AD-A047 613 CALSPAN CORP BUFFALO N Y F/G 8/3
AN INVESTIGATION OF THE METEOROLOGY, PHYSICS, AND CHEMISTRY OF --ETC(U)
OCT 77 E J MACK, U KATZ, C W ROGERS N00019-76-C-0657
UNCLASSIFIED CALSPAN-CJ-6017-M-1 NL

1 OF 2
AD
AD47613

Calspan

AN INVESTIGATION OF THE METEOROLOGY, PHYSICS, AND CHEMISTRY OF MARINE BOUNDARY LAYER PROCESSES.

By
E.J. Mack, U. Katz, C.W. Rogers, D.W. Gaucher,
K.R. Piech, C.K. Akers, and R.J. Pille

Calspan Report No. CJ-6017-M-1

CALSPAN-

Report on
Project Sea Fog,
Fifth Annual Summary Report, no. 5,

Prepared For:

NAVAL AIR SYSTEMS COMMAND
WASHINGTON, D.C. 20360
CODE AIR-370C

CONTRACT NO. N00019-76-C-0657

OCTOBER 1977

32 p.

Calspan Corporation
Buffalo, New York 14221

407727

ABSTRACT

During late September and early October 1976, Calspan participated in CEWCOM-76, a research cruise aboard the Naval Postgraduate School's R/V ACANIA to investigate marine boundary-layer phenomena in the offshore waters of southern California. The objective of the four-week cruise was to investigate marine fog, aerosol characteristics, and evolutionary processes which affect optical propagation in the marine atmosphere. Measurements of visibility, scattering coefficient, winds, air and sea surface temperatures, dew point, total particulate concentration, CCN activity spectra, and fog microphysics were obtained, and hi-vol samples of the ambient aerosols and discrete samples of fog water were collected for later chemical analysis. The data were analyzed to provide descriptions of the microphysics and chemistry of marine fogs and the areal distribution of "clear air" visibility, CCN activity spectra, and aerosol concentration and composition in a 150,000 km^2 area extending approximately 500 km SW of Los Angeles. The data are compared with those obtained on previous investigations conducted off both the East and West Coasts. In addition, limited experiments were conducted to determine if laser beam enlargement could be detected using a low-power laser over short propagation paths and if such measurements might be useful in assessing optical parameters such as size and concentration of aerosols and levels of turbulence in the marine boundary layer.

TABLE OF CONTENTS

TABLE OF CONTENTS (Cont.)

LIST OF FIGURES

LIST OF FIGURES (Cont.)

LIST OF FIGURES (Cont.)

LIST OF FIGURES (Cont.)

LIST OF TABLES

Section 1

INTRODUCTION AND SUMMARY

For the fifth consecutive year, Calspan Corporation under Contract No. N00019-76-C-0657 from the Naval Air Systems Command is continuing its investigation of marine boundary-layer phenomena. In previous investigations, attention was focused on determination of the formation mechanisms, life-cycle variations, and physical and chemical properties of marine fogs occurring off the coasts of California and Nova Scotia. Results of those efforts are described in annual summary reports (Ref. 1-4).

In consonance with the Navy's expanded interest in meteorological effects on the performance of electro-optical equipment, the scope of the current effort has been expanded to include investigation of aerosol characteristics and evolutionary processes which affect optical propagation in the marine atmosphere. To this end, Calspan participated in a four-week research cruise (CEWCOM 76--Cooperative Experiment in West Coast Oceanography and Meteorology-1976) conducted off the coast of southern California during late September and early October 1976. The cruise was performed aboard the Naval Postgraduate School's (NPS) R/V ACANIA and involved a general study of the optical properties of the marine boundary-layer with participation by the NPS, the Naval Oceanographic Systems Center (NOSC), the Naval Avionics Facility-Indianapolis (NAFI), the Naval Research Laboratory (NRL), and Airborne Research Associates. Calspan's role was to obtain measurements of micrometeorological parameters, visibility, aerosol concentration and chemical composition, and fog microphysics. While a substantial quantity of data was acquired during episodes of fog, the primary objectives of this year's effort were to describe the aerosol population and to investigate factors which influence "clear air" visibility.

The expedition was based out of San Diego, with the ACANIA departing its home base at Monterey on 20 September and returning on 15 October 1976. Ship's tracks for the first (20 September-2 October) and second (3-15 October) segments of the cruise are depicted in Figures 1a and 1b, respectively.

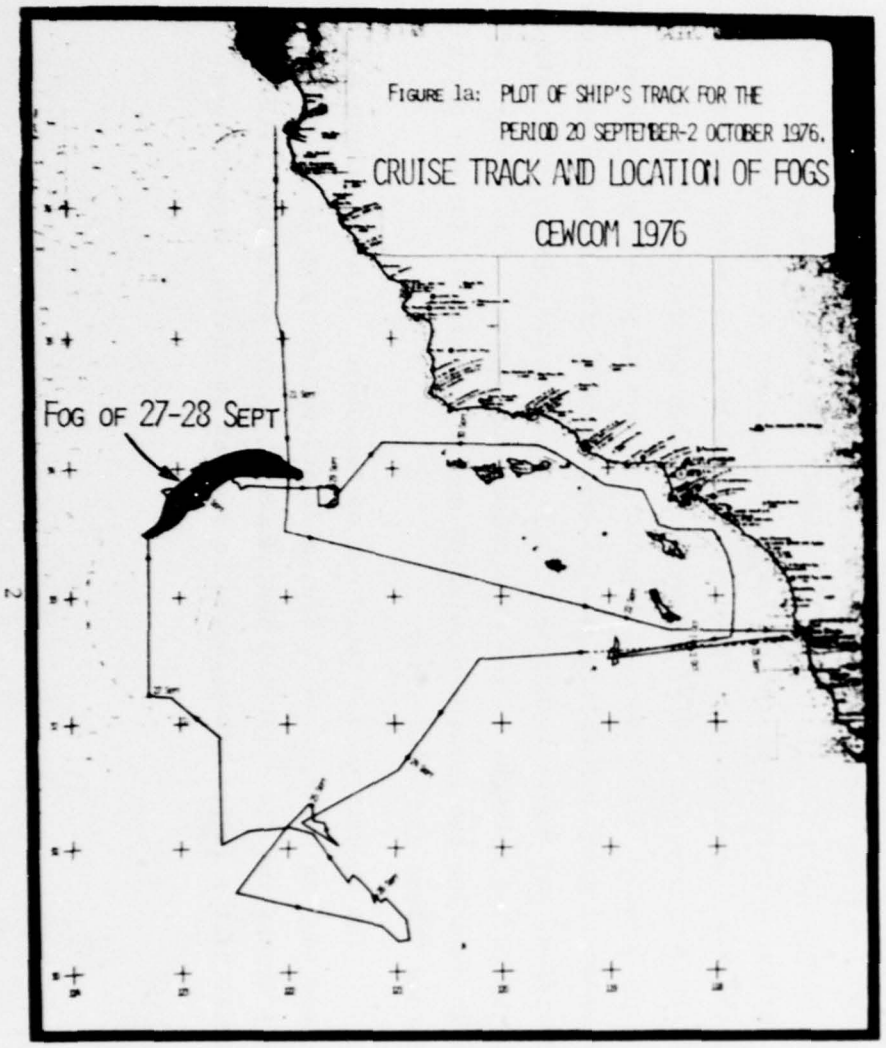

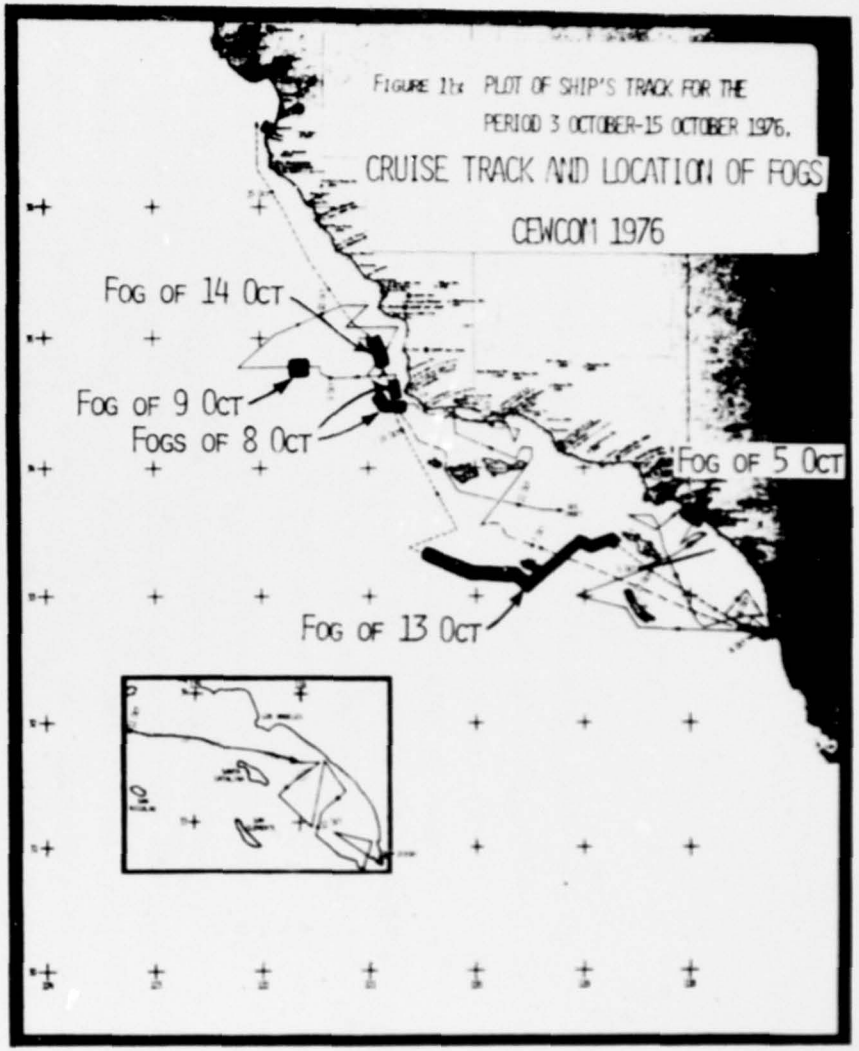

Figure 1: Ship's Track and Location of Fogs Observed During the September-October 1976 Cruise of R/V ACANIA Off Southern California.

(The dates shown along the track refer to the 0000 hour, PDT, of the respective days.) As shown by Figures 1a and b, measurements were obtained over a 150,000 km^2 area in the region of the Los Angeles Bight, extending seaward approximately 500 km SW from San Diego and 200 km W of Pt. Conception.

Calspan instrumentation employed during the field study are listed in Table 1. Calspan's atmospheric research van was hoisted aboard the ACANIA and housed all recorders, a "clear-air" visibility monitor, and nuclei sampling apparatus. Temperature and dew point instrumentation were mounted on the 20 m tower on the foredeck of the ACANIA; fog microphysics and hi-vol aerosol-sampling instrumentation were mounted on a specially-constructed bow platform; the fog visibility monitor was installed on the roof of the pilot house; and sea surface temperature was monitored from a specially-designed vehicle towed along side the ship. Detailed descriptions of this instrumentation may be found elsewhere (e.g., Ref. 1-4).

Throughout the cruise, scattering coefficient, visibility, sea surface temperature, air temperature and dew point were monitored continuously; true winds, wet and dry bulb temperatures, and total particulate (Aitken Nuclei) concentration were recorded hourly. In addition, 112 measurements of the cloud nucleus (CCN) spectra, 100 hi-vol samples of atmospheric aerosols (for chemical analysis) and 42 cascade impactor samples (of aerosols) were obtained during non-fog periods. In the six fog situations encountered, approximately 30 hours of fog data were logged. In addition to continuous records of visibility and micrometeorological parameters, approximately 360 drop samples and 370 ml of fog water (for chemical analysis) were collected during episodes of fog. Some of these data are provided in Appendices B and C and discussed in detail in Sections 2 and 3. (A complete list of all fogs observed to date on this program is provided in Appendix A.)

Results of analyses of aerosol data obtained off the West Coast may be briefly summarized as follows: (1) total particle concentrations increased nearly monotonically with proximity to the coastline apparently reflecting increasing continental influences; (2) most of the aerosols existent in the marine boundary layer off the West Coast were active at 1.0% supersaturation;

Table 1

Calspan Instrumentation Installed on the R/V ACANIA

September-October, 1976

Instrument/Parameter	Height Above Sea Surface
Temperature sensors (Foxboro)	sea sfc., 3.5, 8.5, 18.5 m
Dew point sensors (Foxboro)	8.5, 18.5 m
Sling Psychrometer	4 m
Forward scatter visibility (fog) (EG&G)	7.5 m
Nephelometer visibility (clear air) (MRI)	6 m
Cloud nucleus chamber (Calspan)	6 m
Total particulate monitor (Gardner)	6 m
Aerosol chemistry (2 Hi-Vol Samplers)	5 m
Cascade impactor (Battelle type)	5 m
Fog droplet sampler (Calspan)	5 m
Fog water collector (Calspan)	5 m

(3) larger particles (i.e., CCN active at 0.2% S) in general also increased with proximity to the coast but localized "pockets" of higher concentrations suggest localized sources for these aerosols; (4) since most of the observed ambient aerosol were active as CCN and therefore size-dependent on relative humidity, fluctuations in both aerosol concentration and relative humidity were found to be responsible for fluctuations in clear-air visibility; (5) the chemical composition of the ambient aerosols varied considerably over the cruise area; SO_4^{--}, NO_3^-, NH_4^+, Ca and Al tended to higher concentrations nearer the coast, while concentrations of Cl^- were greater, on the average, farther to sea; Na and Mg concentrations, on the average, remained constant over the cruise area; (6) ratios of chemical constituents suggest that the observed aerosols were primarily of marine origin (sea salt) farther to sea, with increasing quantities of continental/anthropogenic species (superimposed

on the marine aerosol) with proximity to the coast; (7) the data further suggest that the oxidation of gaseous SO_2 to particulate SO_4^{--} in the presence of marine aerosols was responsible for losses of Cl^- and hence a major change in the composition of aerosols in the marine boundary layer closer to the coast. The data on which these conclusions are based is discussed in greater detail in Section 2.

During the cruise, six fogs were encountered at offshore locations depicted in Figure 1. Analyses of fog microphysics data and samples of fog water may be summarized as follows: (1) with the exception of the two fogs observed closest to shore, the microphysical features of the observed fogs were similar to those of fogs previously observed off the West Coast; the near-shore fogs exhibited characteristics more closely resembling those of Nova Scotia fogs; (2) chemically, fog water was comprised of nearly equal concentrations of SO_4^{--} and Cl^- with lessor amounts of Na, NO_3^-, and NH_4^+; (3) fog water concentrations of SO_4^{--} were similar to those measured in Nova Scotia fogs, while Cl^- concentrations were found at levels typical of West Coast fogs and considerably higher than those observed in Nova Scotia fogs; (4) the fogs were apparently nucleated by (or scavenged) both sulfate and chloride aerosols in amounts corresponding to approximately 30-50% of the mass available in the ambient aerosols. These data are discussed in greater detail in Section 2.7.

Case studies for three of the six fogs observed during the cruise are presented in Section 3. The fog of 27-28 September developed behind a cold front over the open ocean ~300 km offshore and persisted for more than 20 hours. The fog of 9 October occurred as a result of lowering stratus, and analysis of the available data showed that a change in the height of the inversion base relative to the lifting condensation level was responsible for initial stratus formation. The third fog discussed in Section 3 was observed over cold water within 20 km of the coast under conditions of high pressure aloft and offshore flow in the surface layer on 8 October.

In addition to direct measurements of the micrometeorological and physical characteristics of the marine boundary layer, a laser imaging experiment was conducted jointly with J.B. Russell of NAFI. The amount and form of laser beam enlargement might be useful in assessing important optical parameters such as size and concentration of aerosols and levels of turbulence in the boundary-layer atmosphere. The primary objective of the experiment was to determine if laser beam enlargement can be observed using a low-power laser over short propagation paths in the marine boundary layer. Laser imaging experiments were conducted on two separate days off the Pacific coast near the NOSC facility at San Diego and, subsequently, on two separate days in February 1977 from the Naval Coastal Systems Laboratory's platform located in the Gulf of Mexico ~20 km off Panama City, Florida. While only a limited effort was feasible within the scope of the experiment, laser imaging data were obtained at ranges from 2 to 18 km, and a significant amount of beam spreading about the forward direction was detected. However, analysis of the imagery data indicated that a laser of 3-5 times greater intensity is required to obtain data at ranges >4 km when ambient visibilities are < 20 km. These experiments and data are discussed in greater detail in Section 4.

Section 2

PHYSICAL AND CHEMICAL CHARACTERISTICS AND AREAL DISTRIBUTION OF AEROSOLS IN THE OFFSHORE REGION OF SOUTHERN CALIFORNIA DURING SEPTEMBER AND OCTOBER 1976

The primary objective of the September-October 1976 cruise aboard the R/V ACANIA was to obtain data describing the aerosol population off the coast of southern California. As a result, a considerable quantity of data was acquired in an effort to delineate the spatial and temporal variations of aerosols in the marine boundary layer. These data include hourly observations of total particulate concentration, scattering coefficient, visibility, relative humidity, and winds. Frequent measurements of condensation nucleus (CCN) spectra (2-6 times daily) and hi-vol samples (2-4/day) of ambient aerosols (for bulk chemical composition analysis) were obtained during non-fog periods. In addition, during the 30 hours of fog encountered during the cruise, measurements of droplet spectra and samples of fog water (for chemical analysis) were obtained. Detailed analyses of these data are presented and discussed within this section.

2.1 General Meteorological Conditions

During the cruise, the sea surface temperature was monitored continuously, and the data from both halves of the cruise were composited to produce the sea surface isotherm chart shown in Figure 2. Despite the three-plus weeks required to obtain the data and the considerable liberty taken in smoothing of small scale temperature fluctuations particularly in the vicinity of the Channel Islands, it is felt that the surface isotherm chart is reasonably representative of the gross features of the surface temperature pattern existent during the period. The data show that the coldest water was centered about the 122 W meridian and that, with the exception of a cold spot along the shore north of Pt. Conception, the sea surface gradually warmed with proximity to the coast.

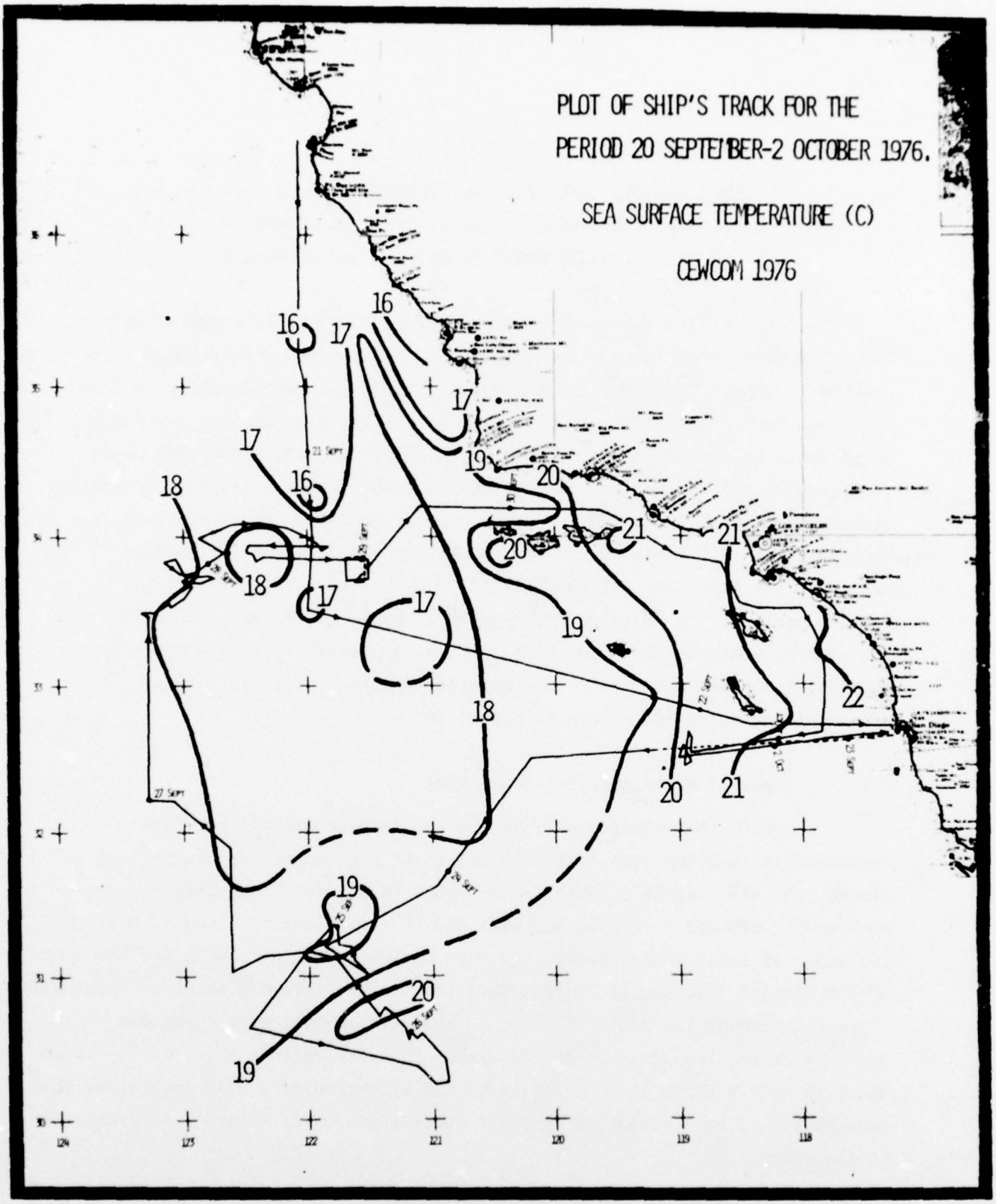

FIGURE 2: MEAN SEA SURFACE TEMPERATURE PATTERN MEASURED FROM ACANIA OFFSHORE SOUTHERN CALIFORNIA, 20 SEPTEMBER-13 OCTOBER 1976.

Observations of winds were obtained hourly from the ship's anemometer along with ship's heading and speed. These data were combined in a computer routine to provide calculations of true wind. As much of these data as possible have been plotted as a function of ship's position and are shown in Figures 3a, b, and c. For the most part, winds were "on shore" and >5 m sec^{-1} at distant offshore locations, and "light and variable" (< 5 m sec^{-1}), with predominantly offshore flow in the area between the Channel Islands and the coast.

Data depicting the general visibility levels in "clear air" conditions (i.e., in the absence of fog) during the first half of the cruise are presented in Figure 4. In order to smooth out small scale fluctuations, the visibility isopleth chart in Figure 4 was constructed from hourly observations averaged over six-hour periods. These data thus provide a synopsis of the mean visibility levels for the initial 12-day portion of the cruise. It is seen from the data that an area of reduced visibility existed, in the mean, in the vicinity of San Nicolas and San Clemente Islands and that the clearest air was observed in the southwest portion of the cruise area. (Because of the amount of fog observed on the second half of the cruise, it was not possible to construct a comparable visibility chart for that portion of the cruise.)

An overview of the "clear air" conditions encountered during the cruise is provided in greater detail by data shown in Figure 5. At the bottom of the figure measurements of CCN concentrations* active at 0.2% S and 1.0% S** are plotted as functions of time for the duration of the cruise.

---

*These data have not been corrected for vapor depletion and sedimentation effects (Ref. 5).

**According to theory and experimental evidence (e.g., Ref. 6), CCN active at 0.2 and 1.0% S correspond to particles of ~0.075 and 0.025 μm diameter (dry size), respectively.

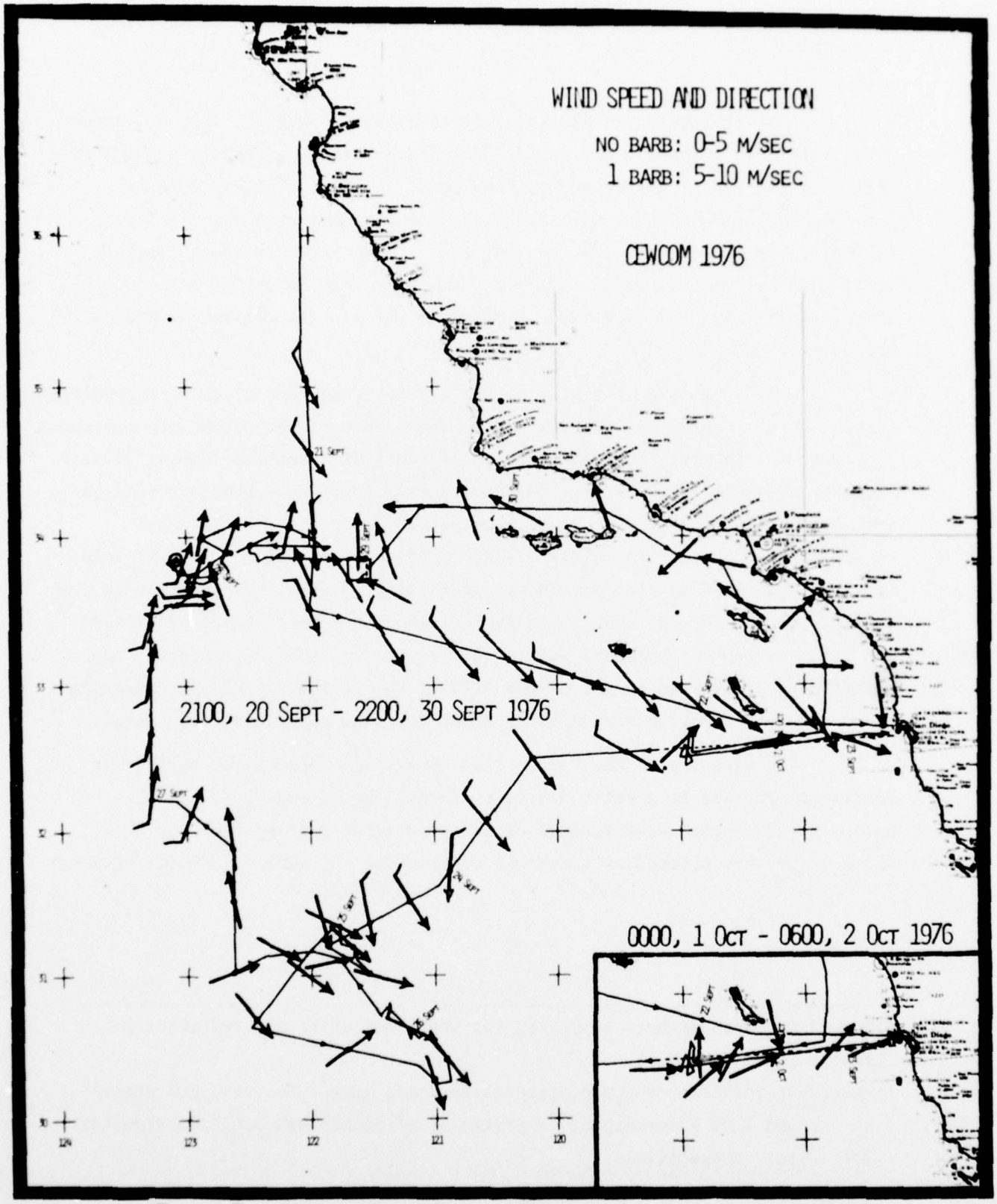

FIGURE 3A: WINDS FOR THE PERIOD 20 SEPTEMBER TO 2 OCTOBER 1976

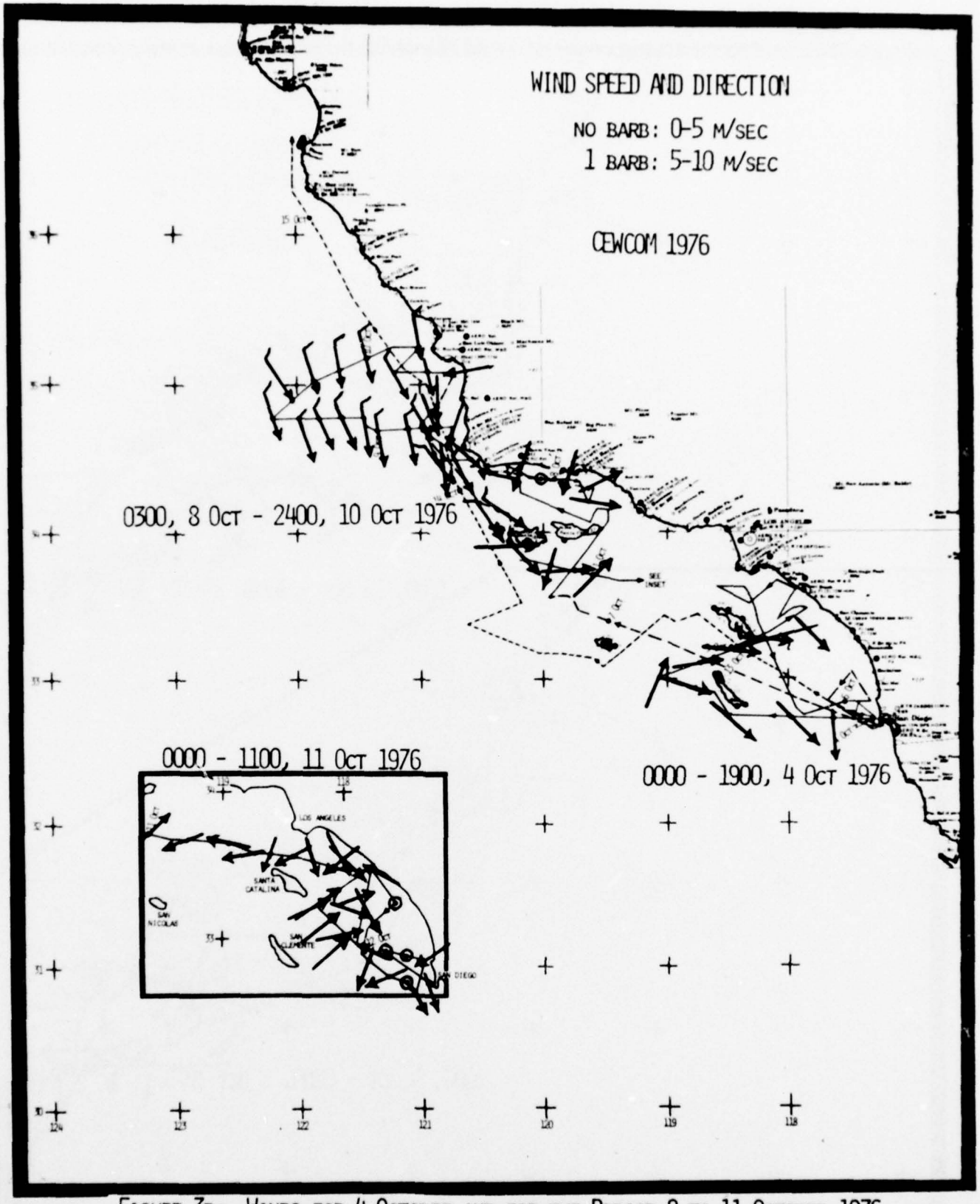

FIGURE 3B: WINDS FOR 4 OCTOBER AND FOR THE PERIOD 8 TO 11 OCTOBER 1976

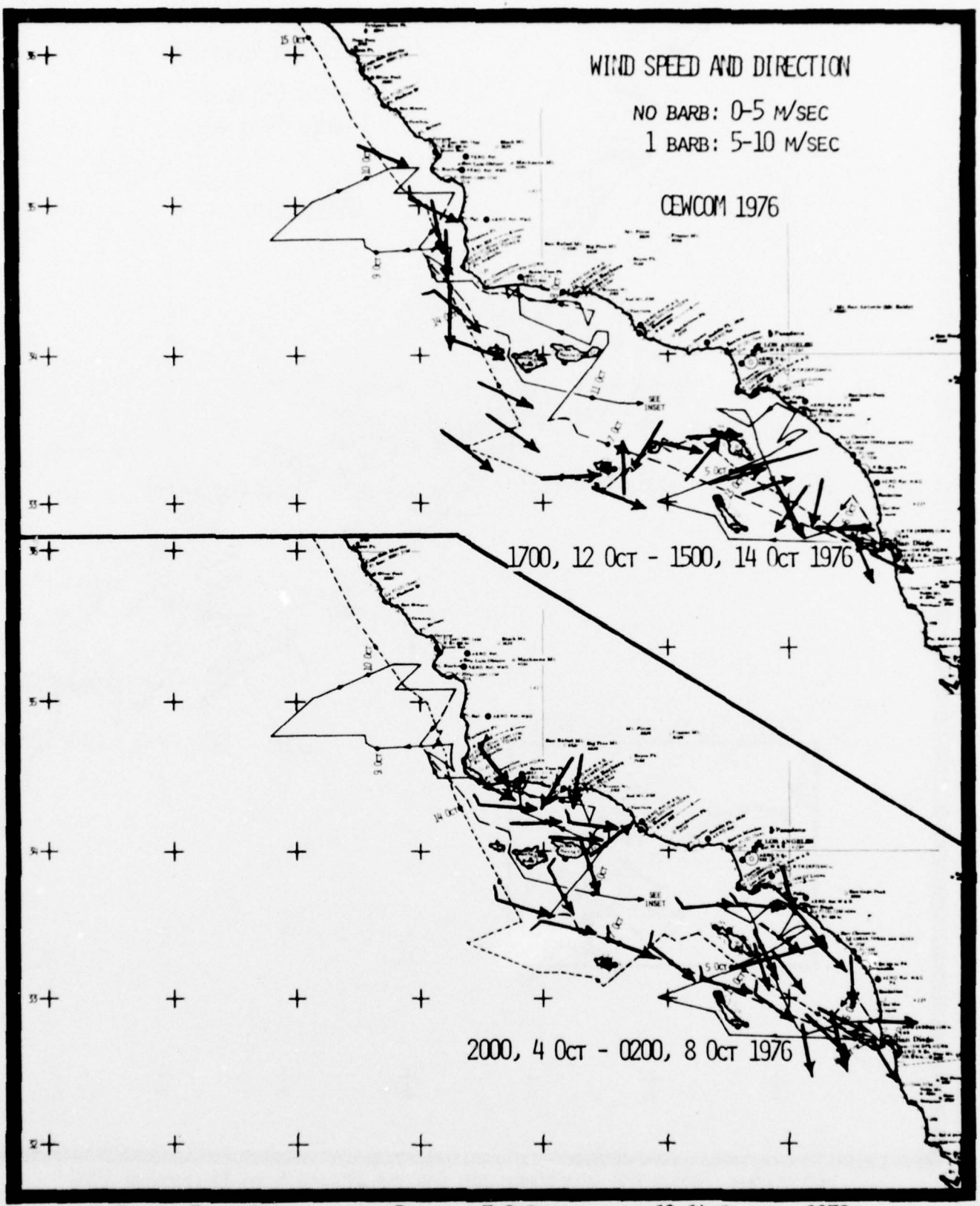

FIGURE 3C: WINDS FOR THE PERIODS 5-8 OCTOBER AND 12-14 OCTOBER 1976

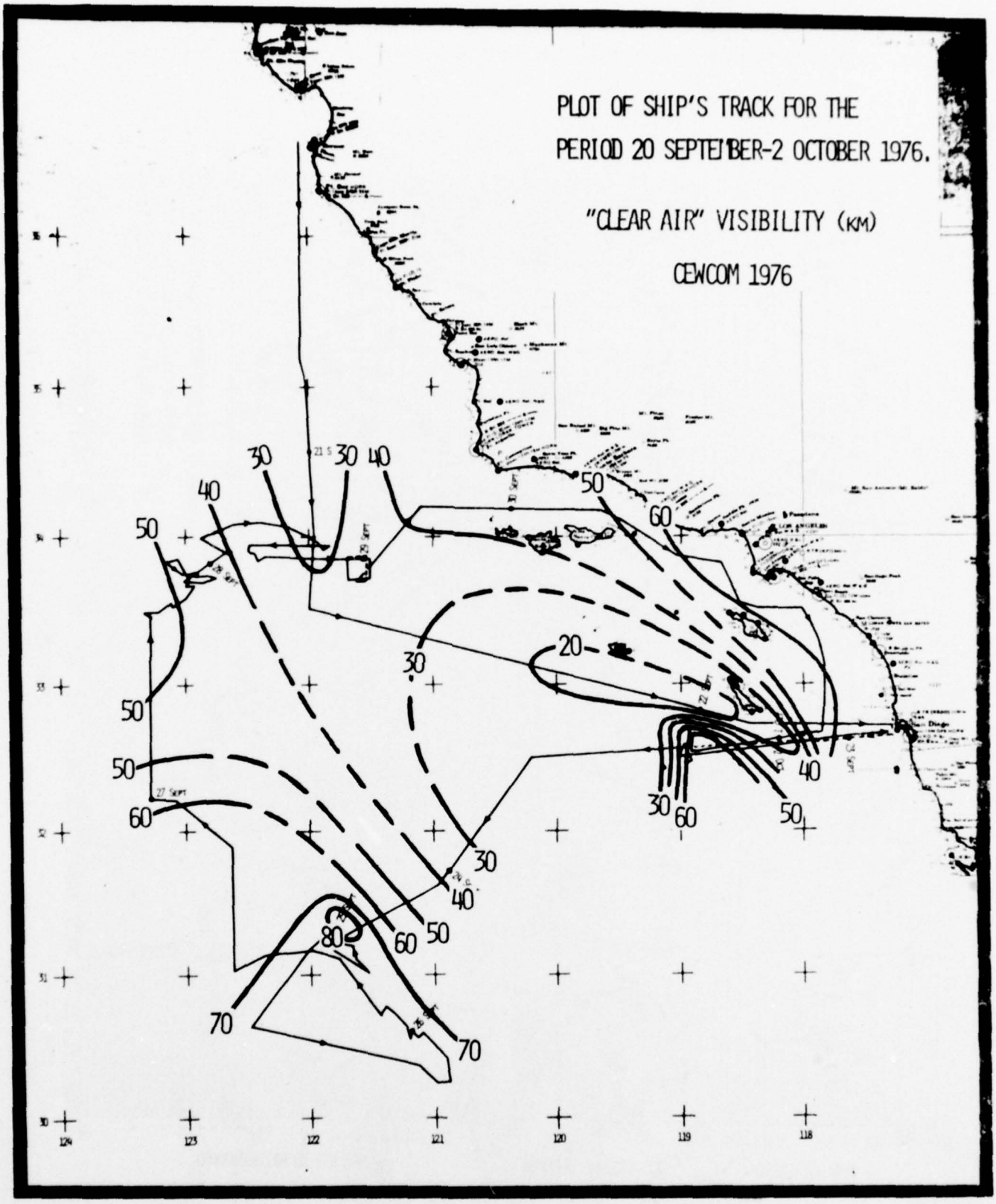

FIGURE 4: ISOPLETHS OF "CLEAR AIR" VISIBILITY (KM) OFFSHORE SOUTHERN CALIFORNIA, 20 SEPTEMBER-2 OCTOBER 1976

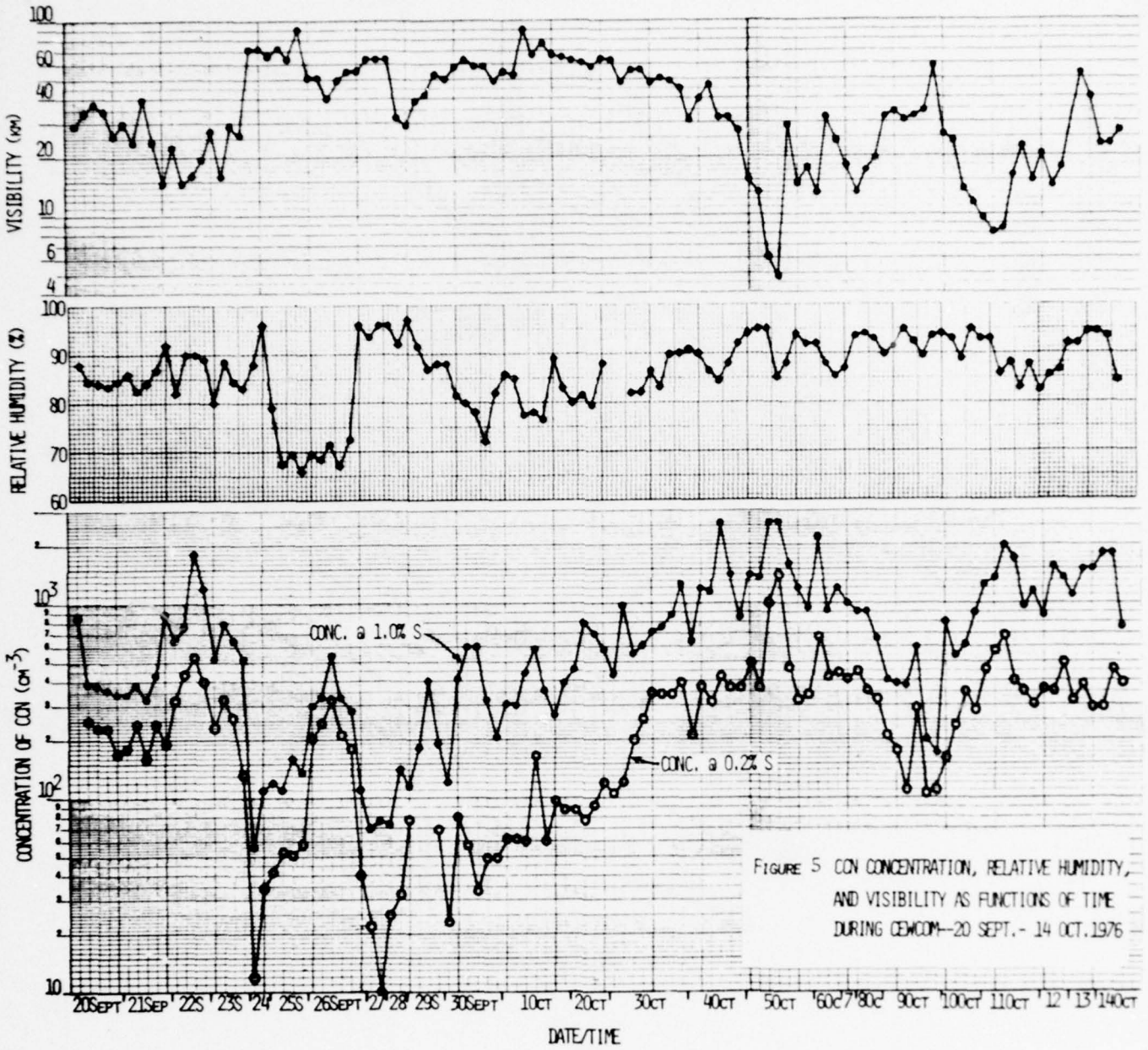

FIGURE 5 CCN CONCENTRATION, RELATIVE HUMIDITY, AND VISIBILITY AS FUNCTIONS OF TIME DURING CEWCOM--20 SEPT.- 14 OCT. 1976

The CCN data are sequential observations, and it should be noted that the time scale on the figure is nonlinear. As can be seen from the data, CCN concentrations at the two supersaturations differed by a factor of approximately 2-5 but fluctuated sometimes synchronously throughout the cruise, each varying in magnitude from one locale to another by a factor of about 30.

2.2 Spatial Variations of Aerosols and CCN Off the Southern California Coast

The fluctuations evident in the CCN data shown in Figure 5 in general reflect the various activities depicted by the cruise tracks (Figure 1). Highest CCN concentrations were observed near shore, in the vicinity of San Nicolas and San Clemente Islands on 22 September, and on 4 and 13 October, and in the region between Los Angeles and San Diego on 4-6 October and again on 11 October. The lowest CCN concentrations were observed at the most distant offshore positions (i.e., on 24 and 25 September, 27 through 30 September and on 9 October). CCN concentrations gradually increased as the ship neared the coast on 29 September and sailed down the Santa Barbara Channel to the vicinity of San Diego.

When plotted as functions of ship's position, the aerosol data reveal consistent patterns and trends apparently associated with the wind field and proximity to the coast. For example, in Figure 6, isopleths of total particle concentration (Aitken nuclei) are shown for the first and second halves of the cruise. These data were obtained hourly and averaged over six hour intervals to produce the distribution charts shown in Figure 6. As shown by the figure, total particle concentrations increased steadily from minimum detectable levels (i.e., < 200 cm^{-3}) at the seaward edge of the cruise area to values in excess of 2000 cm^{-3} near shore. These data no doubt reflect the increasing influence of continental sources, and perhaps surf action, on the total aerosol burden with proximity to the coastline.

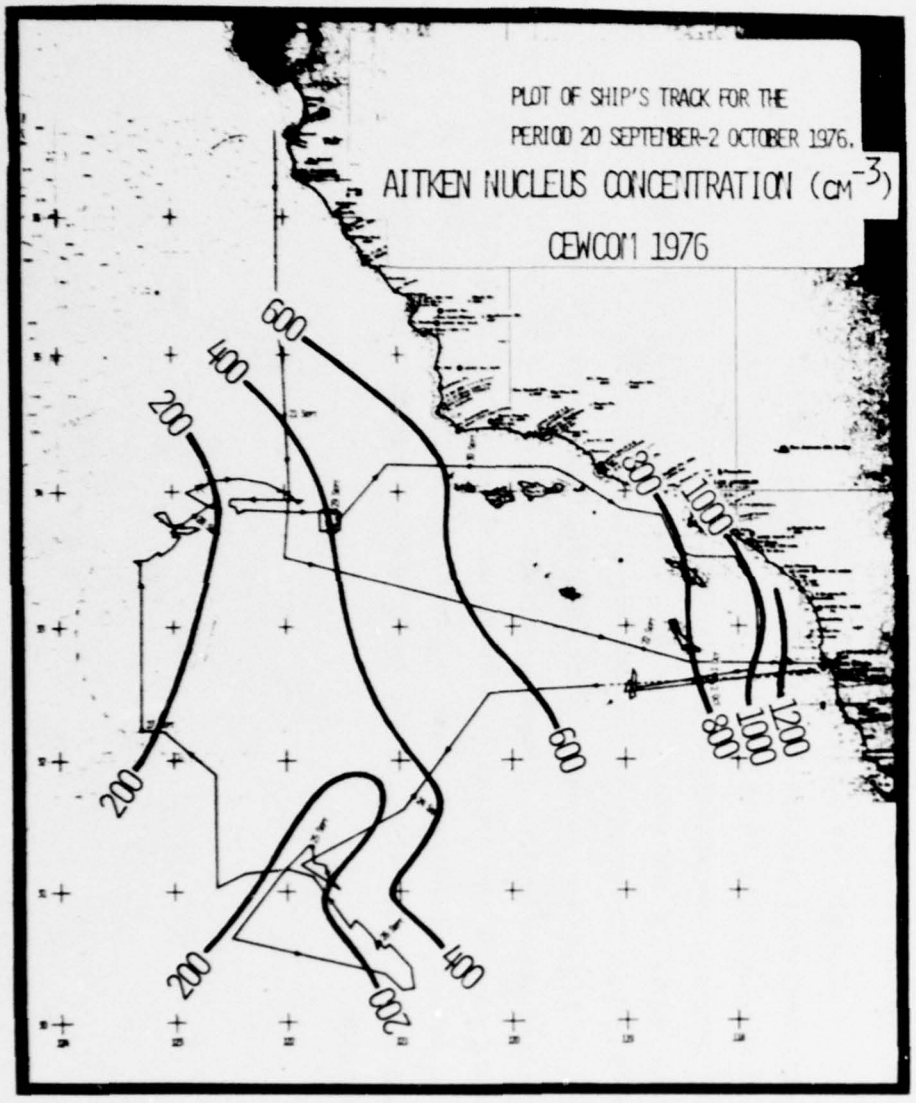

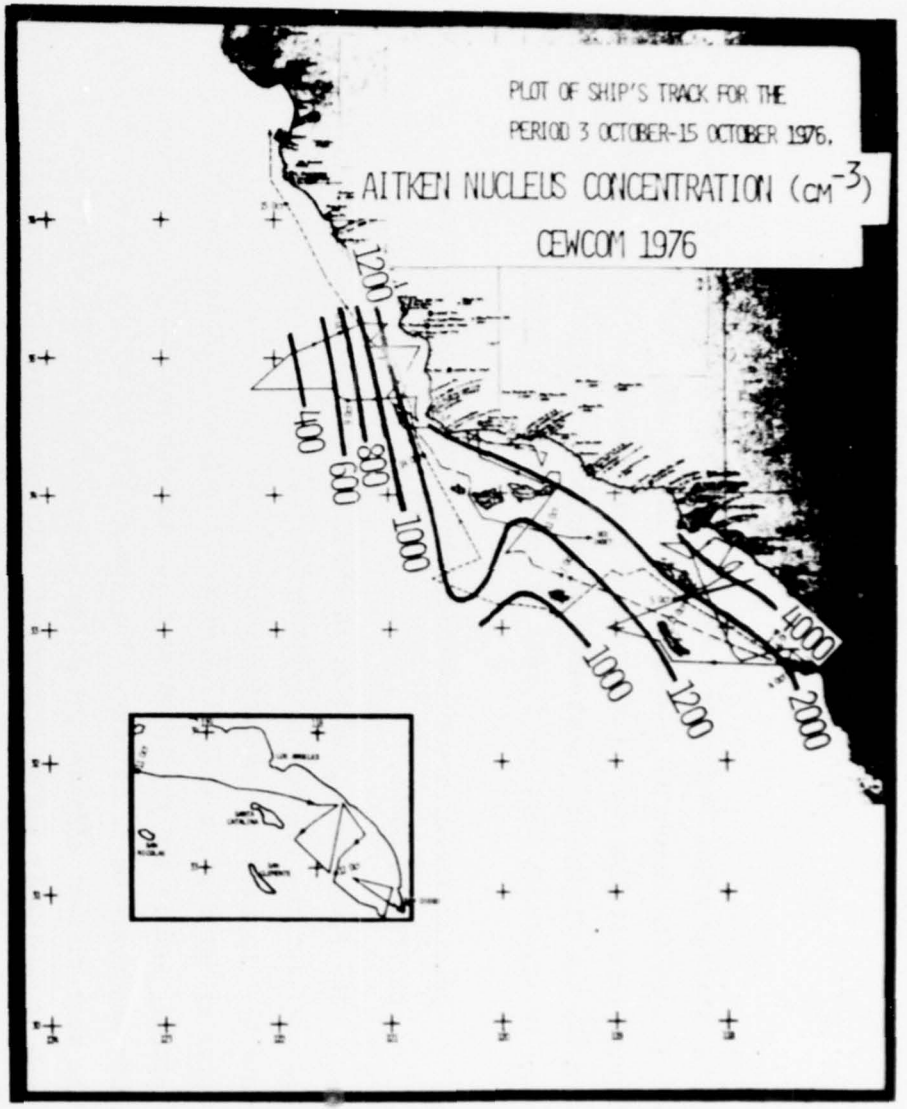

FIGURE 6: ISOPLETHS OF TOTAL PARTICLE CONCENTRATION (CM^{-3}), OFFSHORE SOUTHERN CALIFORNIA, SEPTEMBER-OCTOBER 1976.

Similar data describing the distribution of CCN concentrations are shown in Figures 7 and 8 for particles active at 1.0% S (>0.025 μm, dry size) and 0.2% S (>0.075 μm, dry size), respectively. (The CCN data used to produce the plots are individual observations obtained at frequencies of from two to six times daily). As was the case for total particle concentration, a general trend of increasing CCN concentrations with proximity to the coast is evident in both figures. The distribution plots of the CCN data, however, are not as uniform as those of total particle concentration, exhibiting minima and maxima and suggesting localized sources for these aerosols.

The extent to which the CCN distribution plots are affected by the lack of data as extensive as those of total particle concentration is not known. In Figure 9, total nucleus concentration is plotted as a function of the simultaneous concentration of CCN active at 1.0% S. It is evident from this presentation that most of the aerosols observed during the cruise were active at 1.0% S--a result reported for marine air masses by a number of previous investigators (e.g., Ref. 7). However, the number of departures from the 1:1 line in Figure 9 suggest that a 1:1 relationship is not always the case; and therefore that there are, at times, differences in the production mechanisms for Aitken nuclei and CCN, even in the marine boundary layer.

2.3 CCN Activity Spectra

In total, more than 110 measurements of the CCN activity spectra were obtained during the September-October cruise. When plotted together, the CCN data were found to fall into well-defined groupings as illustrated in Figures 10a and b. Five distinct, mean activity spectra were identified by this comparison, and these are presented in Figure 11. It is readily seen that the mean CCN spectra differed chiefly in the absolute magnitude of the respective aerosol concentrations--with the exception of the spectrum represented by the square symbol and which exhibits a much steeper slope than those of the other spectra.

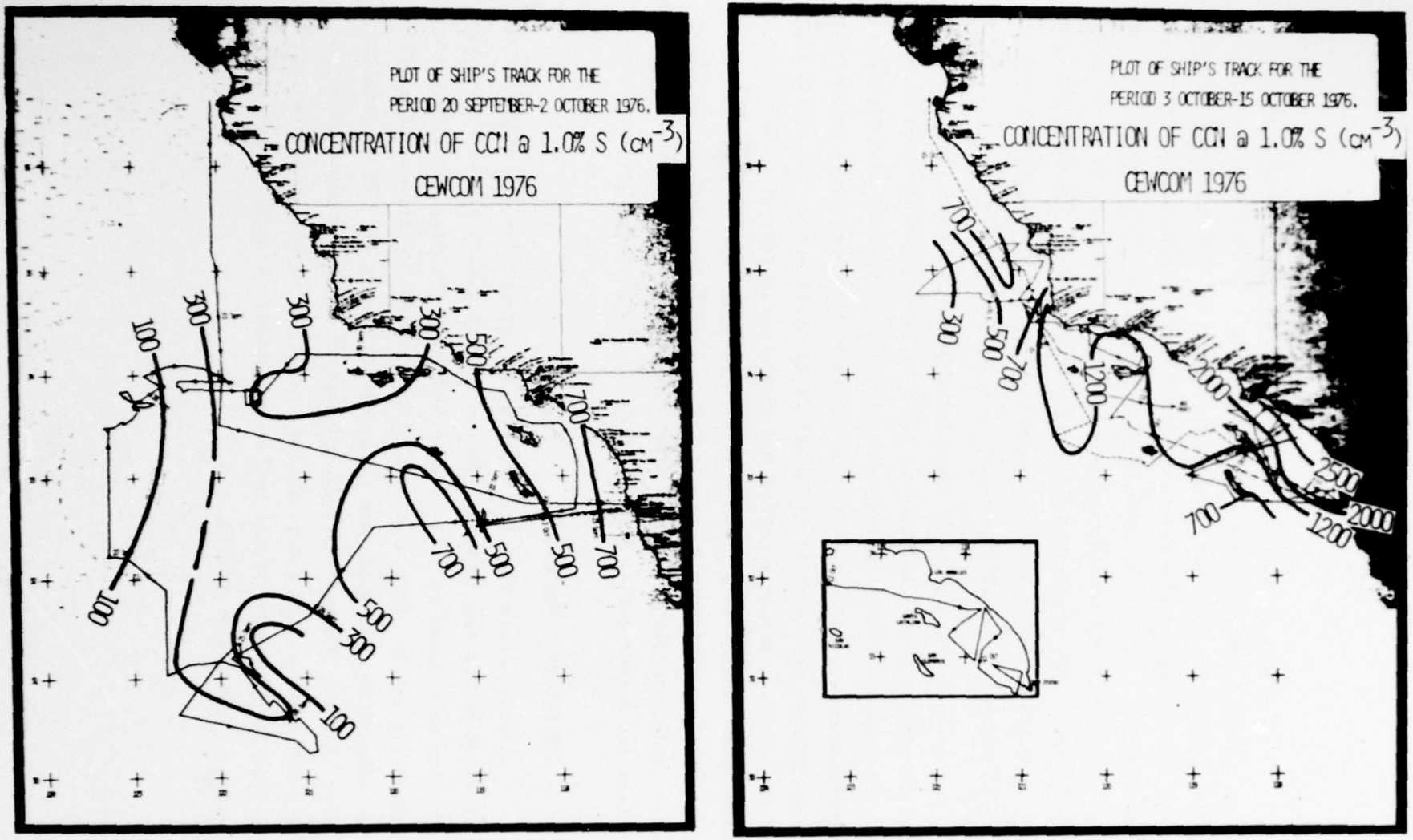

FIGURE 7: ISOPLETHS OF CONCENTRATIONS OF CCN (ACTIVE AT 1.0% SUPERSATURATION), OFFSHORE SOUTHERN CALIFORNIA, SEPTEMBER-OCTOBER 1976.

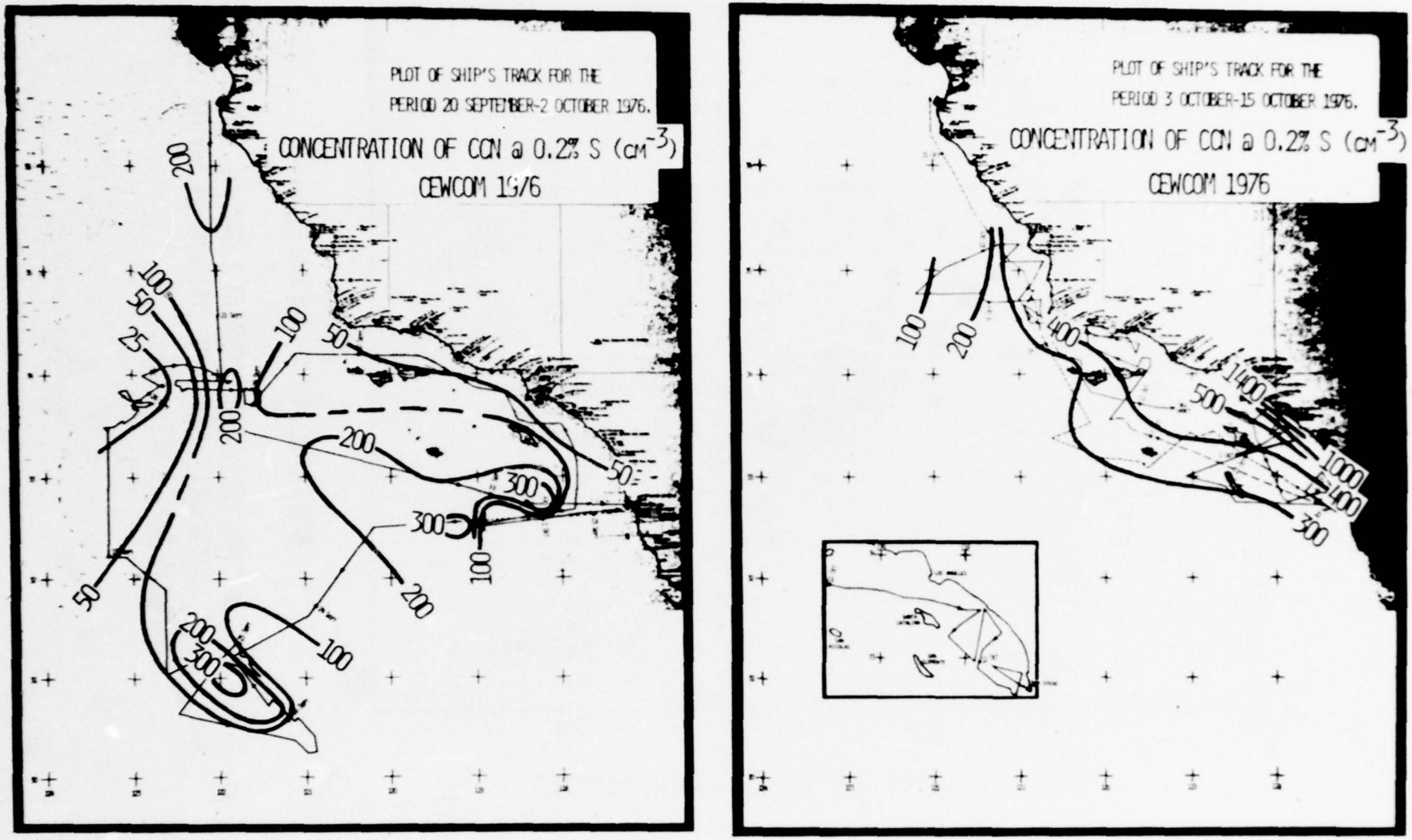

FIGURE 8: ISOPLETHS OF CONCENTRATIONS OF CCN (ACTIVE AT 0.2% SUPERSATURATION), OFFSHORE SOUTHERN CALIFORNIA, SEPTEMBER-OCTOBER 1976.

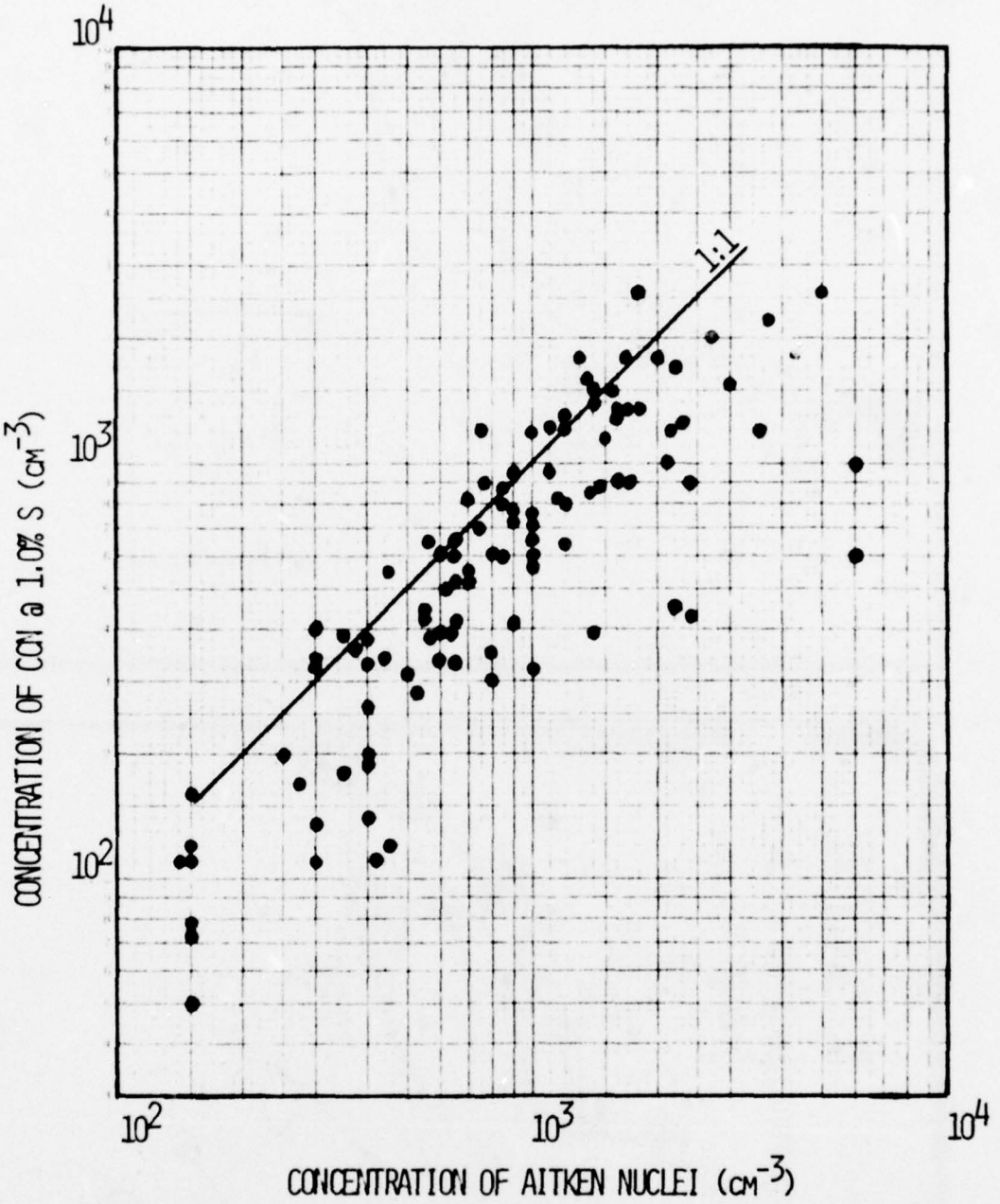

FIGURE 9 CONCENTRATION OF CCN ACTIVE AT 1.0% S vs. CONCENTRATION OF AITKEN NUCLEI, OFFSHORE SOUTHERN CALIFORNIA DURING CEWCOM, SEPT.- OCT., 1976.

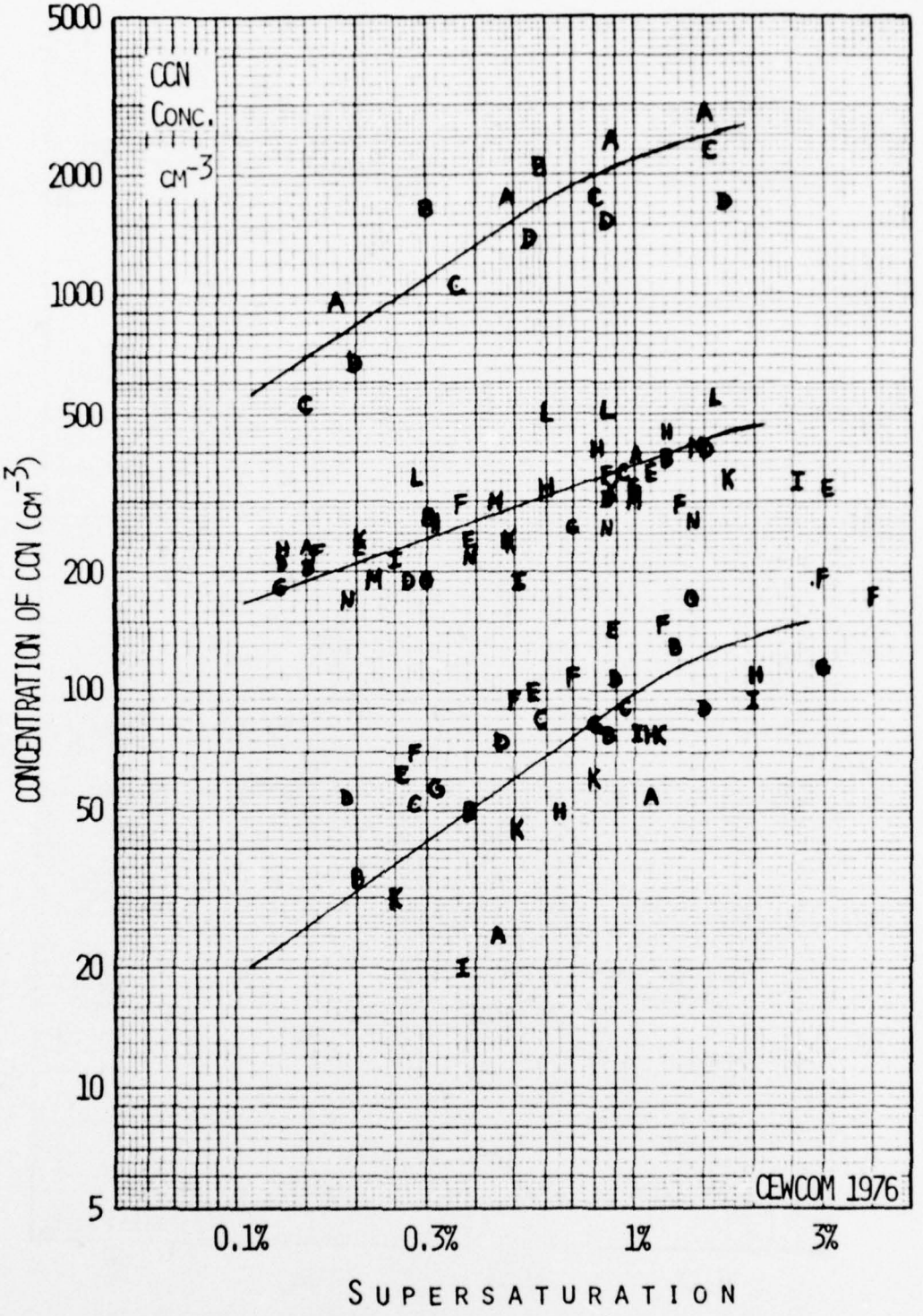

FIGURE 10A: CCN ACTIVITY SPECTRA MEASURED OFF THE COAST OF SOUTHERN CALIFORNIA, SEPTEMBER-OCTOBER 1976.

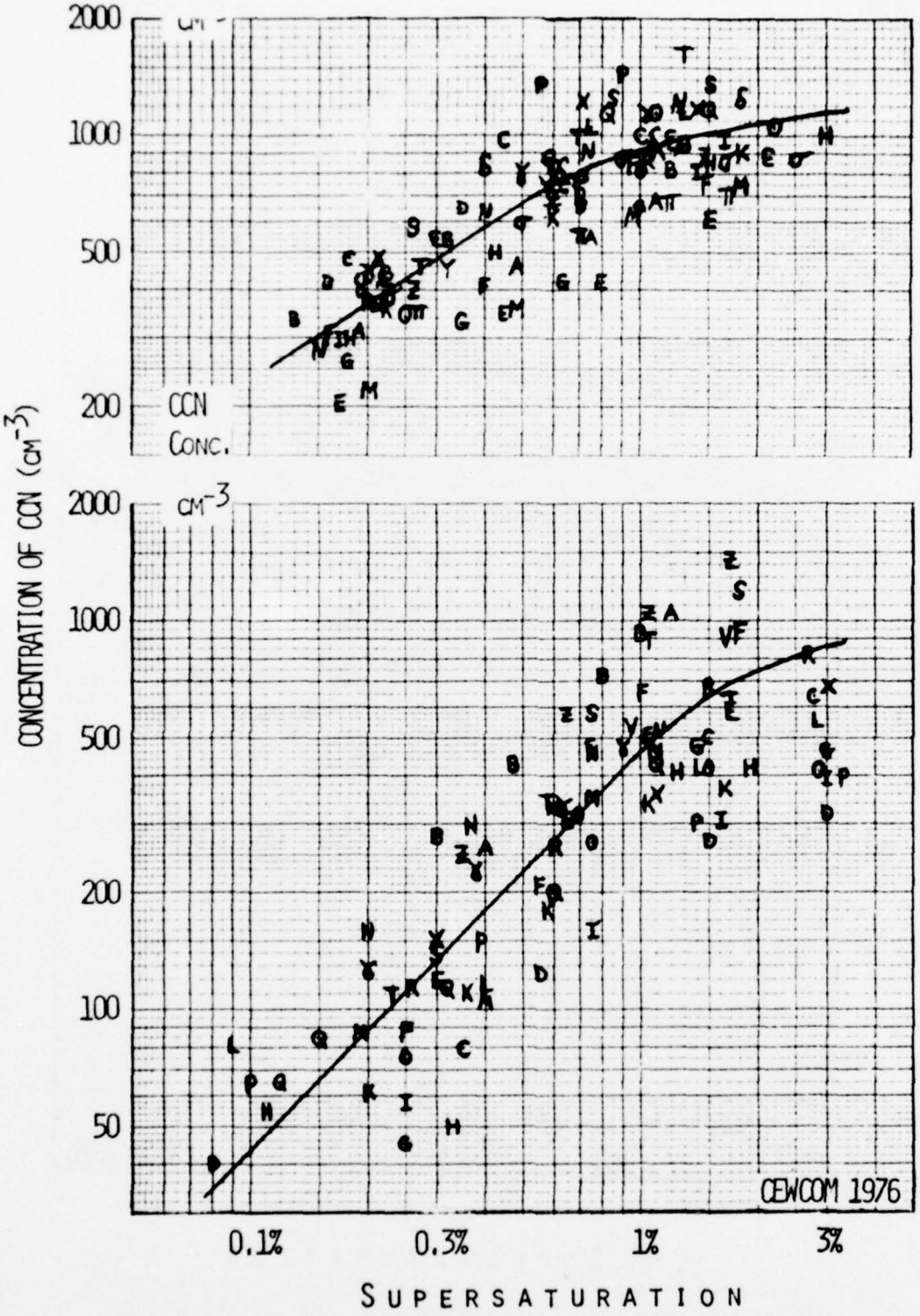

FIGURE 10B: CCN ACTIVITY SPECTRA MEASURED OFF THE COAST OF SOUTHERN CALIFORNIA, SEPTEMBER-OCTOBER 1976 (CONT.)

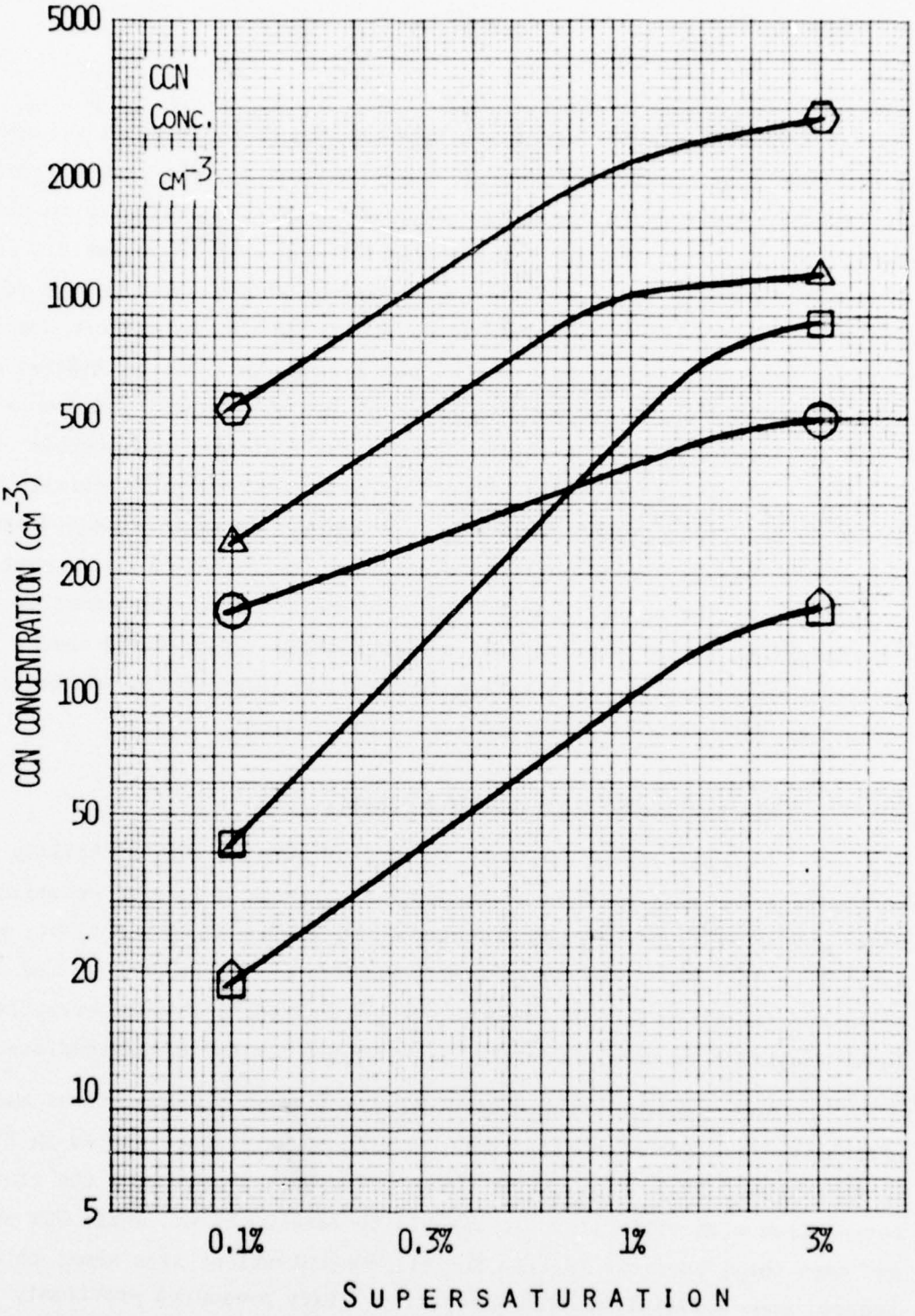

FIGURE 11 AVERAGE CCN ACTIVITY SPECTRA OBSERVED OFF THE COAST OF SOUTHERN CALIFORNIA DURING CEWCOM, SEPT.-OCT., 1976.

When plotted as a function of measurement location (i.e., along ship's track) as shown in Figure 12, the five mean activity spectra defined a pattern suggestive of increasing continentality with proximity to the coastline. The data show that the lowest CCN concentrations (at all supersaturations between 0.1 and 3.0%) were observed at the seaward edge of the cruise area (presumably clean marine aerosols), while the highest concentrations were measured inside the Channel Islands between Los Angeles and San Diego (presumably continental/pollutant aerosols superimposed on a marine background). In the region between the coastline and distant offshore (i.e., the general area of the Channel Islands) observed CCN activity spectra appear to be "transitional" between the primarily-continental and clean marine aerosols of the respective locations. The "transitional" spectra (designated by the square and triangular symbols) being characterized by low concentrations at low supersaturation (presumably larger-sized marine aerosols) and high concentrations at high supersaturations (presumably smaller-sized combustion and photooxidation products).

2.4 Fluctuations in Clear-Air Visibility

A comparison of CCN data shown in Figure 8a with visibility data in Figure 4 for that portion of the cruise suggests a general correlation between visibility and concentrations of CCN active at 0.2% S (i.e., particles $\geq$ 0.075 μm dia, dry size). Similar features are also evident in the data presented in Figure 5. As expected, in general but with some exceptions, lower visibilities were associated with higher aerosol concentrations.

The observed relationship between aerosol concentrations and visibility (scattering coefficient) is more clearly demonstrated in Figure 13. In the figure, it is seen that CCN active at 0.2% S exhibited the closest correlation with visibility (at visibility levels < 50 km) while CCN at 1.0% S and even total particle (Aitken Nuclei) concentrations also show, to a lesser degree, some correlation with visibility. Data presented previously in Figure 9 showing that nearly all the particles observed during the cruise were active at 1.0% S explains the correlation between visibility and Aitken nucleus concentration.

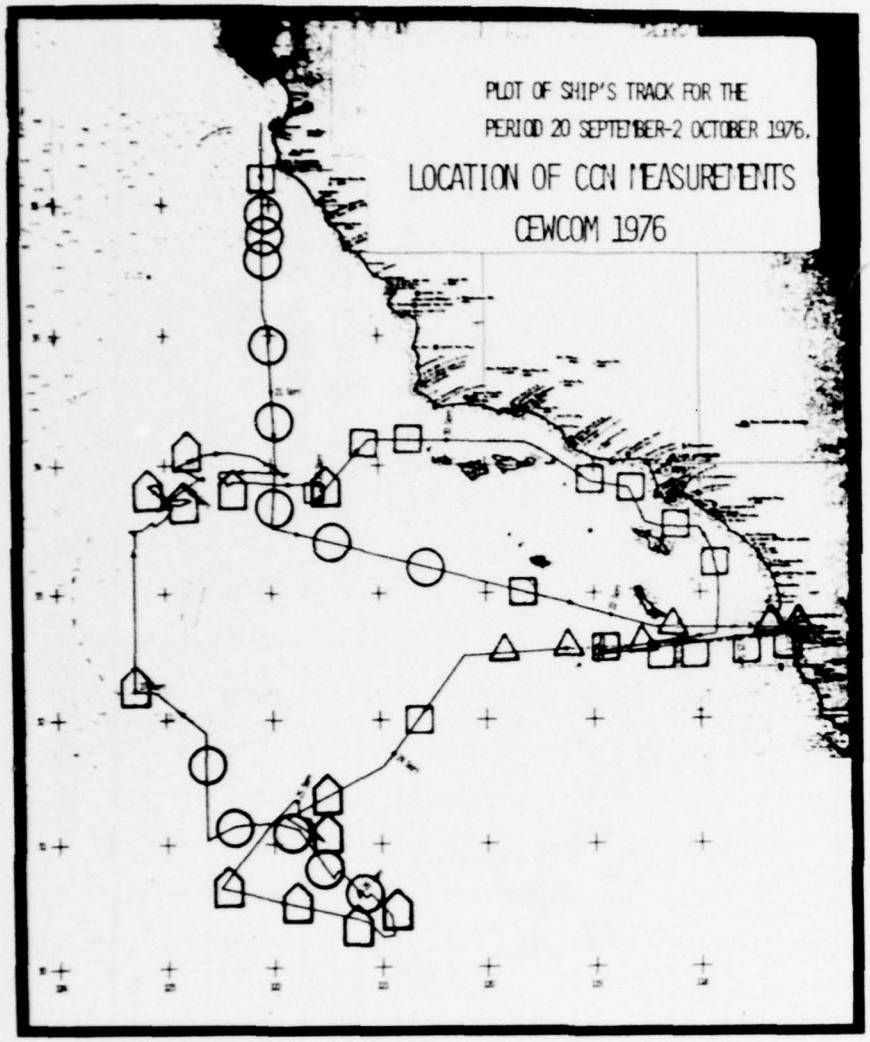

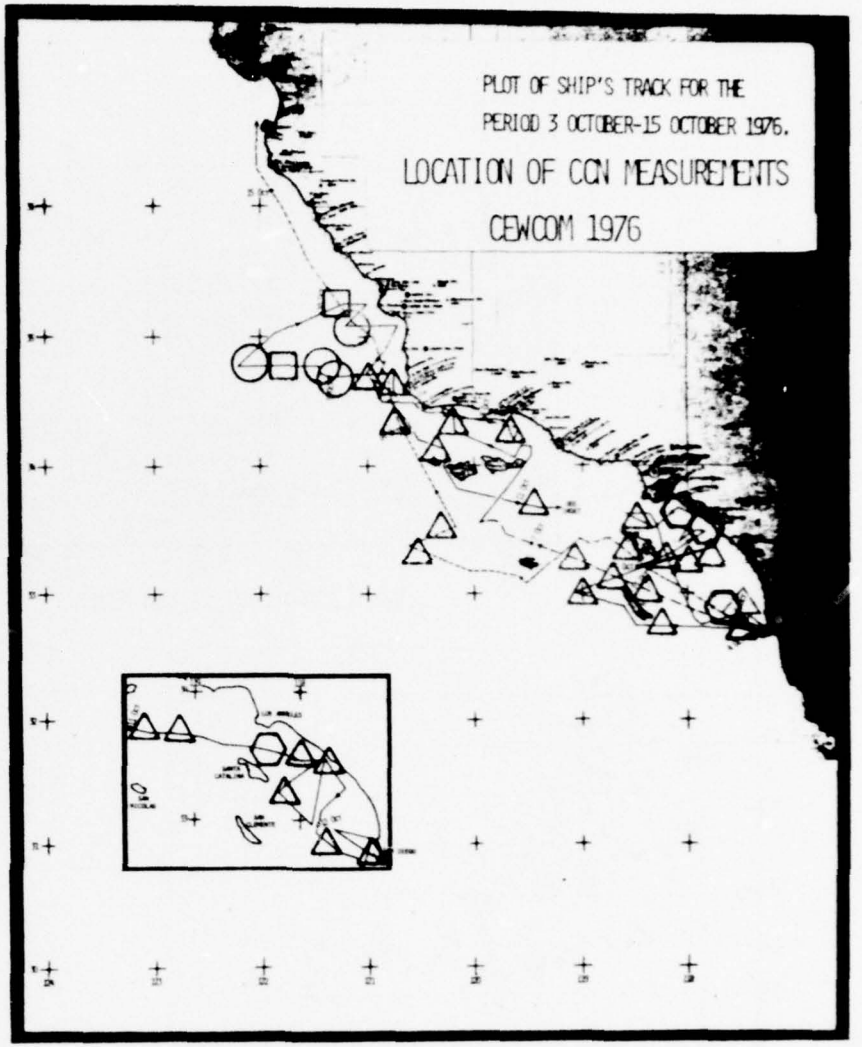

FIGURE 12: AREAL DISTRIBUTION OF AVERAGE CCN ACTIVITY SPECTRA, OFF THE COAST OF SOUTHERN CALIFORNIA, SEPTEMBER-OCTOBER 1976.

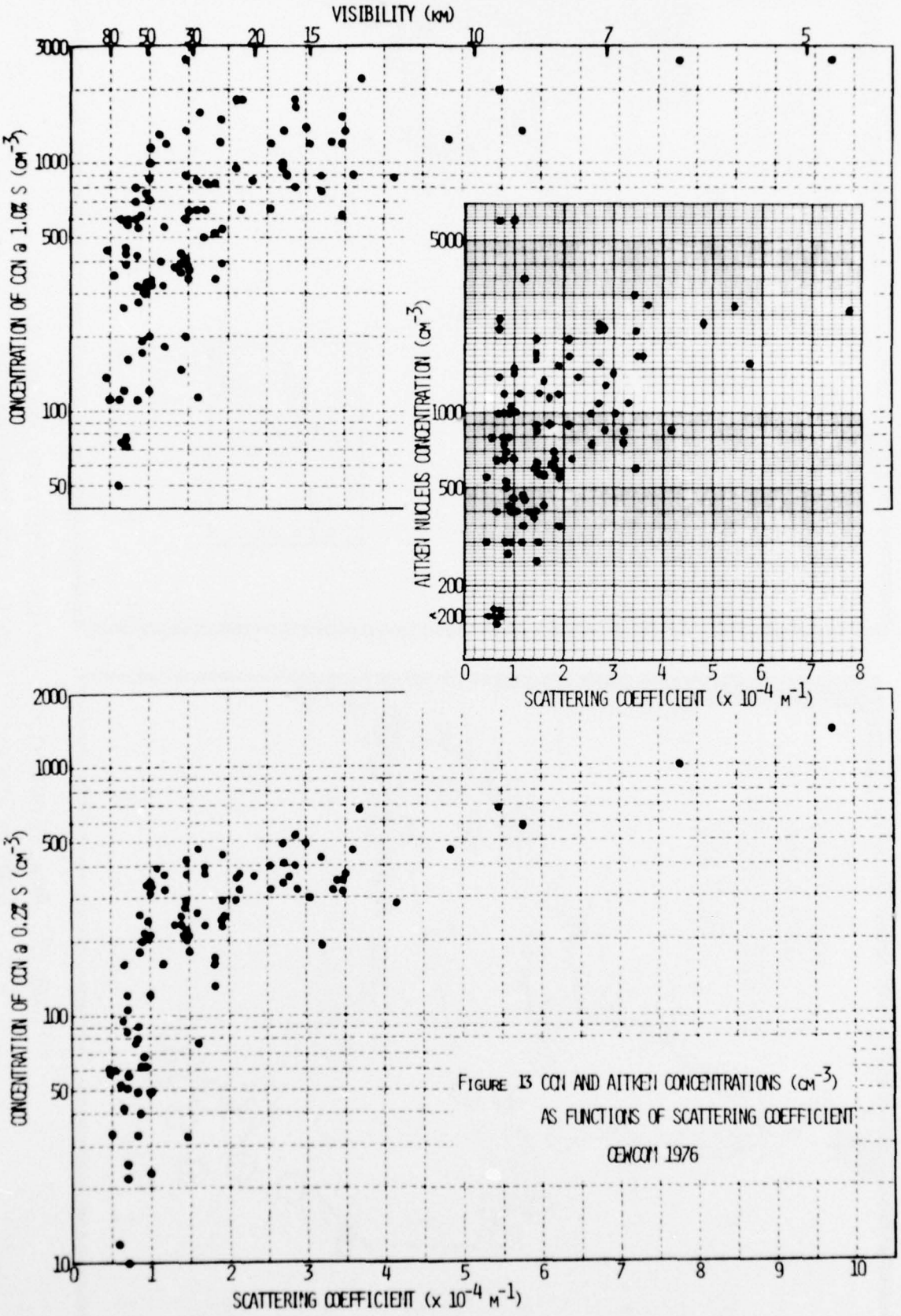

FIGURE 13 CCN AND AITKEN CONCENTRATIONS (CM^{-3})
AS FUNCTIONS OF SCATTERING COEFFICIENT
CEWCOM 1976

Visibility (V) in the atmosphere is dependent on the threshold contrast of a target and on the optical properties of the intervening air and is usually described by the Koschmieder relation: $V = 3.91/\beta$, where β is the atmospheric extinction coefficient. Total atmospheric extinction (β) is the sum of Rayleigh scattering (β_r) by air molecules and particles small ($< .05$ μm) compared to wavelength, Mie scattering (β_m) by aerosols of size (>0.1 μm) comparable to wavelength, and absorption (α) by both gaseous and particulate elements. In the typical, aerosol-laden boundary layer, β_r and α due to gas molecules are small and relatively constant, and β_m is sufficiently large so that β_r and α due to aerosols can be neglected. Since β_m is dependent on the refractive index, concentration and size of aerosols, visibility fluctuations in the atmosphere become primarily dependent on the integrated fluctuations of aerosol composition, concentration and size in the Mie scattering regime (e.g., Ref. 16, 17).

Obviously, in view of aerosol-scattering relationships, aerosols (CCN) at dry sizes of < 0.1 μm will have less influence on visibility than particles of larger size. In a recent investigation by these authors in the Gulf of Mexico, aerosols of diameter >0.5 μm (the smallest size measured) were found to be closely correlated with MRI Nephelometer-measured visibility restrictions (Ref. 12). However, that the CCN of the current study are aerosols active at supersaturations as low as 0.2% S is indicative of their deliquescence properties and potential response to changes in relative humidity (RH). At the high relative humidities typical of the marine boundary layer (i.e., 70-90%--see Table 2, Section 2.5) hygroscopic aerosols (CCN) composed of sulfates, nitrates and chlorides (see Section 2.6) are expected to exhibit equilibrium sizes ∿2-3 times larger than their dry sizes (e.g., Ref. 18). Thus, the measured CCN (dry size >0.075 μm) were likely existent in the ambient conditions at sizes >0.2 μm diameter and therefore should exhibit some correlation with visibility.

Since relative humidity can be expected to control the sizes of hygroscopic aerosols (CCN), it follows that fluctuations in RH will produce changes in visibility through a given population of aerosols (e.g., Ref. 12, 17). This conclusion is substantiated, in part, by data presented in Figure 5. While it has been shown previously (Figures 5 and 9) that number concentrations of CCN active at 0.2% S are grossly correlated with visual range, low relative humidity on 26 September apparently prevented severe visibility degradation during a period of high CCN concentration. Similarly, decreasing RH on 29 and 30 September, in the face of increasing CCN (at 0.2% S) was apparently responsible for the observed increase in visibility. Further, the combination of increasing RH and increasing CCN concentration from 2 October to 5 October was apparently responsible for the gradual decrease in visibility observed during that period.

Similar evidence of a dual dependence of visibility on both aerosol concentration and relative humidity is presented in Figures 14 and 15. In the figures, detailed observations of total aerosol concentration, relative humidity and visibility are plotted as functions of time for two selected 16-hour periods. (CCN measurements were obtained only twice during each of the two periods shown in Figures 14 and 15). In Figure 14, data are presented for a period on 9 and 10 October as the ACANIA sailed from ∿130 km offshore to near the coast at Vandenberg (see Figure 1). Note that, under conditions of nearly constant RH, a rapid and sustained increase in total particle concentration was accompanied by a rapid decrease in visibility. On the other hand, data in Figure 15 suggest that a major increase in relative humidity beginning at about 2200 PDT on 7 October was responsible for a decrease in visibility during a period of highly-fluctuating particle concentrations.

In summary, the data show that clear-air visibility fluctuations can be a result of a complex combination of fluctuations in both particle concentration and relative humidity. Sufficient data were not obtained in the current study to allow exact determination of the relative importance of particle size and composition on visibility. However, of the two parameters for which detailed observation are available, data and experience suggest that

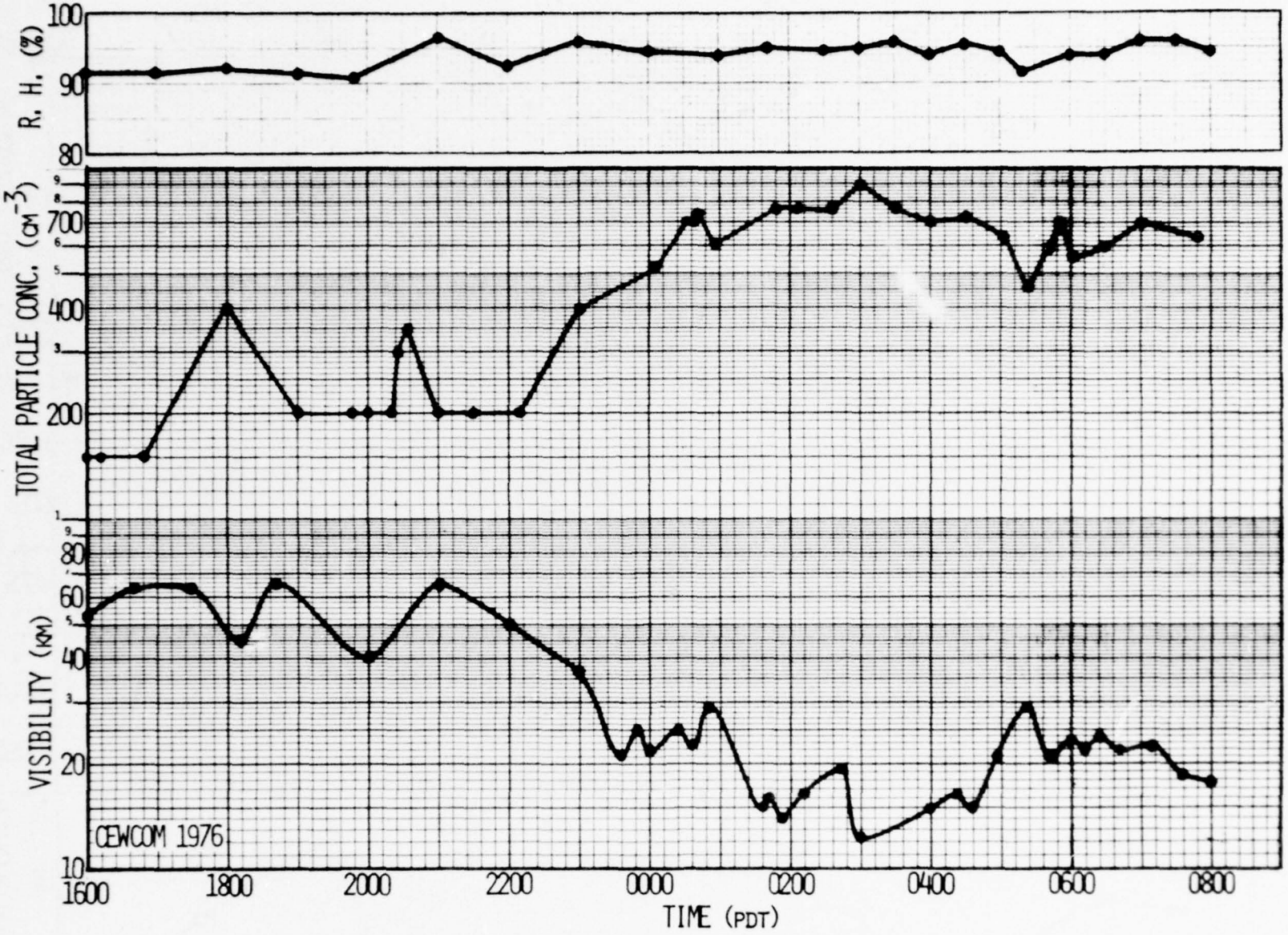

FIGURE 14: "CLEAR AIR" VISIBILITY, TOTAL PARTICLE CONCENTRATION AND RELATIVE HUMIDITY FOR THE PERIOD 1600 TO 0800 PDT, 9-10 OCTOBER 1976

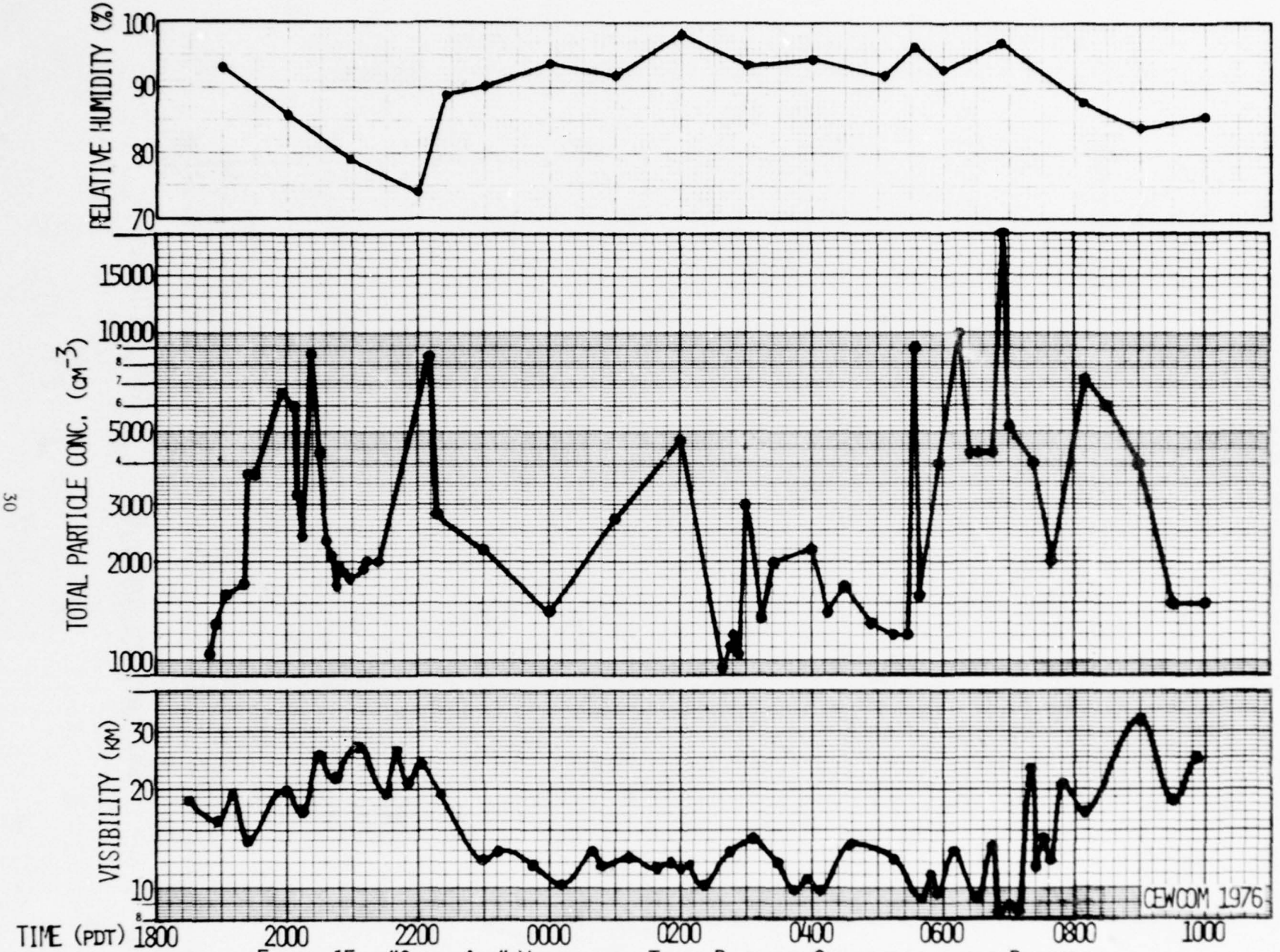

FIGURE 15: "CLEAR AIR" VISIBILITY, TOTAL PARTICLE CONCENTRATION AND RELATIVE HUMIDITY FOR THE PERIOD 1800 TO 1000 PDT, 7-8 OCTOBER 1976

relative humidity is a more conservative parameter than is aerosol concentration, particularly near coastlines. Hence, variations in visibility due to the influence of RH are expected to be more conservative than those due to changes in aerosol concentration. That is, visibility fluctuations due to changes in RH are expected to be long-term, gradual changes while those due to particle concentration can be extremely rapid as illustrated by the data in Figure 15.

2.5 Summary of General Meteorological and Physical Characteristics of the Marine Boundary Layer off Southern California and Elsewhere

During the course of eleven at-sea and four coastal-site field studies conducted since 1970, Calspan has collected a considerable quantity of data describing the aerosol population and other characteristics of the marine boundary layer (Ref. 1-4, 8-15). In earlier studies (Ref. 1-3, 8-10) attention was focused on the physical properties and formation mechanisms of marine fog, and aerosol data were acquired as auxillary-support information. In more recent studies (Ref. 4, 11-15) including the current investigation, the distribution and composition of the aerosol population in the marine boundary-layer have become the primary focus of our at-sea studies. The aerosol-related data acquired during these investigations are summarized in Table 2.

Table 2 provides a synopsis of Calspan data describing the physical characteristics of the marine boundary layer (in the absence of fog) at various locations around the world. These data* include typical values of

*Relative humidity data were acquired with a sling psychrometer and visibility and scattering coefficient were measured with an MRI Integrating Nephelometer. Total aerosol concentration was monitored by a Gardner Small Particle Detector; aerosol concentrations for sizes >0.01 and >0.10 μm by a Thermo Systems Electrical Aerosol Analyzer; concentrations or particles of "dry" sizes >0.025 and >0.075 by a Calspan thermal gradient diffusion chamber; and concentrations of particle sizes >0.3 μm by a Royco Optical Particle Counter.

TABLE 2: AEROSOL-RELATED CHARACTERISTICS OF THE MARINE BOUNDARY

Location	Distance		Ref.	Date	Meteorological Variables		
					RH (%)	Vsby. (km)	Scat. Coeff. (10^{4} m^{-1})
Pacific Coast of Wash.	0.1 km	INLAND	8	Feb 70			
Los Angeles	0.5 km		9	Nov 71			
Vandenberg AFB	1.4 km		9, 10	Sept 71 Jul 72			
Gulf of Mexico — Marine Air	20 km	OFFSHORE	12, 13	Feb 77	67-98	15-80+	0.5-3.0
Gulf of Mexico — Continent. Air	20 km		12, 13	Feb 77	41-76	25-65	0.7-2.5
Nova Scotia	300 km		4	Aug 75			
East Coast, USA	200-400 km		4	Aug 75			
N. Calif., USA	0-15 km		1, 3	Aug 72			
N. Calif., USA	15-150 km		2, 3	Aug-Sept 74			
S. Calif., USA	0-50 km		15	Jul 77	76-98	6-80+	0.7-8.0
East Coast	100-300 km		14	May-Jun 77	65-75	60-80+	0.3-0.8
Nova Scotia	100 km		14	May-Jun 77	67-87	20-80+	0.3-2.2
Mid-Atlantic			14	May-Jun 77	48-77	70-80+	0.23-0.6
SW Coast of Europe	150-500 km		14	May-Jun 77	73-83	30-50	0.9-1.5
SW Coast of Europe	50-150 km		14	May-Jun 77	73-82	17-25	1.9-2.7
SW Coast of Europe	0-50 km		14	May-Jun 77	72-89	16-80	0.6-3.0
Western Mediterr.			14	May-Jun 77	65-80	60-80+	0.55-0.7
Central Mediterr.			14	May-Jun 77	67-73	25-45	1.0-1.9
S. Calif., USA	0-50 km		*	Sept-Oct 76	70-95	5-30	1.5-9.5
S. Calif., USA	50-150 km		*	Sept-Oct 76	70-95	8-60	0.8-6.0
S. Calif., USA	150-500 km		*	Sept-Oct 76	70-95	15-80+	0.55-3.1

*Data From Current Study

LAYER AT VARIOUS LOCATIONS (IN THE ABSENCE OF FOG)

Aerosol Concentrations

(No./cm^3 Larger Than Indicated Diameter)

Total >.0025 μm	CCN (Dry Size) >.025 μm	>0.075 μm	>0.1 μm	>0.3 μm	>0.5 μm	>1.2 μm	>1.4 μm	>3.0 μm
6000	530	230						
6000-20000	800-3000	500-1300						
800-4000	600	200-300						
1300-7000					0.9-3.7		0.1-1.3	.02-.35
2500-8000					1.8-9.0		.15-1.2	.01-.07
400-2000	450	130						
2000-6000	1350	580						
1000-2500	380	180						
600-1200	250	50						
1200-20000			400-5000	20-390		1-50		.007-.21
3000-12000			1300-3500	1.8-12.		0.34-1.4		.03-.18
1500-9000			900-4500	5.4-40		0.7-5.4		.07-.36
<< 200-600			20-110	2.1-9.0		0.6-3.0		.04-.30
700-1300			350-700	13-21		1.4-3.2		.03-.06
1100-3000			800-1000	50-60		4.6-6.1		.07-.21
1500-5000			1000-1600	10-60		2.7-5.7		.07-.21
1500-3000			220-850	6.8-11		1.4-1.7		.06-.10
1300-3500			600-1100	14-27		1.6-2.9		.09-.20
1000-4000	400-2200	90-1000						
400-1000	400-1000	40-250						
< 200-600	100-400	20-170						

relative humidity, visibility and scattering coefficient, and cumulative aerosol concentrations at representative size intervals spanning a range of about three orders of magnitude (i.e., from >0.0025 μm to >3.0 μm). All of the over water data were obtained at heights within 20 m of the sea surface. It should be noted that the data presented were obtained over different time intervals at the different locations. For example, the Transatlantic/ Mediterranean data of May 1977 are ∿24 hour averages, while the remainder of the data are averages over longer periods, i.e., up to four weeks. For this reason, where available, the typical range of fluctuation for each parameter is given rather than an average.

The data show that considerable variations in aerosol-related parameters occur in the marine boundary layer. Temporal variations approach the scale of spatial variations, no doubt reflecting the major influences of wind speed and direction, fetch, sea state, relative humidity and air mass history. Climatologies such as that represented by Table 2 will obviously require repeated observations as functions of meteorological conditions before they can be considered representative.

2.6 Chemical Composition of Boundary Layer Aerosols

During the September-October 1976 cruise, samples of atmospheric aerosols were collected nearly continuously, weather and winds permitting. The samples were obtained, utilizing a hi-vol filter technique, on 10 cm diameter Tissuquartz filters* and subsequently analyzed by standard analytical techniques in Calspan's Chemistry Laboratories. A description of analysis procedures may be found elsewhere (e.g., Ref. 4).

Two samplers were operated simultaneously on the bow platform, as far forward on the ship as possible and at a height of 5 m above the sea surface. A great deal of care was taken to ensure that samples not be contaminated by ship's exhaust and environment or by sea spray; any obviously contaminated samples were discarded. Sampling periods ranged from 1.5 to 9 hrs, and the samplers were operated at a flow rate of $\sim 0.3\ m^3\ min^{-1}$. In toto, data were obtained at 57 sampling sites, 50 of which are designated by circles in Figure 16. Results of the chemical analyses of these samples are tabulated in Appendix B.

*Pallflex Corp., No. 2500 QAO

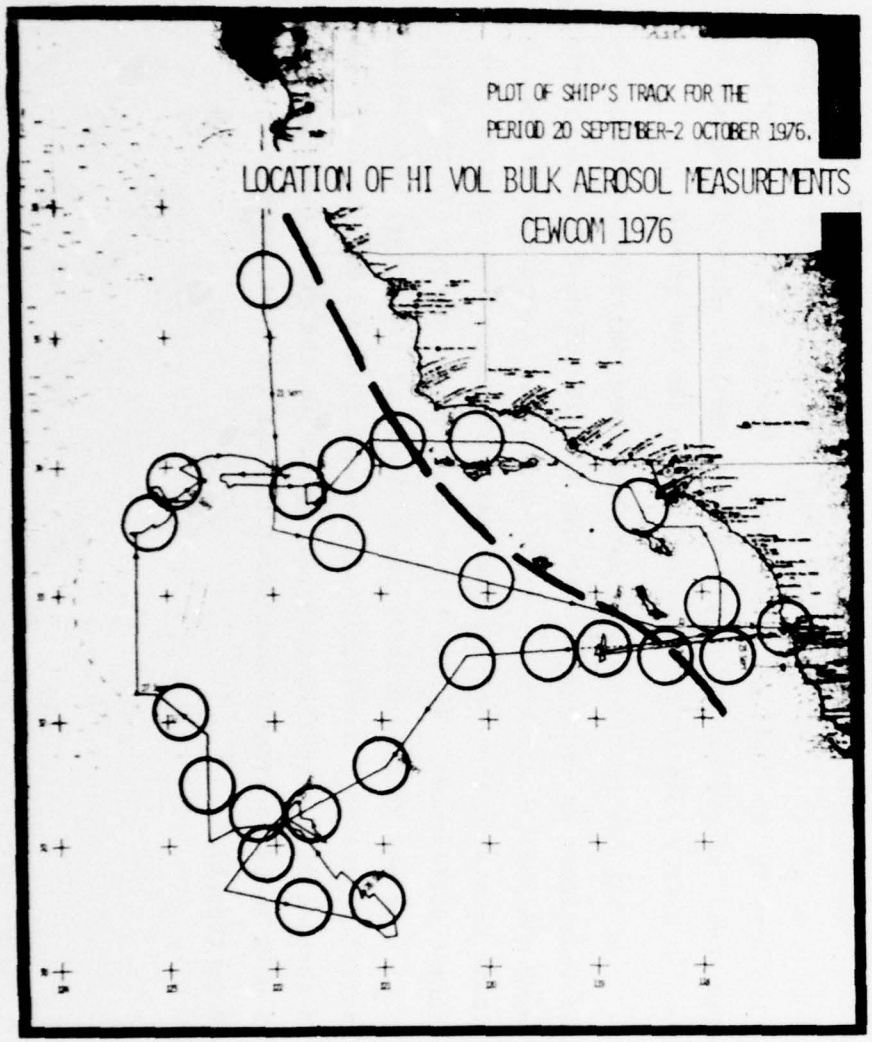

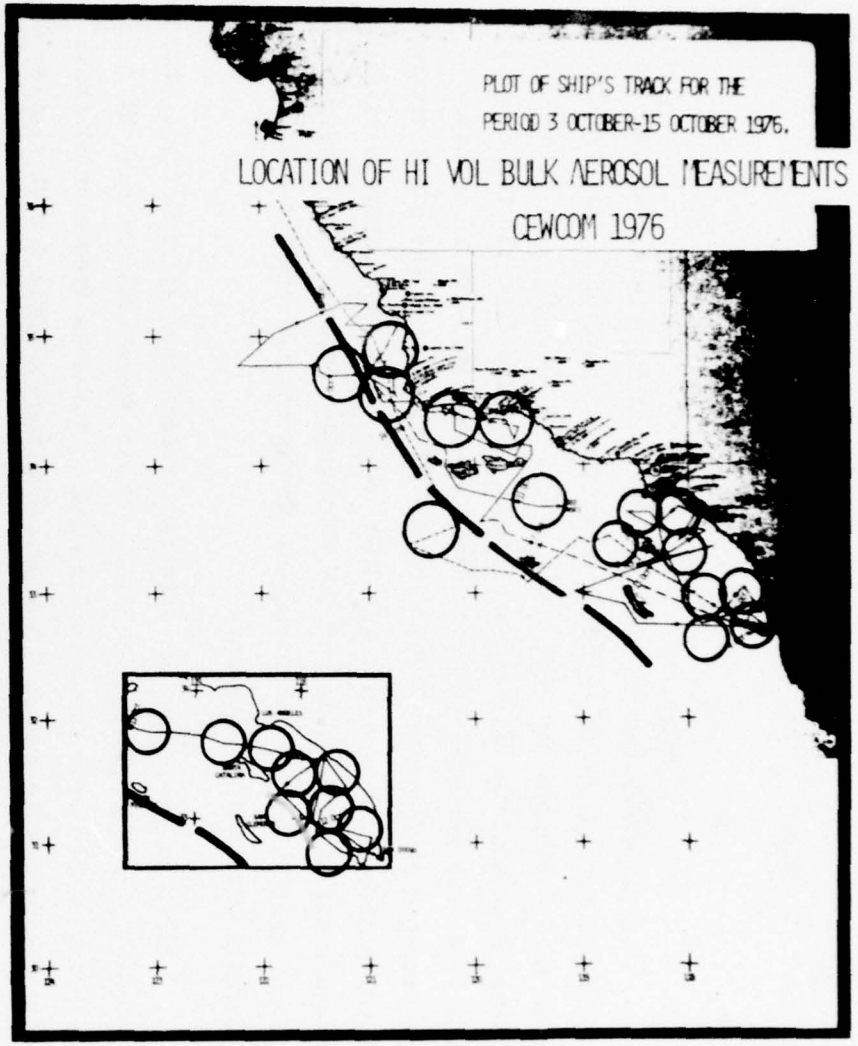

FIGURE 16: LOCATION OF HI-VOL BULK AEROSOL MEASUREMENTS. (HEAVY DASHED LINE SEPARATES "NEAR SHORE" SAMPLES FROM "AT SEA" SAMPLES.)

With a few exceptions due to sampler malfunctions, two samples were obtained at each of the sites indicated in Figure 16. Analytical analyses were performed for SO_4^{--}, Cl^-, NH_4^+, Na, Al, NO_3^-, K, Mg and Ca, and after adjustment for filter background, the data from the two samples at each site were averaged to produce the values tabulated in Appendix B and illustrated in Figures 17-20. Figures 17 to 20 show the areal distribution of selected chemical components (Cl^-, Na, SO_4^{--}, and NH_4^+, respectively) of the ambient air mass aerosols sampled during the cruise. From these data it is obvious that absolute concentrations of the various constituents varied considerably over the cruise area.

Based on geography and attendant meteorological conditions, the data were grouped into two categories: i.e., "near shore" and "at sea" as defined by the heavy dashed line shown in Figure 16. The data from each of these respective groups were averaged and are compared in Table 3 with similar data obtained on a previous cruise off the East Coast (Ref. 4). With respect to the California offshore data, as expected, constituents of presumably continental origin (i.e., SO_4^{--}, NH_4^+, NO_3^-, Ca, Al) were present in greater concentrations in the "near shore" samples. Average Cl^-, concentrations, on the other hand, were greater in the "at sea" samples, while Na, Mg and K were observed in nearly identical concentrations in the two groups.

At the bottom of Table 3, data are shown which were obtained by similar techniques during a cruise to the vicinity of Nova Scotia in which only aged continental air masses were encountered. Comparison of the current West Coast data with those of the previous East Coast study reveals some significant differences. In the highly maritime air masses off the West Coast, Cl^-, Na and Mg (the primary constituents of sea water) were found in substantially greater concentrations than were observed off the East Coast in the absence of a significant marine input. On the other hand, SO_4^{--}, NH_4^+, and Al were found in greater concentrations off the East Coast--i.e., downwind of the continent.

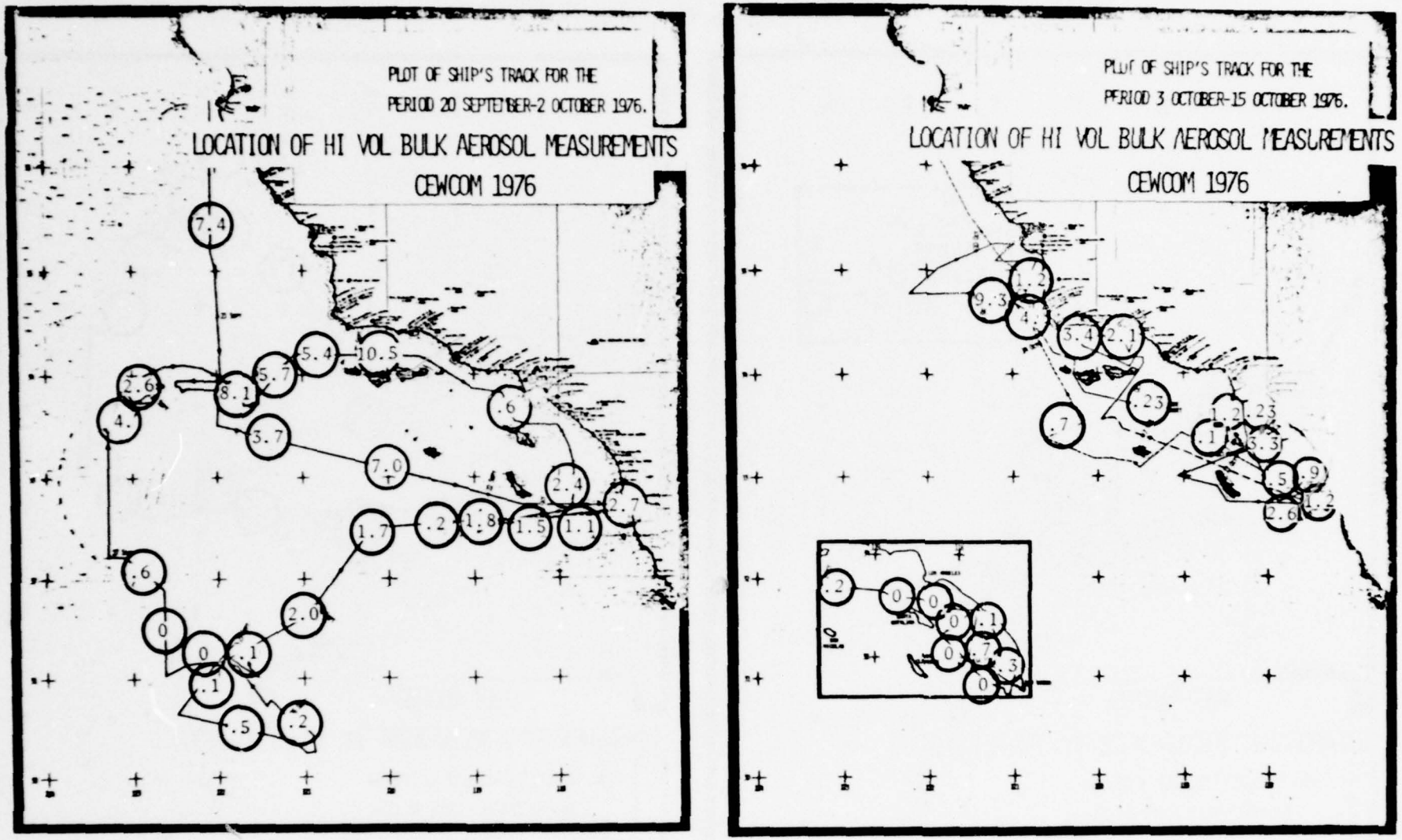

FIGURE 17: ABSOLUTE CONCENTRATION ($\mu G/M^3$) OF CL^- OBTAINED BY HI-VOL AEROSOL SAMPLES AT INDICATED LOCATIONS, OFFSHORE SOUTHERN CALIFORNIA, SEPTEMBER-OCTOBER 1976.

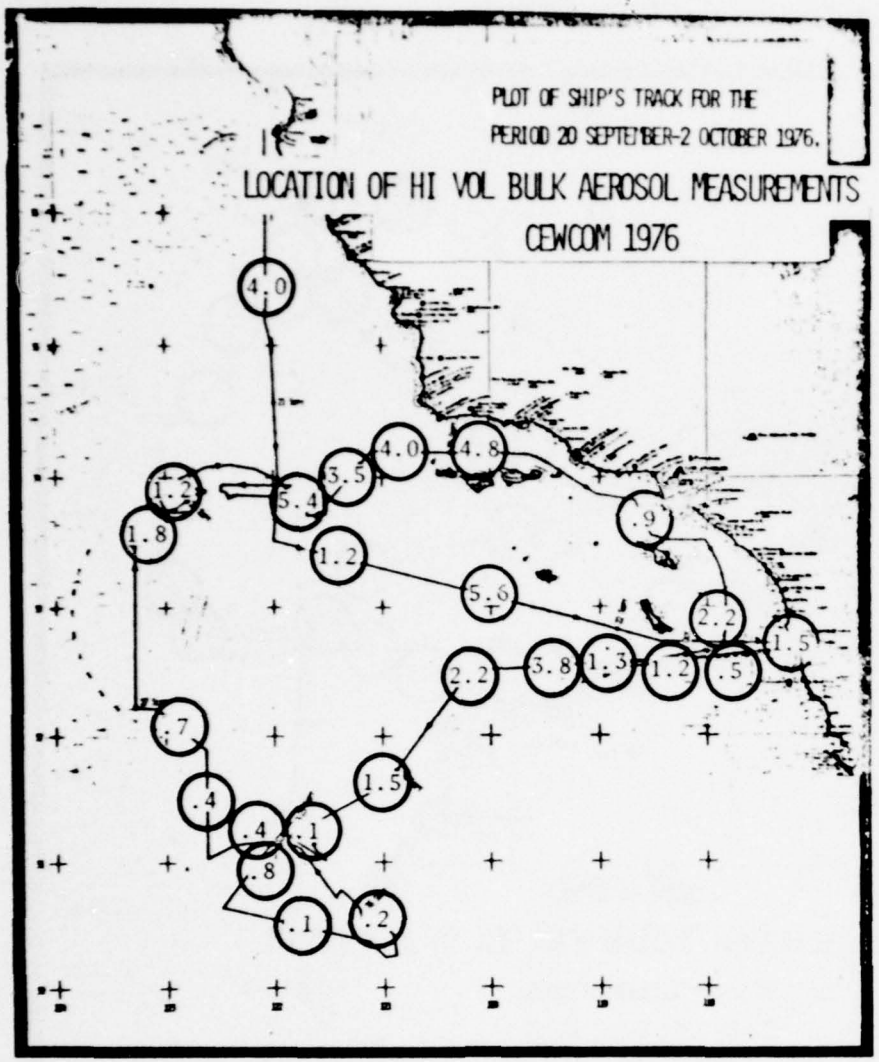

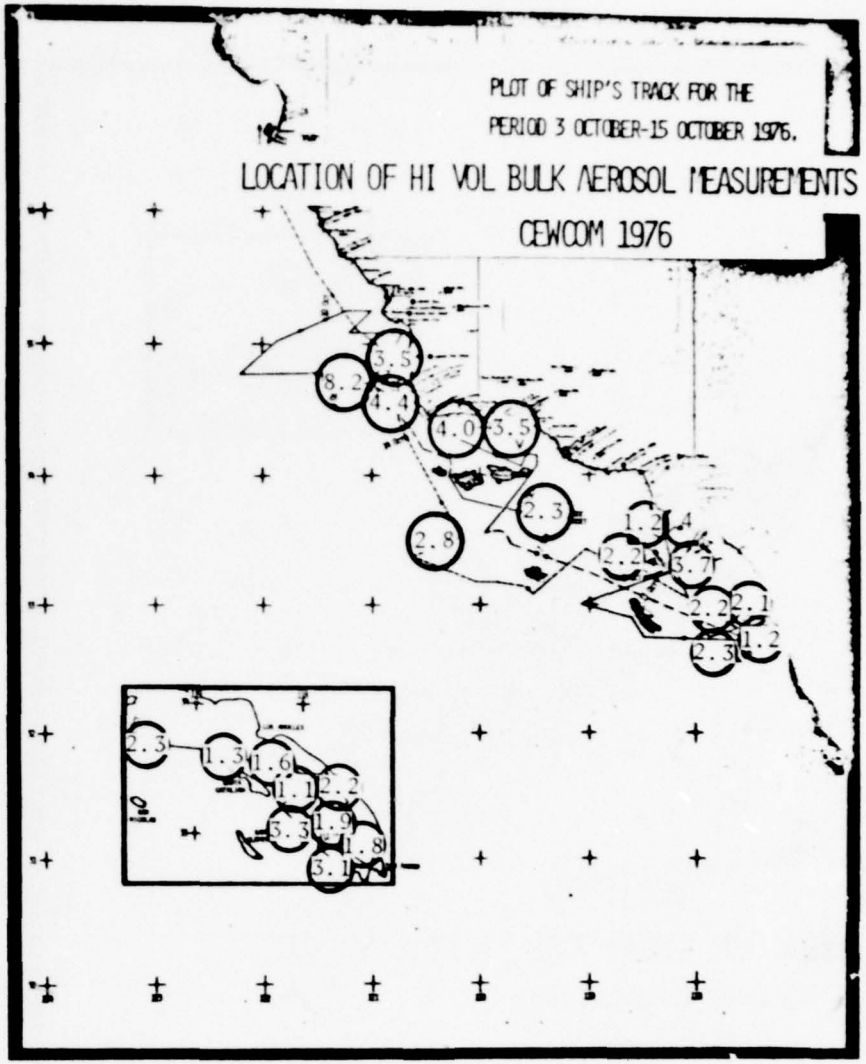

FIGURE 18: ABSOLUTE CONCENTRATION ($\mu G/M^3$) OF NA OBTAINED BY HI-VOL AEROSOL SAMPLES AT INDICATED LOCATIONS, OFFSHORE SOUTHERN CALIFORNIA, SEPTEMBER-OCTOBER 1976.

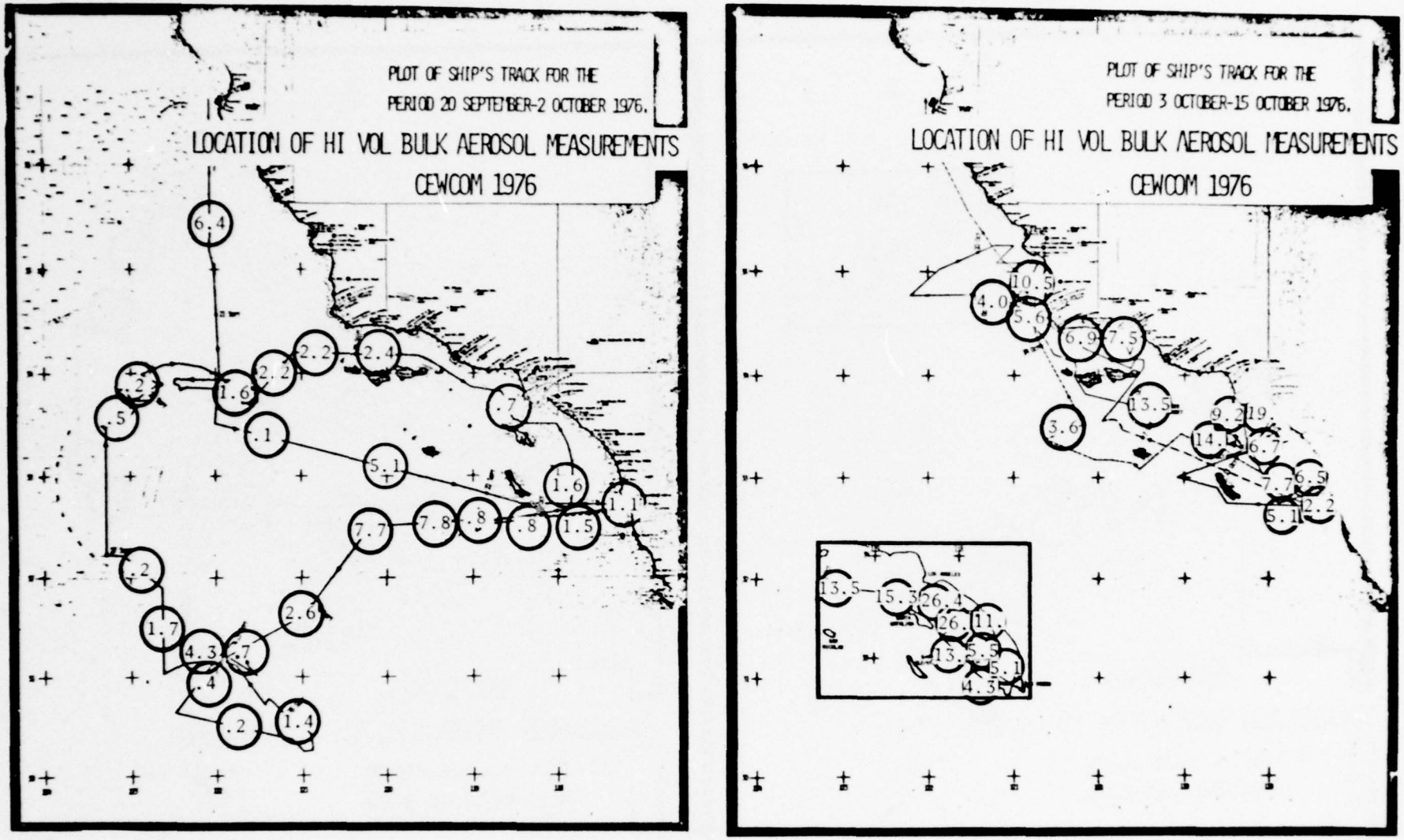

FIGURE 19: ABSOLUTE CONCENTRATION ($\mu G/M^3$) OF SO_4^{--} OBTAINED BY HI-VOL AEROSOL SAMPLES AT INDICATED LOCATIONS, OFFSHORE SOUTHERN CALIFORNIA, SEPTEMBER-OCTOBER 1976.

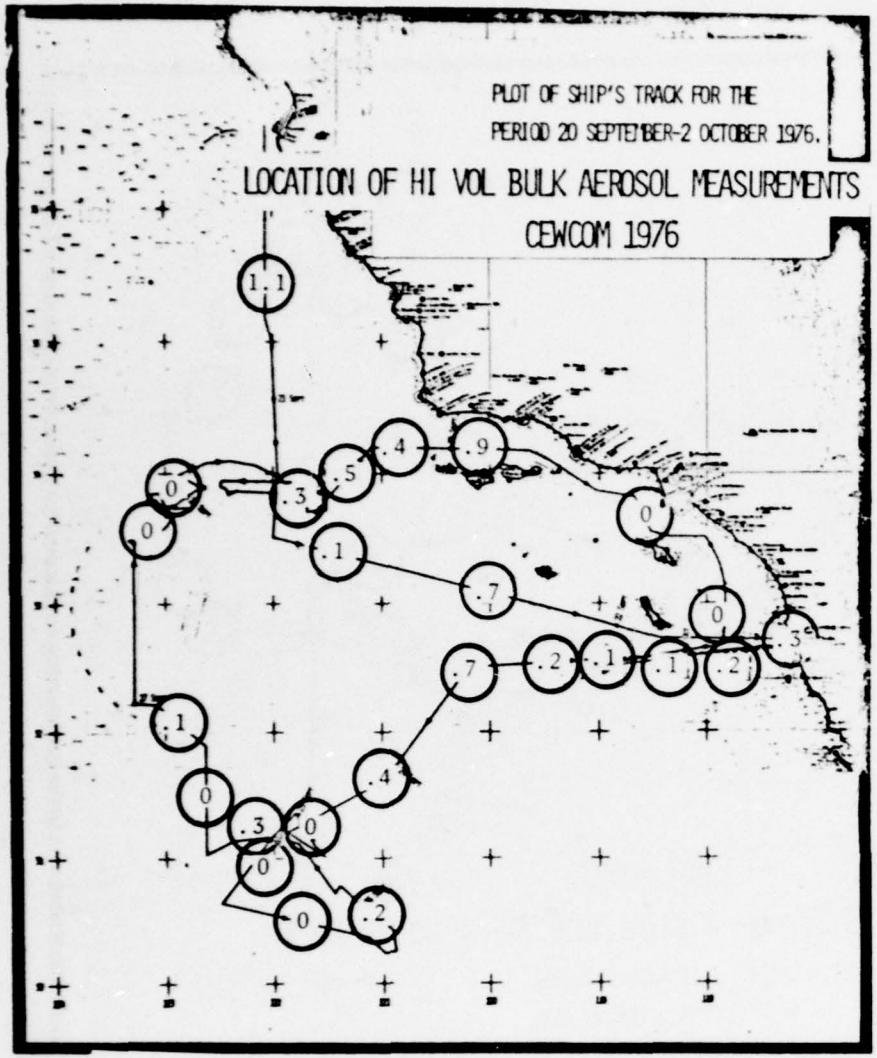

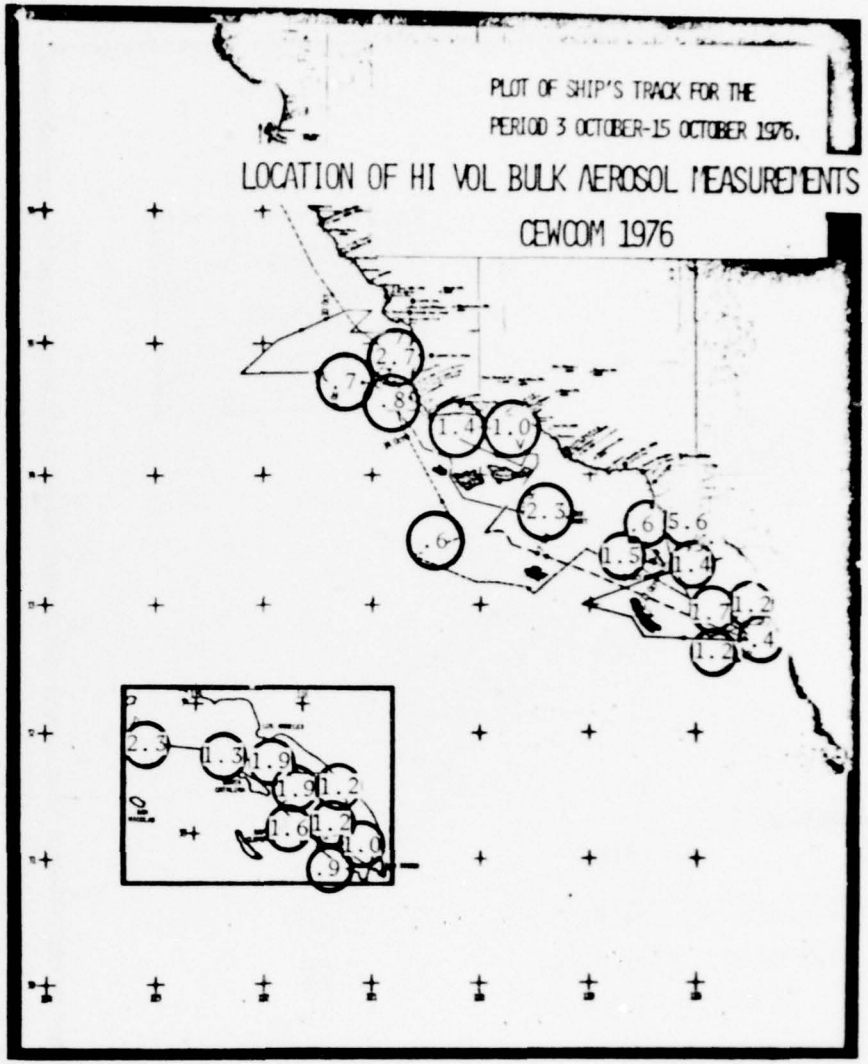

FIGURE 20: ABSOLUTE CONCENTRATION ($\mu G/M^3$) OF NH_4^+ OBTAINED BY HI-VOL AEROSOL SAMPLES AT INDICATED LOCATIONS, OFFSHORE SOUTHERN CALIFORNIA, SEPTEMBER-OCTOBER 1976.

Table 3 Average Concentrations of Selected Constituents of Hi-Vol Aerosol Samples Collected Off the East and West Coasts

Absolute Concentration $\mu g/m^3$

	SO_4^{--}	Cl^-	Na	NH_4^+	K	Mg	Ca	Al	NO_3^-
Sept-Oct 1976									
Southern California "At Sea"	2.5	3.1	2.4	0.3	.14	.30	.08	.004	.42
Southern California "Near Shore"	8.4	1.2	2.1	1.3	.20	.31	.19	.013	.73
August 1975									
Off Coast of Nova Scotia	4.0	< .02	0.9	0.7	.19	.05	.09	.22	
Enroute, off Washington-Boston Coast	14.0	< .02	1.3	2.5	.22	.12	.13	.26	

Additional insight into the overall chemical characteristics of the aerosols observed off Southern California is provided by the Sodium ratios of the various constituents of the aerosols. In Figure 21, measured concentrations of Cl^- are plotted against measured concentrations of Na for each sample. The symbols delineate the "at sea" and "near shore" data, and the solid line represents the sea water value of the Cl^-/Na ratio (1.8). Note that "at sea," Cl^-/Na ratios are grouped about the sea water value, while the "near shore" data suggest either an increase in Na (with respect to Cl^-) or a decrease in Cl^- with respect to Na.

Sodium ratios for all constituents and all samples are tabulated in Appendix B and shown for selected constituents in Figure 22. In Figure 22 the Sodium ratios for Mg, Cl^-, and SO_4^{--} are differentiated with respect to "at sea" and "near shore" data and compared with respective sea water values. The data show that Mg/Na ratios were nearly identical and approximated the sea water value (0.12) in both sample sets, suggesting that Na concentrations of aerosols originating from the sea remained constant over the cruise area. The data in Table 3 show that average Na concentration was the same in the "near shore" and "at sea" sections of the cruise area, implying that a loss of Cl^- with respect to Na occurred in the aerosols existent in the near shore region.

A mechanism whereby the presence of NaCl in solution droplets would cause an increase in the oxidation rate of SO_2 and in the process release chlorine as hydrogen chloride to the atmosphere has been hypothesized (Ref. 19). In support of this hypothesis, gaseous SO_2 would be expected in higher concentrations (on the average) near shore. While SO_2 was not measured during the cruise, SO_4^{--}, (arising from the oxidation of SO_2) was found in the "near shore" samples in average concentrations approximately three times greater than the average of the "at sea" samples (Table 3). Further, data in Figure 22 show that SO_4^{--}/Na ratios were consistently higher than the sea water value in the "near shore" data and occasionally higher in the "at sea" data. When plotted as a function of the Cl^-/Na ratio for each sample, as shown in Figure 23, high SO_4^{--}/Na ratios were found consistently associated with low values of the Cl^-/Na ratio; although low values of Cl^-/Na were not necessarily

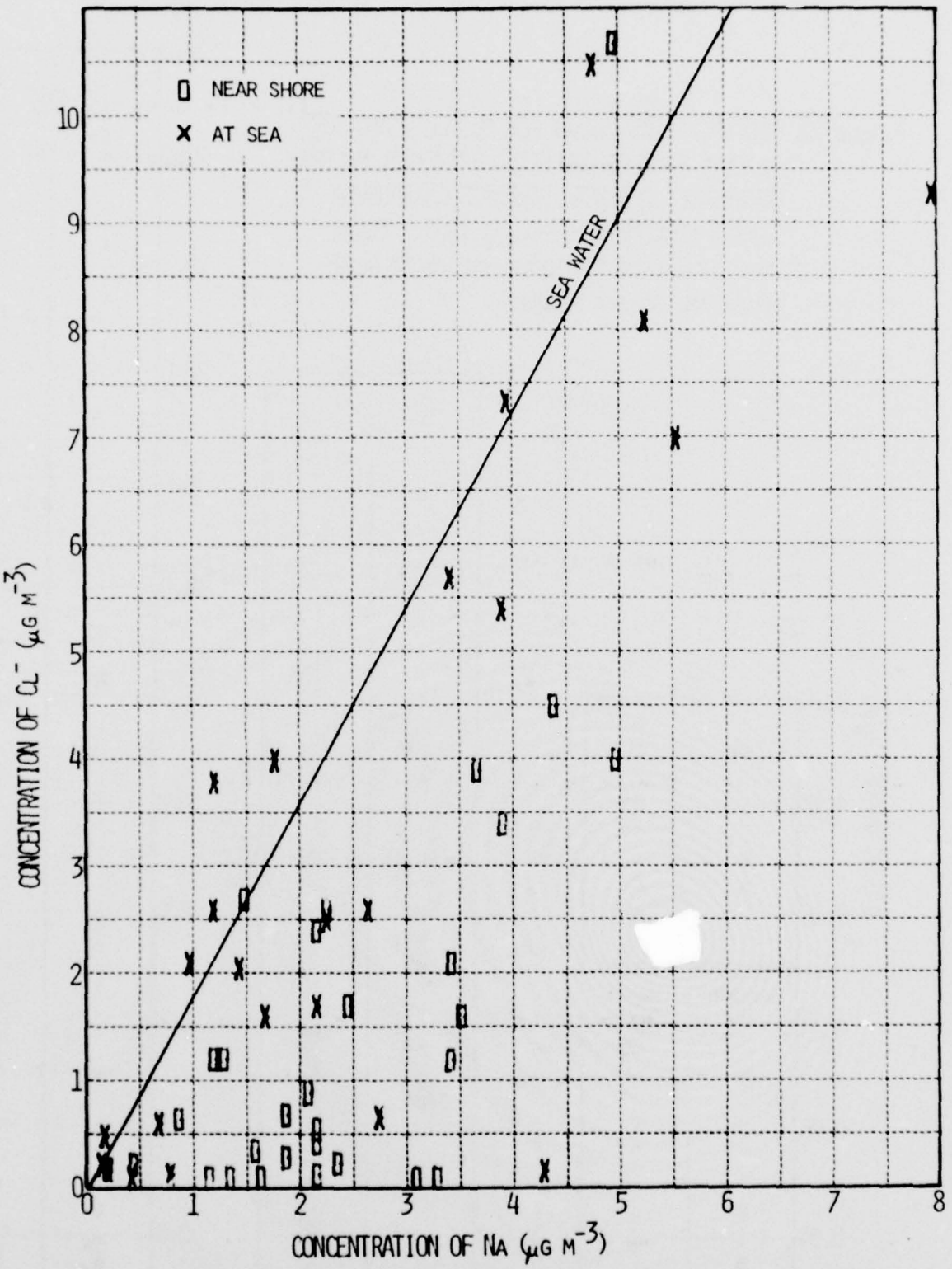

FIGURE 21 CONCENTRATION OF CL^- AS A FUNCTION OF NA IN HI-VOL AEROSOL SAMPLES COLLECTED OFFSHORE SOUTHERN CALIFORNIA DURING CEWCOM, SEPT.- OCT.,1976.

FIGURE 22 SODIUM RATIOS (x/Na) FOR Mg, Cl^-, AND SO_4^{--} AEROSOL SAMPLES COLLECTED BY HI-VOL FILTER TECHNIQUE, OFFSHORE SOUTHERN CALIFORNIA DURING CEWCOM, SEPT.-OCT., 1976. (DATA ARE DIFFERENTIATED WITH RESPECT TO NEAR-SHORE AND AT-SEA SAMPLES.)

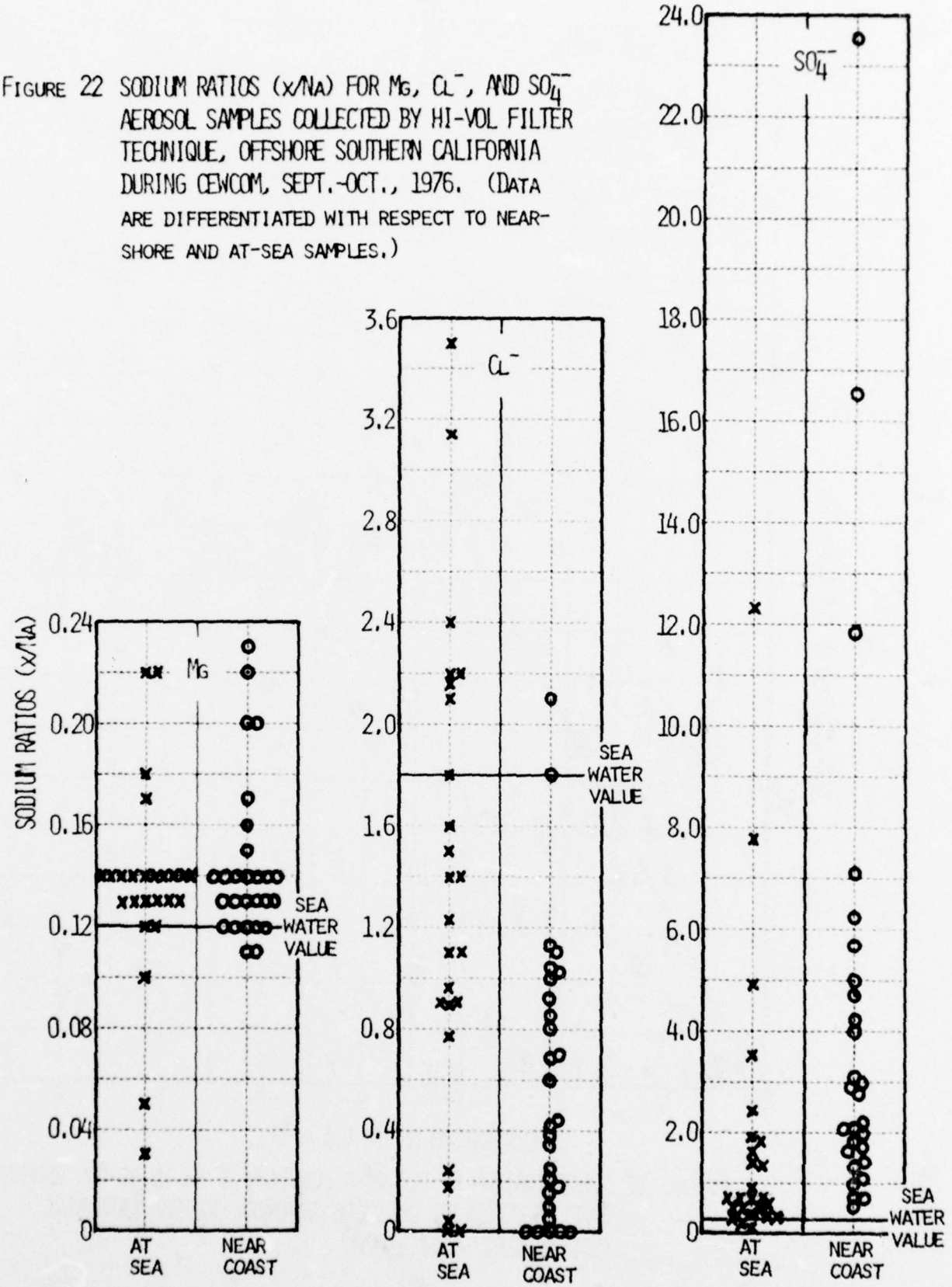

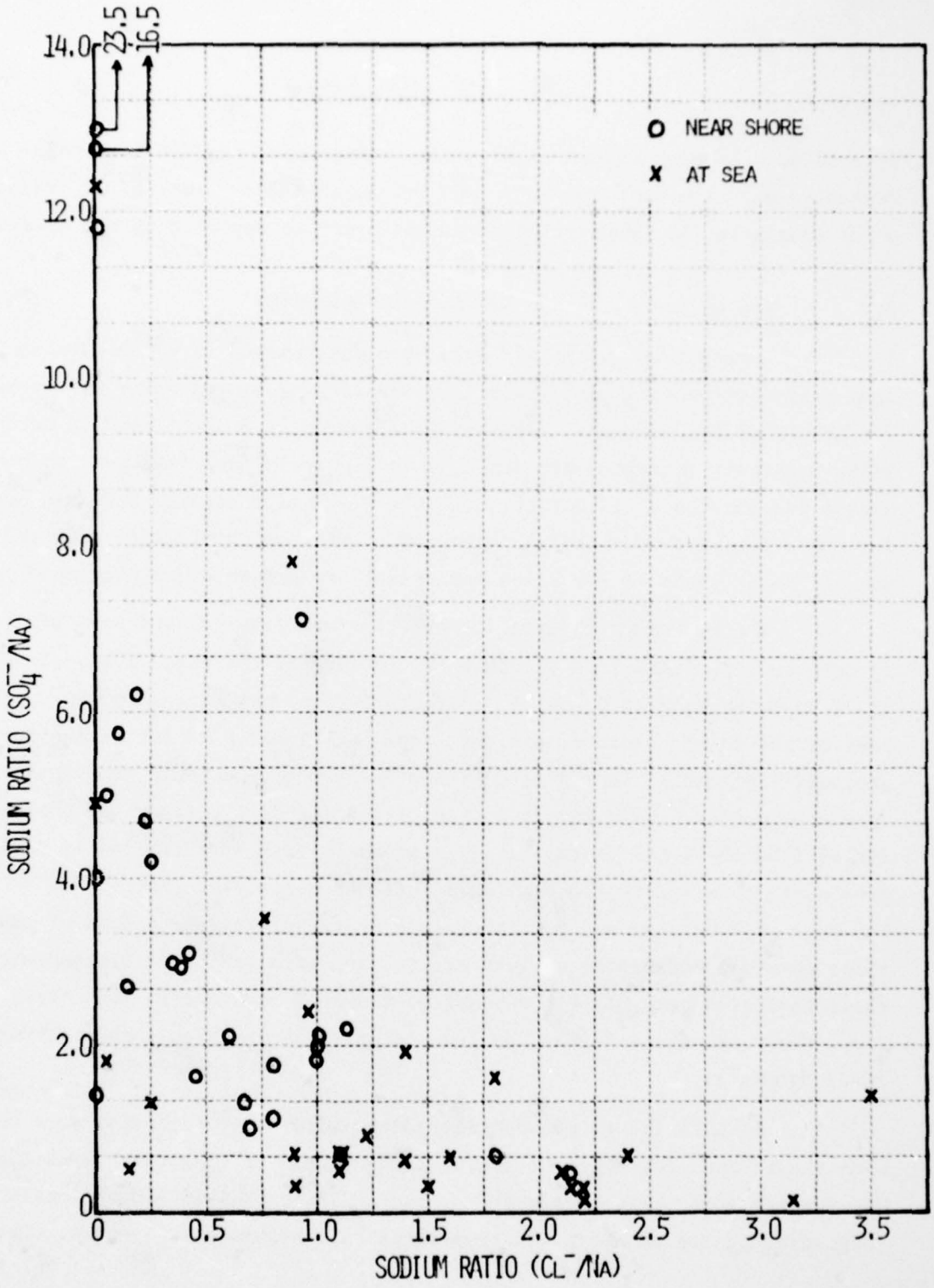

FIGURE 23 PLOT OF SODIUM RATIOS (Cl^-/Na vs. SO_4^{--}/Na) FROM BULK AEROSOL SAMPLES OBTAINED OFFSHORE SOUTHERN CALIFORNIA DURING CEWCOM-1976.

associated with high values of SO_4^{--}/Na. These data suggest that the mechanism may have been operative and responsible for a loss of Cl^- and a major change in the composition of marine aerosols approaching the coast.

2.7 Fog Microphysics and Fog Water Composition

During the cruise, six fogs were encountered in which data including drop size distributions and visibility and samples of fog water were obtained. The fogs were observed on 27-28 September and on 5, 8, 9, 13 and 14 October 1976, and their locations are depicted in Figure 1. All data were reduced, except for the fog of 14 October, and the visibility records and drop spectra for these fogs are provided in Appendix C. Micrometeorological data and a discussion of probable formation mechanisms are presented in Section 3.

The microphysics data for the observed fogs (except that of 14 October) are summarized in Table 4. In some of the fogs (i.e., those of 27-28 September and 13 October), characteristics varied considerably from one area of the fog to another, and data from individual portions of the fogs are averaged separately; in the situation of 8 October, possibly two separate fogs were encountered. With the exception of the fog of 5 October and the second fog of 8 October, the characteristics of these fogs were similar to those previously observed by these authors off the West Coast (Ref. 1-4). The fogs of 5 October and 8 October were observed closest to land of any of those observed during the current cruise, and both exhibited microphysical characteristics more closely resembling those of Nova Scotia fogs (Ref. 4): i.e., they were characterized by low visibilities and high concentrations of small droplets.

In addition to microphysics data, ∿370 ml of fog water were collected with the Calspan Fog Water Collector for analysis of chemical composition. The samples were collected in 5-7 ml increments over 5-15 minute intervals (depending on fog density) and composited into ∿20 ml bulk samples. The

Table 4 Average Microphysics of Fogs Observed off The Coast of Southern California, September-October 1976

Date	Time (PDT)	Mode Radius (μm)	Mean Radius (μm)	Drop Conc. (cm^{-3})	Avg LWC ($g\ m^{-3}$)	Max LWC ($g\ m^{-3}$)	Avg Min VSBY (m)
27 Sept	1200-1655	7.9	8.4	20	.06	.10	300-600
27 Sept	1910-2010	7.9	8.7	22	.10	.18	200
27-28 Sept	2315-0230	6.7	8.5	32	.11	.14	200-300
28 Sept	0430-0830	7.5	8.3	15	.06	.07	300-500
5 Oct	1000-1020	5.0	5.4	135	.13	.14	150
8 Oct	1045-1225	6.5	6.7	65	.11	.16	200
8 Oct	1530-1730	5.5	6.1	175	.21	.30	80
9 Oct	0840-1000	6.7	6.9	15	.03	.04	900
13 Oct	0525-0740	6.6	7.3	65	.17	.35	150
13 Oct	0815-1100	7.0	6.7	25	.04	.09	500-1000

samples were then further combined to produce larger composite samples corresponding to the fog events designated in Table 4. Subsequent analysis at Calspan utilized the same analytical techniques as were used for the hi-vol aerosol samples.

Results of the chemical analysis of the composite fog water samples are presented in Tables 5 and 6. (Only a small quantity of water (insufficient for analysis) was collected in the fog of 5 October; and fog water composition for the fog of 14 October is shown, whereas microphysics data for this fog were not analyzed.) In Table 5, the absolute concentrations of the constituents of the fog water samples are compared with average data from Nova Scotia fogs (Ref. 4). In Table 6, these data are normalized with respect to Na concentration and compared with that of textbook sea water. It is immediately evident from these data that concentrations of the chemical constituents varied considerably from fog to fog; in some fogs exhibiting Na ratios similar to that of sea water and in others more closely resembling those observed in Nova Scotia fogs. In all of the West Coast fogs, the SO_4^{--}/Na ratio was much greater than that of sea water and the Cl^- concentrations were much greater than those observed in Nova Scotia fogs.

Comparison of data presented in Tables 4, 5 and 6 provide some insight into the aerosol responsible for nucleation of these fogs. Applying the liquid water contents observed during the periods in which fog water samples were collected and assuming that the Fog Water Collector collects fog water quantitatively*, the fog water concentration data may be used to estimate airborne concentrations of these constituents. Results of such calculations for fog events in which both microphysics and composition data are available are

*The nominal 50% collection cutoff for the Fog Water Collector is ∿3 μm radius (i.e., fewer than 50% of the droplets smaller than that size are collected). None of the droplets < 1.5 μm radius are collected.

Table 5 Chemical Composition of Fog Water in Fogs Observed Off the Coast of Southern California, September-October 1976

Absolute Concentration (μg/ml)

Date	Time	SO_4^{--}	Cl^-	Na	NO_3^-	NH_4^+	K	Mg	Ca	Al	Si
27 Sept	1212-1537	2.5	13.7	5.8	12.4	< .06	0.48	0.57	0.58	< .1	< .2
27 Sept	1908-2021	3.2	3.8	1.9	2.2	1.33	0.47	0.21	0.42	"	"
27-28 Sept	2316-0244	3.7	3.4	1.8	11.8	< .06	0.41	0.28	0.18	"	"
28 Sept	0429-0803	3.5	4.8	2.3	1.4	< .06	0.55	0.23	0.31	"	"
8 Oct	1112-1226	23.5	43.8	21.7	1.5	10.4	0.90	2.13	2.05	"	"
8 Oct	1530-1720	13.6	16.7	6.9	11.0	9.2	0.46	0.83	1.01	"	"
13 Oct	0250-0800	15.8	12.7	9.1	14.5	6.2	1.0	1.15	2.62	"	"
14 Oct	0300-1030	10.7	16.0	10.6	1.6	.85	0.33	1.18	1.61	"	"
Average		9.6	14.4	7.5	7.1	3.5	0.58	0.82	1.10	"	"
Nova Scotia Fogs		12.0	3.1	24.	-	0.6	1.8	1.2	0.9	< .1	-

Table 6 Sodium Ratios (X/Na) for Constituents of Fog Water Obtained Off Coast of Southern California, September-October 1976

Date	Time	SO_4^{--}	Cl^-	NO_3^-	NH_4^+	K	Mg	Ca
27 Sept	1212-1537	.4	2.4	2.1	-	.08	.10	.10
27 Sept	1908-2021	1.7	2.1	1.1	0.67	.25	.12	.23
27-28 Sept	2316-0244	2.1	1.9	6.6	-	.23	.15	.10
28 Sept	0429-0803	1.5	2.1	0.6	-	.24	.10	.13
8 Oct	1112-1226	1.1	2.0	0.1	0.48	.04	.10	.09
8 Oct	1530-1720	1.9	2.4	1.6	1.33	.07	.12	.15
13 Oct	0250-0800	1.7	1.4	1.6	0.68	.11	.13	.29
14 Oct	0300-1030	1.0	1.5	0.2	0.1	.03	.11	.15
Average		1.4	2.0	1.7	-	.13	.12	.16
Sea Water		0.2	1.8	---<10^{-6}---		.04	.12	.04
Nova Scotia Fogs		0.5	0.1	-	.03	.08	.05	.04

presented in Table 7. Comparison of these computed values with average data presented in Table 3 and those of individual samples in Appendix B suggests that the fog "scavenged" or was nucleated by approximately 1/3 to 1/2 of the available aerosol mass containing these constituents. Further, these calculations show that, in each of the two fogs (27-28 September and 8 October) which could be partitioned due to differences in the physical features of respective portions of the fog, the absolute chemical characteristics (i.e., airborne concentrations of various chemical constituents) remained relatively uniform throughout a given fog. Similar results have been obtained previously by these authors (Ref. 2-4).

The chemical composition of fog water collected off the West Coast during September-October 1976 may be summarized as follows: (1) sulfate, ammonium and calcium were highest in the fogs observed closest to land as was the case for Nova Scotia fogs; (2) average sulfate, calcium and magnesium concentrations were comparable off both coasts; (3) chloride and ammonium concentrations were considerably higher off the West Coast while sodium concentrations were highest off the East Coast; (4) aluminum and silicates were below minimum detectable levels in fog water at both locations; (5) the sodium ratios suggest that the constituents of fog water off the West Coast were primarily of sea salt origin, but a major contribution by SO_2 oxidation products was also found; (6) concentrations of SO_4^{--}, Cl^-, Na, NH_4^+, K, and Ca incorporated in fog drops were, on the average, a factor of 2-3 lower than the total airborne concentration measured by the hi-vol technique.

Table 7 Calculated Airborne Concentrations of Chemical Constituents of Fog Water, West Coast, September-October 1976

($\mu g/m^3$ of air)

Date	Time	SO_4^{--}	Cl^-	Na	NO_3^-	NH_4^+	K	Mg	Ca
27 Sept	1212-1537	0.15	0.85	0.36	0.77	-	.03	.04	.04
27 Sept	1908-2021	0.31	0.37	0.19	0.22	0.13	.05	.02	.04
27-28 Sept	2316-0244	0.40	0.37	0.19	1.27	-	.04	.03	.02
28 Sept	0429-0803	0.20	0.28	0.13	0.08	-	.03	.01	.02
8 Oct	1112-1226	2.49	4.64	2.30	0.16	1.10	.09	.23	.22
8 Oct	1530-1720	2.80	3.44	1.42	2.27	1.90	.09	.17	.21
13 Oct	0250-0800	2.04	1.64	1.17	1.87	.80	.13	.15	.34
Average		1.20	1.66	0.82	0.95	.98	.066	.093	.13

Section 3

CASE STUDIES OF FOG OCCURRENCE OFF THE COAST OF SOUTHERN CALIFORNIA DURING SEPTEMBER-OCTOBER 1976

A secondary objective of the CEWCOM-76 cruise off the coast of Southern California was to continue our studies (Ref. 1-4) of the microphysical and micrometeorological properties of marine fog. During the cruise, fogs were encountered on 27-28 September and 5, 8, 9, 13, and 14 October at locations shown on the charts in Figure 1. In the fogs, continuous observations of visibility, sea surface temperature, air temperature and dew point were recorded. In addition, frequent measurements of drop size distributions, wet and dry bulb temperatures and winds were obtained along with collections of fog water samples (for chemical analysis). The visibility, temperature and drop spectra records for each of these fogs (except for the fog of 14 October) are provided in Appendix C; fog microphysics and analysis of fog water samples were discussed in Section 2.7. In this section, pertinent meteorological features of three of these fogs are discussed.

3.1 The Fog Event of 27-28 September 1976

The fog of 27-28 September was initially encountered at mid-day over the open ocean approximately 300 km from land. First observed as patchy/light fog at ~1150 PDT 27 September during a frontal passage, the fog persisted for approximately 20 hours. Fig. 24 shows a satellite photograph of the area at 0915 and the position of ACANIA at 0900, just prior to the frontal passage. The cold front with which the fog was associated was oriented north-south along the 124 W meridian, and a second cold front which moved through during the 28th may be seen along the 131 W meridian. The track of ACANIA, periods of reduced visibility, and wind observations obtained during the event are shown in Fig. 25. The visibility, air temperature, and droplet data for this fog may be found in Figures C-1, C-2, and C-3 in Appendix C.

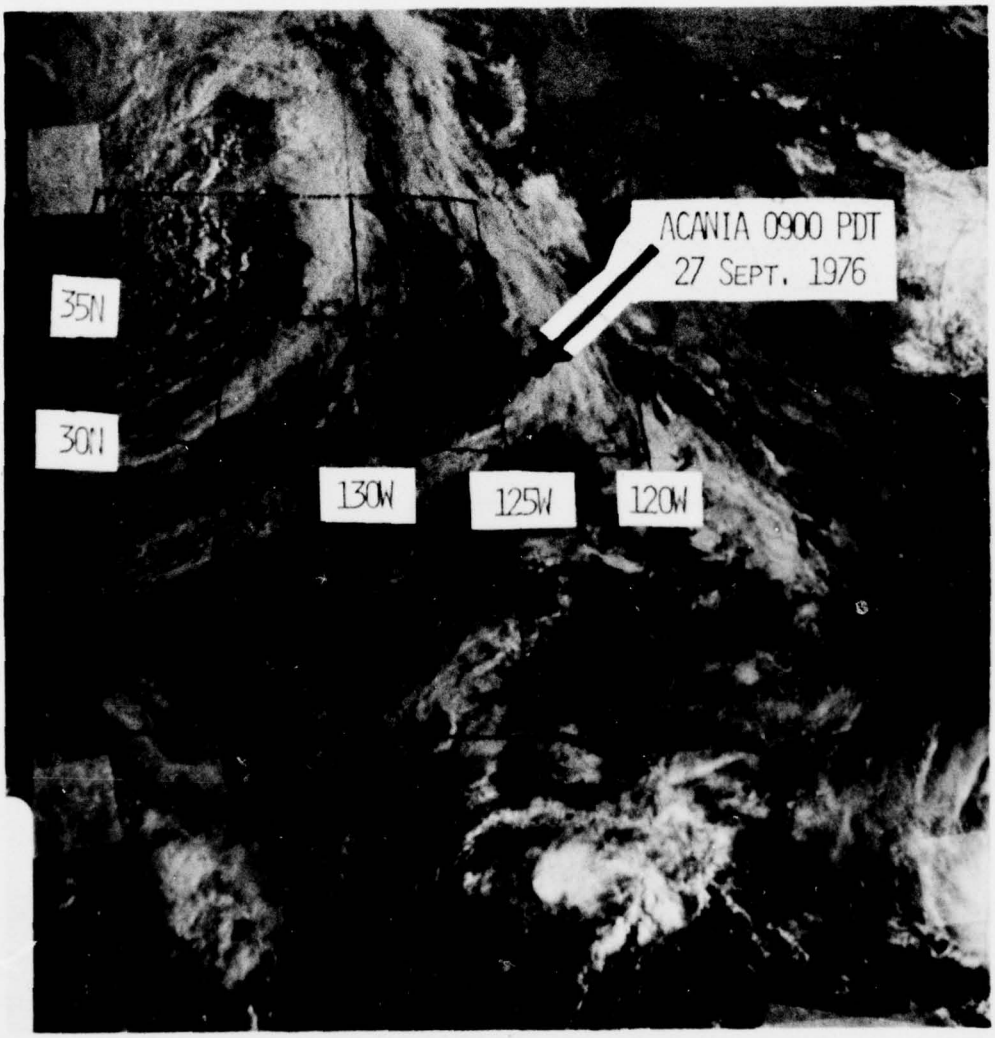

FIGURE 24 SATELLITE PHOTOGRAPH FOR 0915PDT 27 SEPTEMBER 1976
SHOWING LOCATION OF ACANIA . CEWCOM 1976

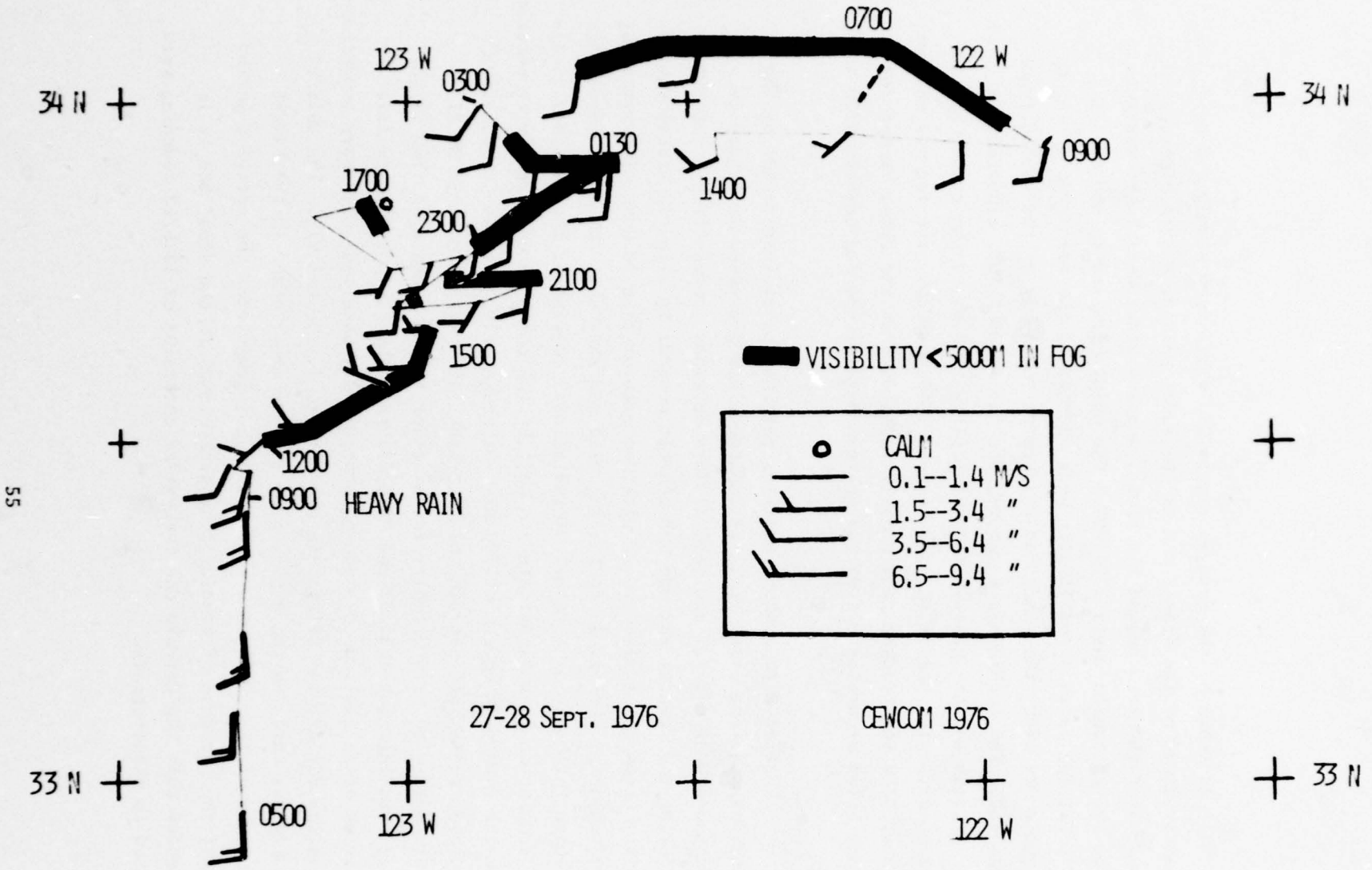

FIGURE 25 SHIP'S TRACK, WINDS AND FOG EPISODES FOR 27-28 SEPTEMBER 1976.

As shown by the data in Figure 25, winds were strong (∿8 m/sec) southerly ahead of the front, and as the front passed, ACANIA experienced a heavy rain shower. Behind the front, surface winds were light westerly during the afternoon until 1700 PDT. The ACANIA cruised in and out of individual fog patches and finally west and out of the main area of fog by 1715 PDT. By 1800, the winds had shifted to southerly as the second front approached. The ACANIA again entered the fog at 1900 PDT, experiencing heavy drizzle and the densest fog (visibility ∿150 m) of the entire episode. After an excursion out of the fog between 2030 and 2300, the fog was entered again at 2300 and tracked continuously until 0900 on the 28th, except for another brief excursion out of the western edge of the fog between 0230 and 0430.

Vertical temperature profiles obtained by radiosonde during the frontal passage/fog event of 27-28 September are presented in Figure 26. The soundings of 0445/27 and 1300/27 were obtained, respectively, prior to and during the frontal passage and exhibit neutral to slightly stable characteristics from the surface to an altitude greater than 2000 m. The remaining three soundings were taken in the fog area and show that low-level inversions developed, probably as a result of radiational cooling of the fog (Ref. 1-4). This conclusion is substantiated in part by the observation that air temperature above the inversion (e.g., at 800 m) remained nearly constant for the five soundings, while just beneath the inversion (at a height of ∿350 m) air temperatures were ∿1.5°C cooler in the three in-fog soundings. Two of the in-fog soundings (at 1620/27 and 0442/28) show the base of the low-level inversion at an altitude of < 400 m, a previously observed necessary condition for marine fog off the California coast (Ref. 3, 20, and 21). The 1915/27 sounding was taken during a period of intense drizzle and in the lowest visibility of the fog event. Satellite photographs for the specific period suggest the presence of cumulus congestus clouds in the area, and it is suspected that the drizzle and the raised inversion of 1915/27 sounding were related to these clouds.

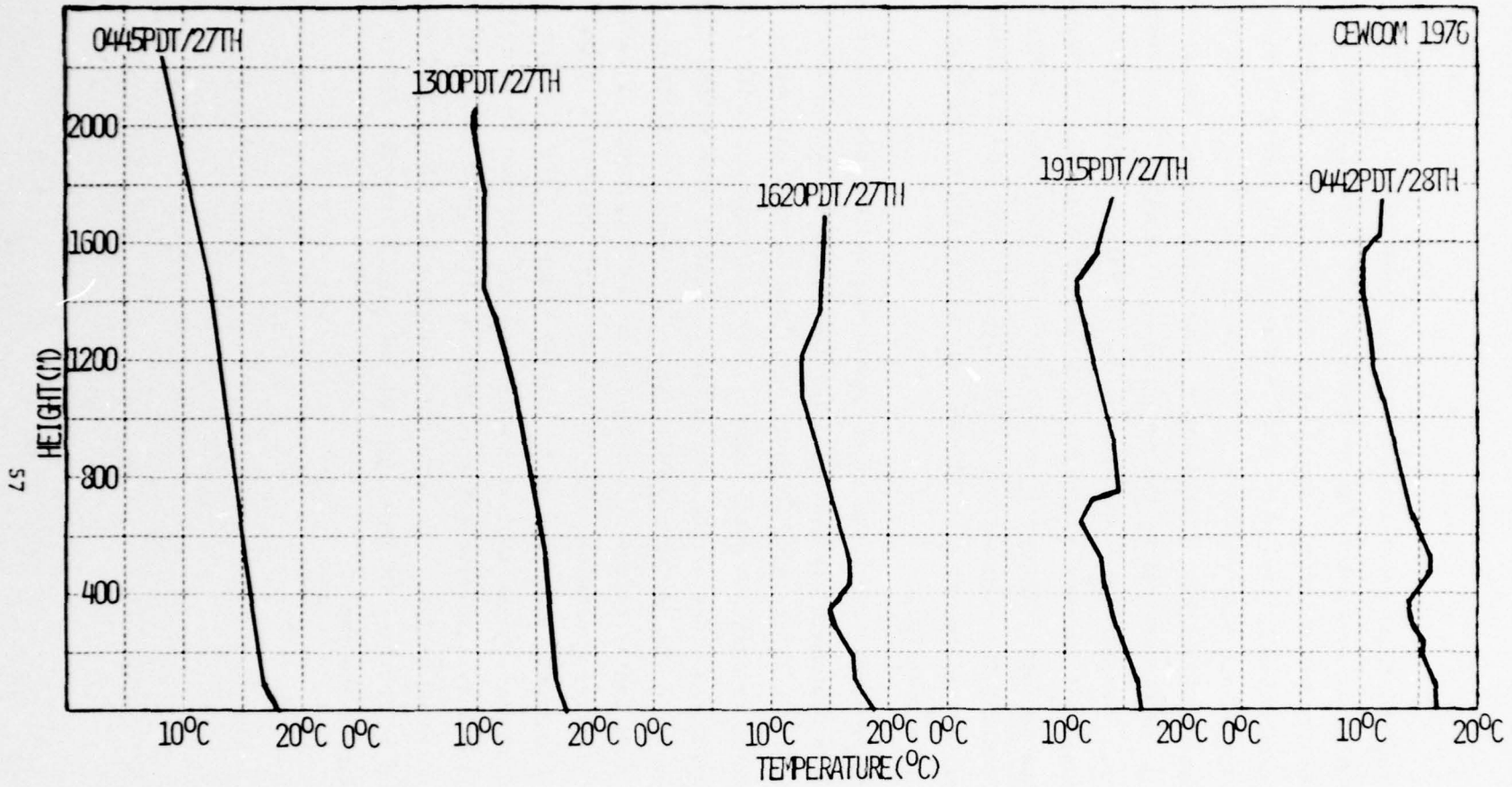

FIGURE 26 VERTICAL TEMPERATURE PROFILES FOR FOG EPISODES OF 27-28 SEPTEMBER 1976.

During the final penetration of the fog from 0400 to 0900 PDT, a period (0505-0630) of less dense fog characterized by high-frequency fluctuations in visibility was observed. As shown by the visibility record in Figure 27, minimum visibilities were ∿1500 m during the period 0505-0630 compared to ∿450 m both east and west of that portion of the fog. In the region of improved visibility, liquid water content and droplet concentrations were reduced to levels preventing the acquisition of statistically meaningful droplet spectra. Sea surface temperature and wind data, provided in Figure 27, show that the area of improved visibility was located downwind of a local warm spot in the sea surface. Apparently heating by the warmer water reduced the liquid water content (by evaporation) of the fog and increased the turbulence intensity (Ref. 22) giving rise to improved visibility and to the high frequency fluctuations in visibility.

Briefly summarizing, the exact mechanisms responsible for triggering the fog of 27-28 September are unknown. The fog developed behind a weak cold front and persisted for at least 20 hours after the initial encounter. Patchy at first, the fog intensified after sunset. Air temperatures in the fog were everywhere cooler than that of the sea surface, becoming even colder during nocturnal hours. In the presence of the fog, a low-level inversion was established--once again indicating the influence and importance of radiative cooling on marine fog processes. Due to a wind shift ahead of a second, approaching cold front, a portion of the latter stages of the fog was advected over water ∿0.5C warmer than that with which the fog had been in equilibrium. Increased instability gave rise to an increase in turbulence intensity which, along with increased heating, was apparently responsible for partial dissipation of the fog and an increase in general levels of visibility from 400 to 1500 m in that portion of the fog.

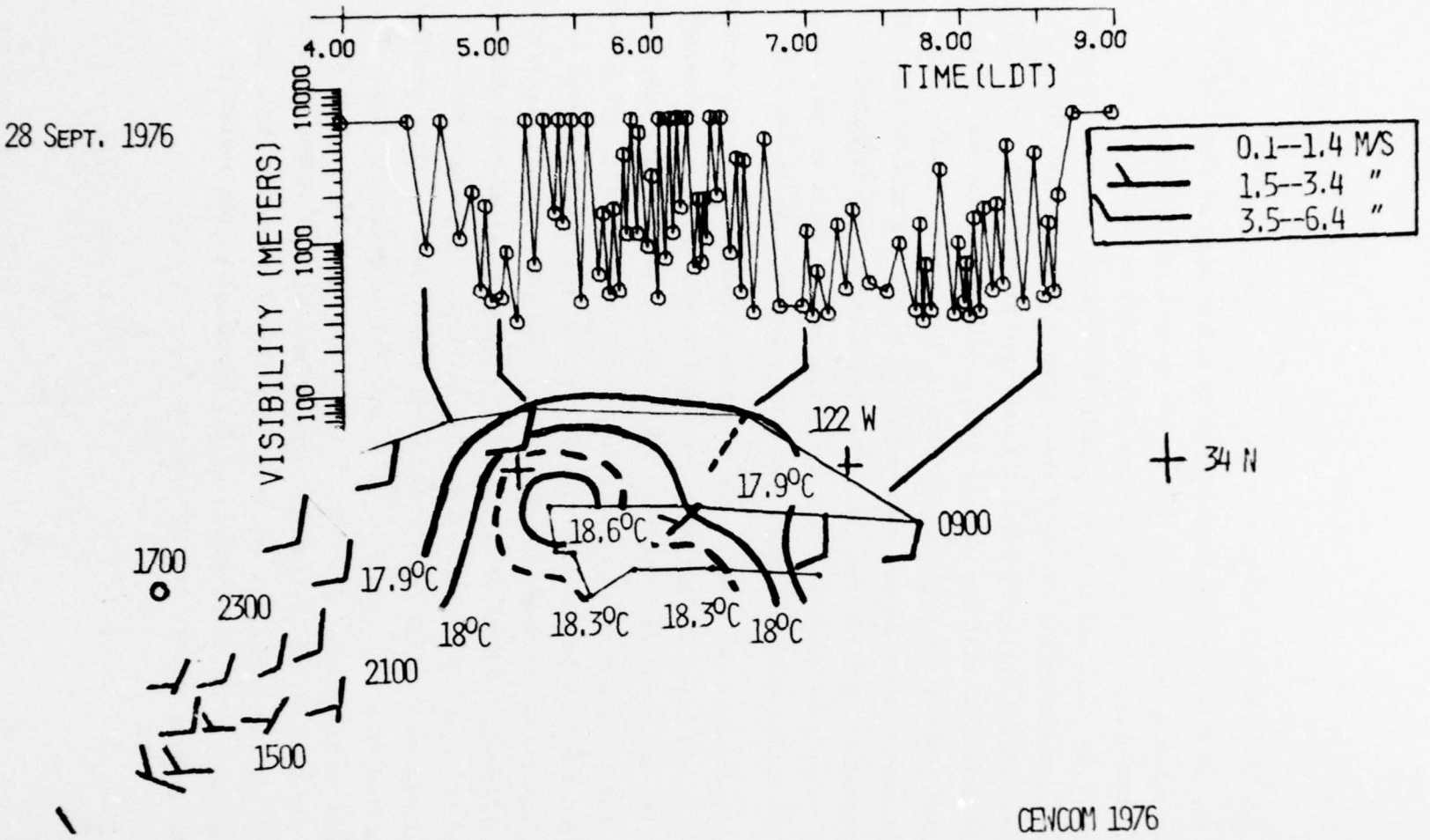

FIGURE 27 SEA SURFACE ISOTHERMS, WINDS AND VISIBILITY FOR FOG WHICH PASSED OVER WARM WATER PATCH.

3.2 The Fog of 9 October 1976

The fog of 9 October was encountered at mid-morning as the ACANIA was steaming westward along 35 N near 122 W, ~85 km west of Vandenberg. The visibility, air temperature and drop spectra records for this fog are provided in Figures C-10, C-11 and C-12 in Appendix C. The air temperature data for a 43 km long portion of the westward track (see Figure 1), including the ~20 km wide fog (surface visibility restriction), are presented in Figure 28. The temperature data show that the air was always colder than the sea surface and that a lapsed temperature profile persisted at low levels throughout the event, with the most intense lapse rate occurring in the fog at 0900 PDT. Radiosonde data obtained at 1011 PDT show that the lapsed conditions extended to the base of an inversion (and hence fog top) at an altitude of 260 m at that time. Winds during the entire westward track were north-northwesterly at 7-9 m sec^{-1}.

Figure 29 shows the time series of visual cloud observations, surface-level visibility, and inversion height as measured by the NPS acoustic sounder (Ref. 23) for the fog event of 9 October. The acoustic sounder data show that the height of the inversion base gradually increased from 100 m to ~275 m above the surface from the east to the west side of the fog; whether the change in height of the inversion was temporal or spatial is unknown. Visual observations indicate the following sequence of events under previously cloud-free conditions: stratus formed aloft at between 0730-0740 PDT, thickened to produce fog and initial visibility restriction (vsby < 6000 m) at the surface by 0810, gradually thinned and lifted from the surface by 1228, and went to broken by 1255. The air temperature record (Figure 28) shows that cooling occurred first at the upper levels (18.5 m) of the instrument tower, beginning at ~0755, 15 minutes before the visibility restriction was measured at the 5 m level. Thus, these data fully support earlier observations of fog formation by the radiative cooling and thickening stratus clouds (Ref. 1).

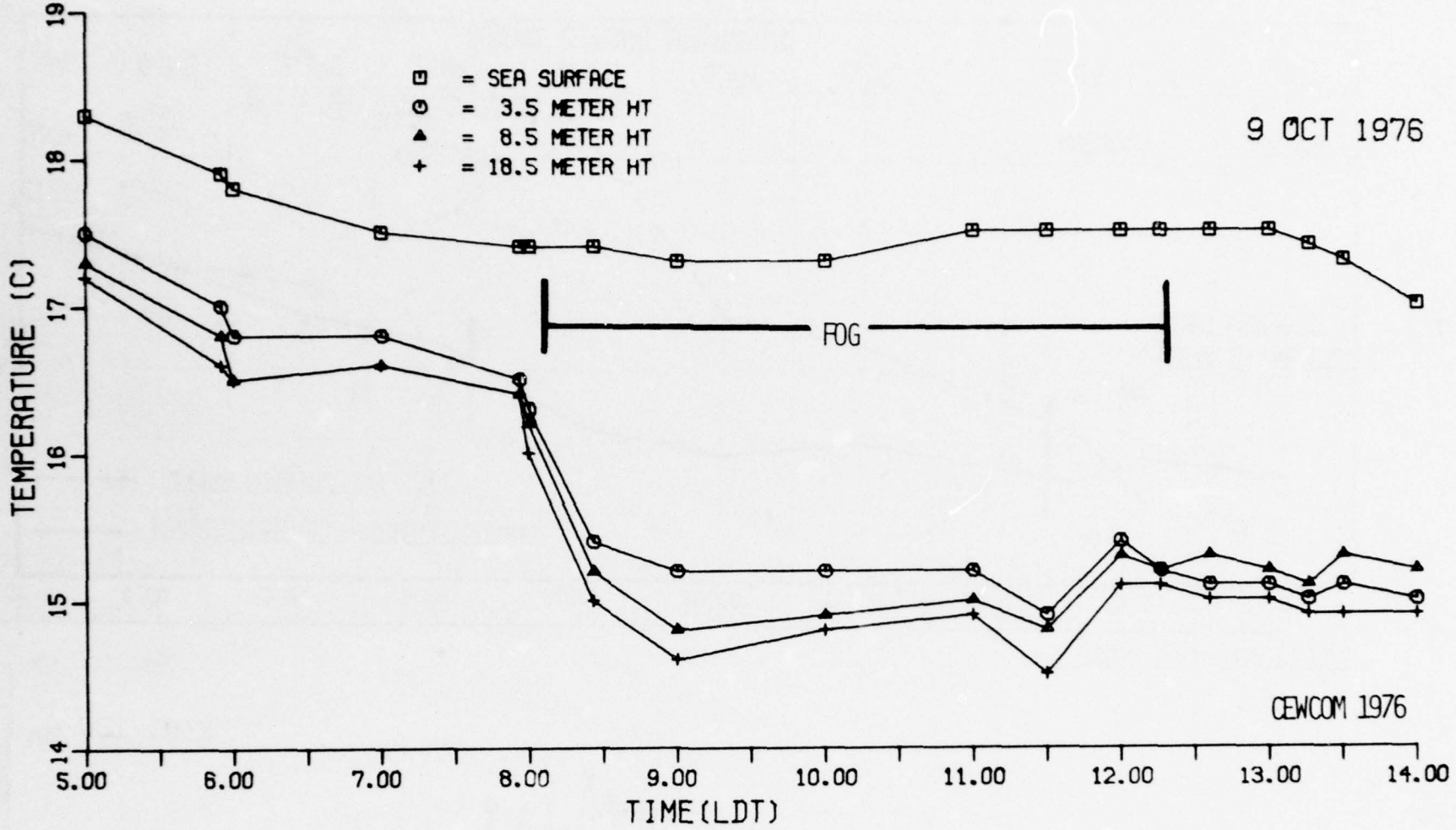

FIGURE 28 SEA SURFACE TEMPERATURE AND AIR TEMPERATURES FOR FOG OF 9 OCTOBER 1976

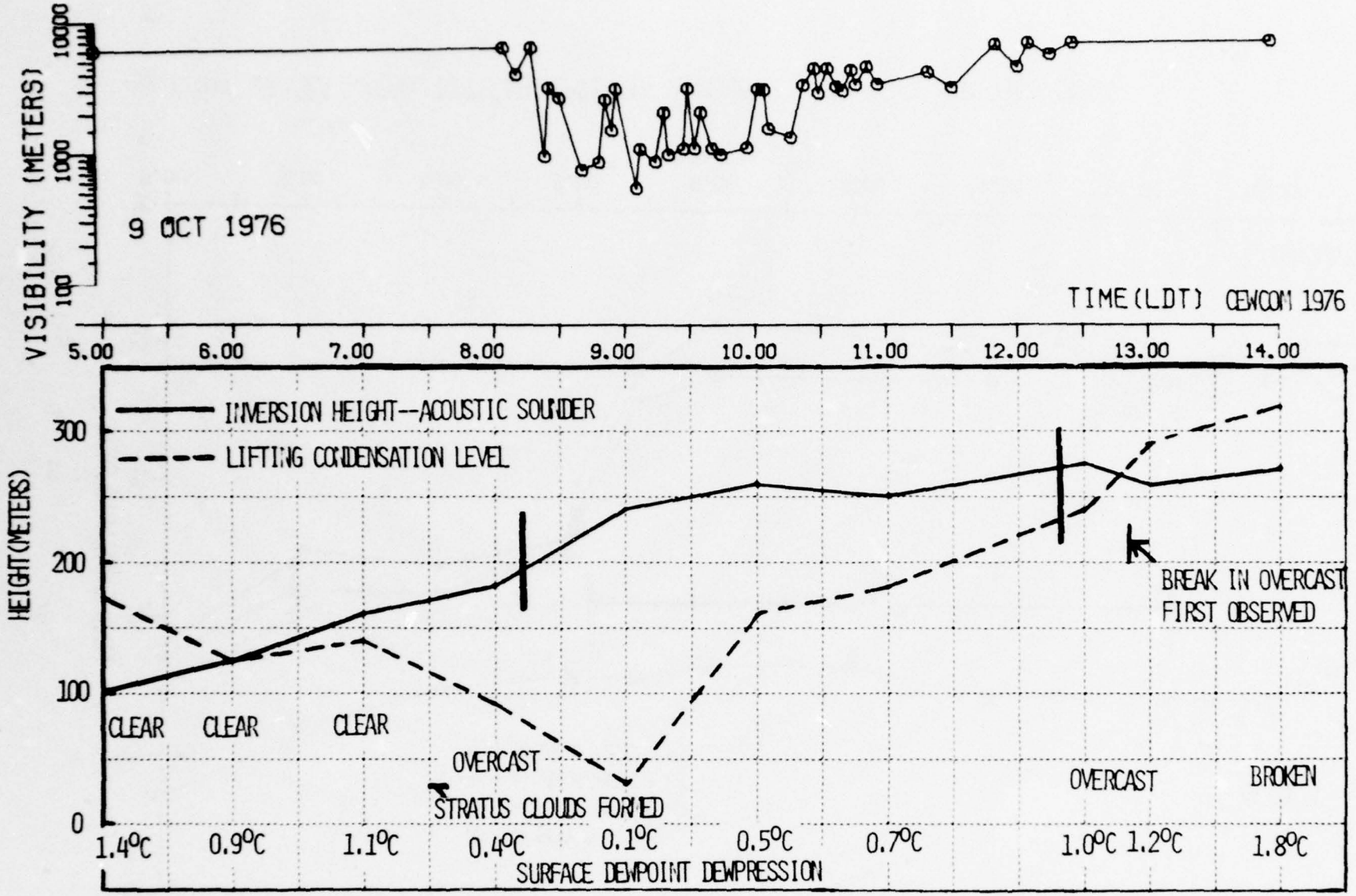

FIGURE 29 VISIBILITY, INVERSION HEIGHT, AND LIFTING CONDENSATION LEVEL FOR FOG OF 9 OCTOBER 1976

In an effort to determine the mechanism responsible for formation of the stratus cloud, the lifting condensation level (LCL)* was computed from surface observations (wet/dry bulb temperatures) obtained during the 9 October event. Computed LCL is shown by the dashed line in Figure 29 as a function of time during the westward track. Comparison of the relative heights of the inversion base and the LCL in Figure 29 clearly demonstrates that the stratus formed when the inversion height rose substantially above the LCL height after ~0730 and began to dissipate when the inversion base and LCL converged at ~1245 PDT.

In summary, fog was again observed to form at sea as a result of stratus lowering (thickening). Stratus formation and subsequent fog development was observed at sea to occur under conditions suggested by previous investigators (Ref. 20, 24) for some California fogs on shore. Anderson (Ref. 20, 1931) and Petterssen (Ref. 24, 1938) examined the correlation between the LCL, inversion height and fog-stratus occurrence and found that when the LCL was above the inversion, fog-stratus would not form in the California marine boundary layer.

The importance of the observations lies in the rapidity with which the inversion height changed and triggered the stratus and subsequent fog occurrence. While the dependence of fog occurrence on the mean, absolute height of the inversion has been long recognized (Ref. 2, 20, 21), the current observations indicate that short-term fluctuations in the height of the inversion may be of equal importance to the occurrence of fog at sea; certainly the short-term fluctuations will be more difficult to detect and forecast.

The change in inversion height is an important consideration in the operational performance of electro-optical equipment even when the inversion remains below the LCL. The increase in maximum relative humidity accompanying an increasing inversion height will cause enlargement of hygroscopic aerosols

---

*The LCL is defined as the height at which condensation will occur in surface air when it is lifted dry adiabatically.

and a consequent increase in optical density beneath the inversion (see Section 2 of this report). Further, the height of the inversion layer controls the length of the optical propagation path in many air-to-sea naval operations. It is therefore recommended that a study of the mesoscale and synoptic scale processes responsible for fluctuations in the height of the marine inversion be initiated.

3.3 The Fog(s) of 8 October 1976

The fog(s) of 8 October were observed over cold water lying just off the California coast at Pt. Arguello. The fog(s) formed under a low-level inversion associated with a high pressure ridge at 500 mb and easterly, offshore flow in the surface levels. At the time of the fog encounter late on the morning of the 8th, the synoptic scale pattern was changing. At 500 mb, the high cell weakened and moved southeasterly, while at the surface high pressure developed off the coast and northwesterly flow became established in the coastal regions. Thus, the observations taken later, upwind of the fog, were probably not representative of "upwind conditions" when the fog was forming. Therefore it was not possible to examine formation processes of this fog, but some observations concerning the behavior and characteristics of this "cold water" fog can be made. Visibility, air temperature and drop spectra records for this event are provided in Figures C-7, C-8, and C-9 in Appendix C.

Figure 30 shows the locale of the fog, the position of radiosonde releases for this fog event, and the track of the ACANIA from 2000 PDT on the 7th until 2200 PDT on the 8th. This figure is shown so that the positions and times of the soundings to be discussed can be appreciated with respect to the location of the fog and the changing synoptic pattern. Five soundings were taken over a 24-hour period and data from the surface up to 1100 m are plotted for each of the soundings in Figure 31. As shown by the soundings, the temperature profiles from 1100 m down to 400 m were strikingly similar. The constancy of the vertical temperature structure during the period 0400-2200 PDT indicates that little change had yet occurred in the synoptic pattern at levels above 400 m.

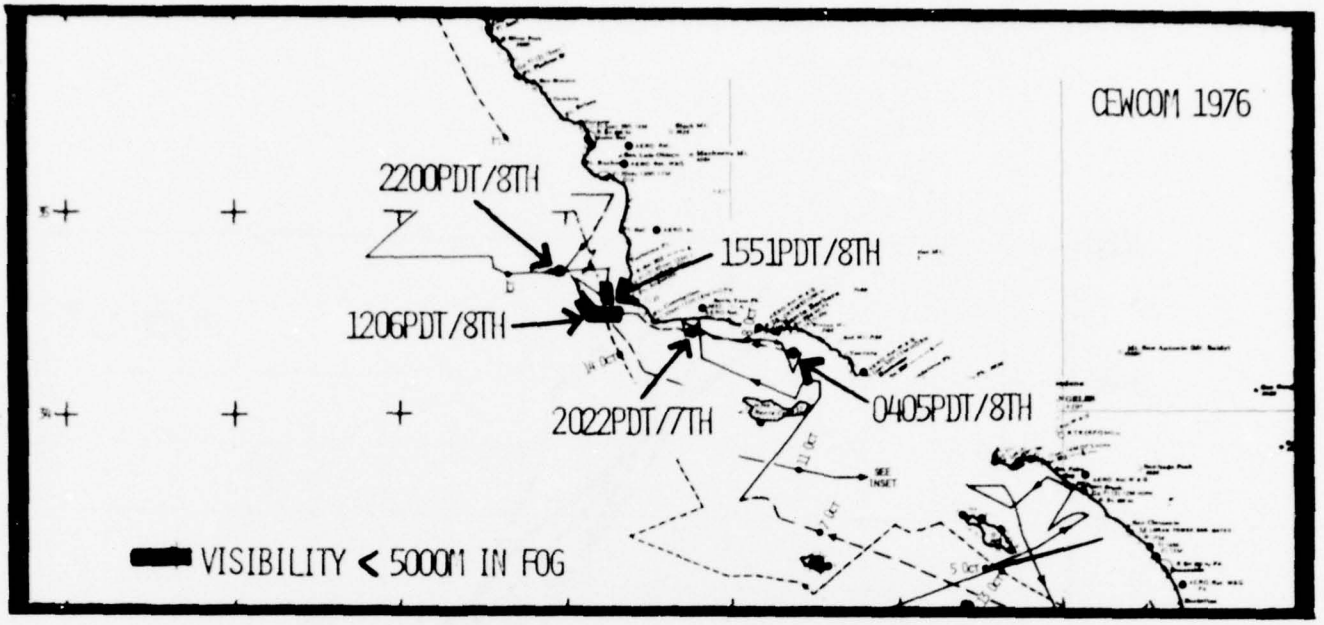

FIGURE 30 LOCATION OF FOGS AND RADIOSONDES FOR 7-8 OCTOBER 1976.

The differences in the soundings below 400 m appear to represent both synoptic scale changes and local effects. For example, the 2022/07 sounding was taken east of Pt. Conception and south of the east-west coastal range and depicts a local effect. The surface wind was northwesterly and the low-level structure of the sounding was probably a result of downslope motion bringing higher level air down to near surface levels.

At the time and location of the 0405/08 sounding, surface winds were west-southwesterly (not downslope) so that the sounding is probably more representative of general conditions in the fog area early on the 8th: i.e., a shallow marine layer topped by a sharp intense inversion. The sounding for 2200 on 8 October was taken in clear air after the fog event and shows the temperature structure in the offshore region as a change to northwesterly flow was occurring: i.e., the inversion was higher and not so sharply defined. The low-level temperature structure in which the fog formed was likely somewhere between these two profiles, probably more like the 0405 sounding rather than the 2200 sounding. The 1206 and 1551 soundings, both obtained in fog,

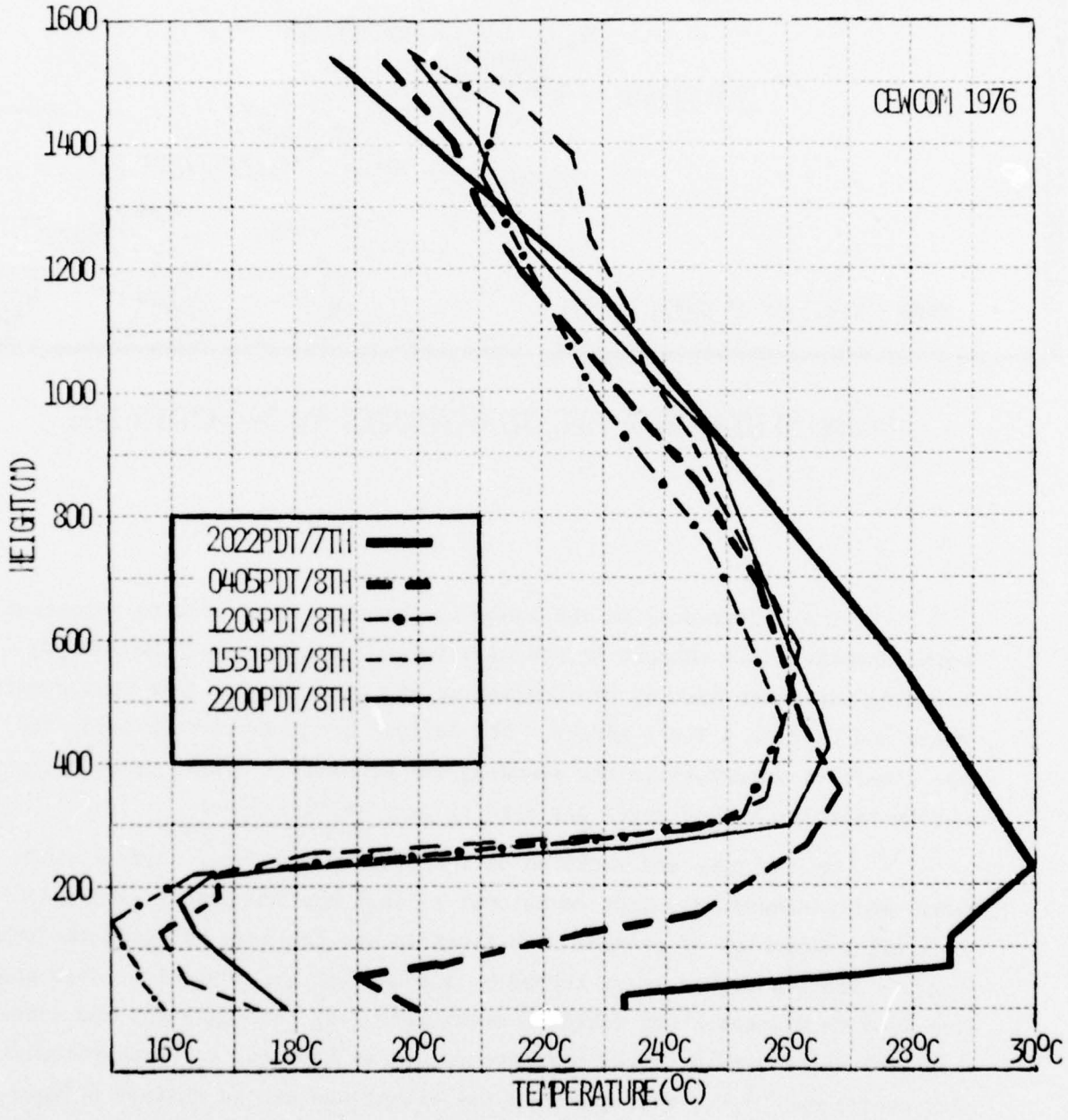

FIGURE 31 VERTICAL TEMPERATURE PROFILES IN FOG AND ENVIRONS FOR FOGS OF 3 OCTOBER 1976.

show a raised inversion level (relative to the 0405 sounding) and a cooler marine boundary layer. The soundings suggest that fog top was at an altitude of approximately 130 m. These data support previous observations of marine fog occurrence and inversion behavior (Ref. 3): i.e., low-level inversions have been found to be requisite to marine fog formation; and in the presence of fog, radiative processes can raise the height of, and strengthen, capping inversions.

As indicated in Figure 30, the fog event of 8 October was encountered in the vicinity of 35 N and 120 W and was comprised of two separate fog patches. The fogs of 8 October may be seen on the satellite photograph taken at 1215 PDT and shown in Figure 32. Note the thin sliver of cloud/fog lying north-south along the coast at Pt. Arguello and the widening of the cloud area toward the south. Visible on the original photograph is a thin east-west break in the cloud area near the northern end of the band, separating the two fog patches observed at the surface from ACANIA.

ACANIA's track, sea surface temperatures, winds, fog boundaries observed by the ACANIA and cloud/fog boundaries from the satellite photograph for the event of 8 October are shown in Figure 33. The first of the two fogs was encountered between 1038 and 1238 PDT as the ship sailed west and then NW completely through the fog. The southern edge of the second fog advected over ACANIA at 1530 from the north and was the cloud/fog patch located north of the break in the clouds seen in the satellite photograph. ACANIA sailed northward through the second fog and stopped just short of the northern boundary at 1720 when fog top lowered to below 20 m. Fog top lowered to below 5 m by 1740 and the northern edge of the fog then advected by ACANIA at 1820 PDT. Reports from a number of ships indicated that the fog had earlier been much further north and had been advecting southward most of the morning.

Comparison of fog boundaries and sea surface isotherms in Figure 33 and visibility and temperature data in Figures C-6 and C-7 (Appendix C) reveals an apparent correlation between sea surface temperature and fog occurrence. The data show that both fog penetrations were nearly centered over a local

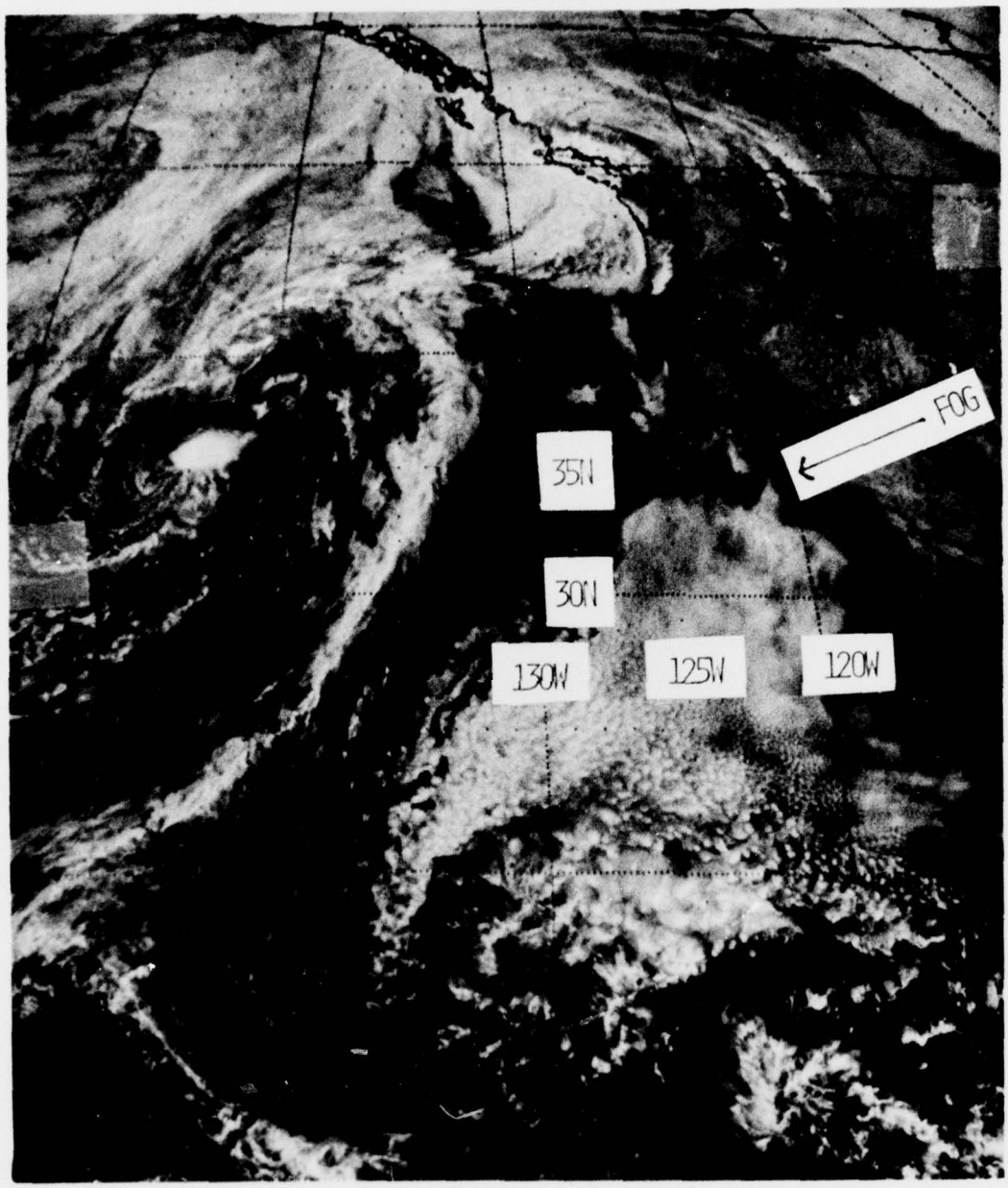

FIGURE 32 SATELLITE PHOTOGRAPH FOR 1215PDT 3 OCTOBER 1976 SHOWING FOG LYING ALONG THE CALIFORNIA COAST. CEWCOM 1976

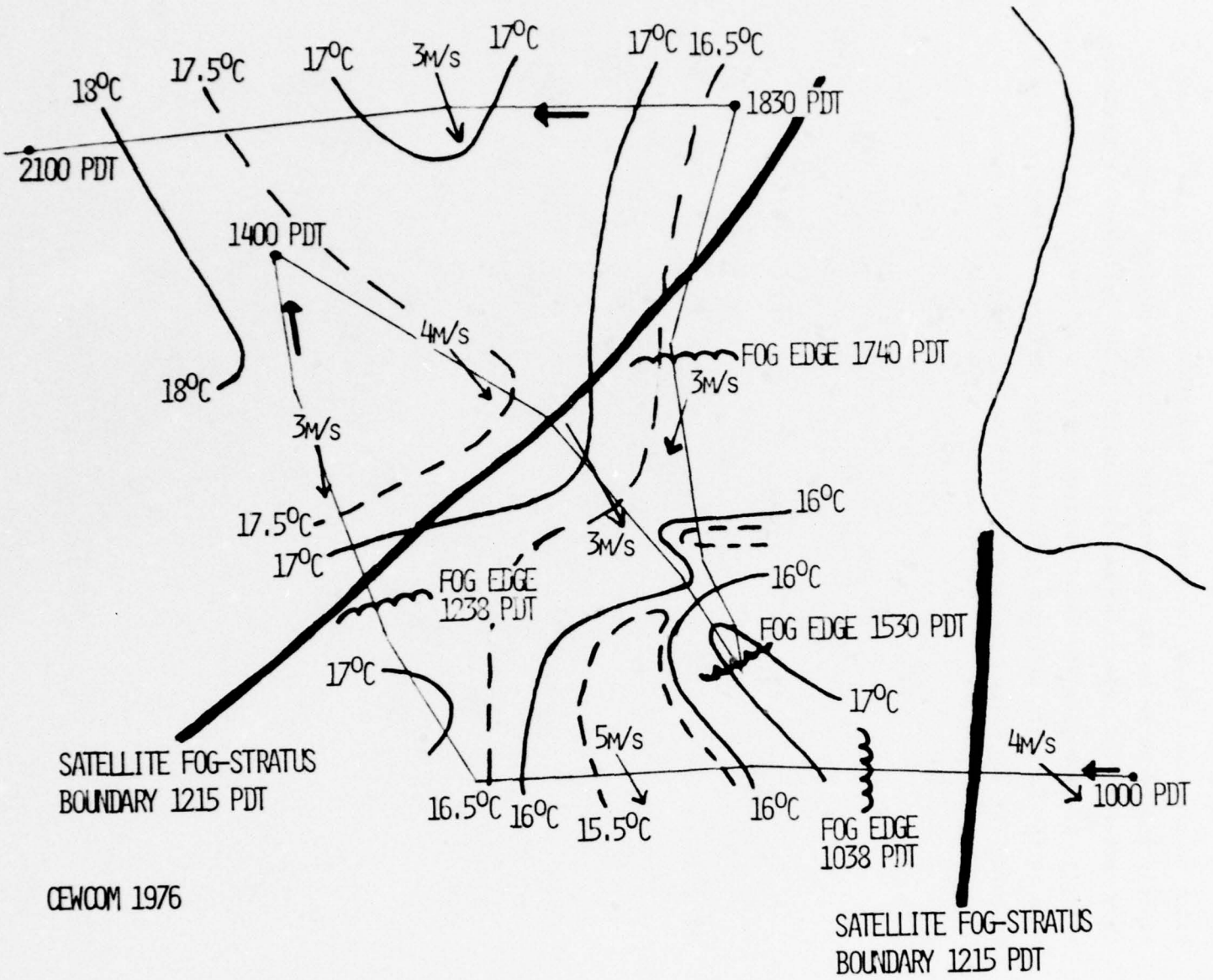

FIGURE 33 SEA SURFACE ISOTHERMS, SHIP'S TRACK, FOG EDGES, AND SELECTED WINDS FOR FOGS OF 8 OCTOBER 1976.

patch of very cold water. Further, air temperatures within the fog were rapidly cooled to below the temperature of the sea surface (except in the very center of the cold water patch) indicating the influence of radiative effects. This may be the first observation of a cold water fog that we have made in the Pacific, although sufficient data are not available for the region in which the fog formed to permit a definite conclusion to be drawn.

Section 4

EXPERIMENTS IN LASER BEAM SPREADING IN THE MARINE BOUNDARY LAYER

4.1 Introduction

As part of a Skylab experiment to evaluate the utility of low power lasers for spacecraft navigation aids and instrument calibration, a low power, visible wavelength laser, located near Goddard, Maryland, illuminated the Skylab spacecraft and was periodically photographed by the on-board astronauts. Analyses of those photographs coupled with visual observations by the astronauts indicated an unusual degree of beam spreading about the forward direction of the laser beam which was tentatively attributed to an atmospheric scattering effect (Ref. 25).

Calspan shipboard investigations off the southern California coast in September-October, 1976, and off the NW Florida coast in February 1977, provided opportunities to conduct similar laser experiments in the marine boundary layer. The experiments were conducted in collaboration with J.B. Russell of the Naval Avionics Facility at Indianapolis who provided and operated the laser. The intent of these experiments was to determine if beam spreading phenomena similar to the Skylab observations could be observed within the marine boundary layer with a low-power laser and at a horizontal range typically 100 times shorter than the Skylab distances. In future experiments, measurements of the amount and form of expected spreading of the laser beam might then be used in an attempt to assess important atmospheric parameters such as size and concentration of aerosols and levels of turbulence.

4.2 Experimental Parameters

Laser imagery data (photographic) were obtained at two separate locations: off the Pacific Coast of California and off the Gulf Coast of Florida. On 9/22/76 and 10/3/76, the laser was located inside a building at the NELC Laboratory on Point Loma, just west of San Diego. In the

experiments of 2/21/77 to 2/25/77, the laser was stationed on the Naval Coastal Systems Laboratory offshore platform, "Stage I," near Panama City, Florida. During both of these data acquisition periods, the laser was bore-sighted at the research vessel with a telescopic site. Photographs of the laser beacon were taken from the ship at varying exposures and distances from the target and at different times of day.

Weather conditions at both stations were nearly duplicated on the days of the experiments. On 9/22/76 (San Diego) and 2/25/77 (Panama City), skies were overcast and a haze persisted which limited visibility to ~15 km. This restricted the sighting of the laser and caused it to appear fainter at ranges exceeding 4 km. On 10/3/76 (San Diego) and 2/21/77 (Panama City), skies were clear and visibility exceeded 40 km. Clear, moonlit conditions existed during the second half (nighttime) of the experiment conducted on 10/3/76. These acquisition parameters are listed in Table 8.

Imagery was collected on 35 mm black and white Kodak Plus X and 35 mm Ektachrome films, using a 200 mm lens during the San Diego experiments and a 105 mm lens at Panama City. Exposures were made using incremental f stops from 5.6 to 22 at 1/125 sec and f 22 at 1/250, 1/500, and 1/1000 sec. Later analysis showed that best exposures were obtained for all images using f stops of 11, 16, and 22 @ 1/125 sec.

The low power laser was a Spectra Physics Helium Neon device operating at a wave length of 6328 Å, providing 2 mW output of randomly polarized, coherent radiation. Beam size was 0.8 mm diameter. Full angle beam divergence was 5.0 mrad at San Diego and 4.3 mrad at Panama City. Radio communications were maintained between the laser operator and the research vessel to ensure that alignment was maintained between the two stations. Range measurements were obtained using ship's radar.

4.3 Imagery Analysis Results - General

The 35 mm imagery collected during the two experimental periods was analyzed using a microdensitometer having a 25 μm aperture. Initial inspection revealed that the beam image varied in size and intensity as functions of both camera exposures and distance from the laser.

Table 8

DATES, TIME OF DAY, RANGES AND WEATHER CONDITIONS
AT TIME OF IMAGERY COLLECTION

Date	Location	Local Time	Range (m)	General Weather Conditions
9/22/76	San Diego	0917	1482	Hazy, overcast-winds 6-9 kts
9/22/76	San Diego	0930	3704	Visibility 5 km
9/22/76	San Diego	1010	7408	
10/3/76	San Diego	1656	1926	Clear Skies - visibility
10/3/76	San Diego	1720	3704	unlimited
10/3/76	San Diego	1756	7408	
10/3/76	San Diego	1837	12,964	Clear
10/3/76	San Diego	1920	18,520	Clear
10/3/76	San Diego	2215	9260	Clear, moonlit skies
10/3/76	San Diego	2323	3704	Clear, moonlit skies
2/21/77	Panama City	1125	3704	Clear - visibility exceeding 15 km
2/21/77	Panama City	1140	7408	Wind 3-5 kts
2/21/77	Panama City	1215	11,112	
2/21/77	Panama City	1245	14,816	
2/21/77	Panama City	1310	7408	
2/21/77	Panama City	1325	3704	
2/25/77	Panama City	0850	3704	Hazy, overcast
2/25/77	Panama City	0915	7408	Visibility less than 7 km
				Wind 3-5 kts

The color of the laser spot itself ranged from bright red to pale pink, and its size varied from slightly less than one to nine meters in diameter.* The shapes of the beam images were also quite random. The beam at times was a perfect circle of red light, while at other times it appeared elliptical or ovate. Several images captured the beam as star shaped, with rays emanating from the central beam spot, similar to the effect encountered with approaching automobile headlights on a rainy night (see Figure 34). These effects were reported by shipboard observers during the experiment. The oblong or elliptical beam spots rotated from one frame to another, such that the long axis was sometimes parallel to the horizon and at other times perpendicular, with intermediate orientations also observed. There is some possibility that the elliptical shapes were due to turbulence with time scales of the order of the film exposure time.

Two photographs obtained on the morning of 22 September are shown in Figure 35 to illustrate the rapid variation of beam appearance. During the approximately 10 seconds which separate the two frames, the major axis of the quasi-elliptic beam image rotated by about 50 degrees. Despite the short range of 1.5 km, the extremely hazy conditions caused the background image to be very faint. Imagery obtained on this day at a distance of 3.7 km was difficult to evaluate, and it was generally impossible to extract data from photographic imagery acquired at distances farther from the laser. In marked contrast, the photographs shown in Figure 36 were obtained in the experiment of 3 October when high visibility allowed imagery to be taken up to a distance of 18 km (a limit imposed by the earth's curvature and the respective heights above sea level of laser and observer). The imagery of Figure 36a and b was obtained at distances of 1.9 and 3.7 km, respectively. Captions to Figures 35 and 36 also include camera settings, distance from laser, beam image size on film and approximate image size.

A portion of the San Diego nocturnal experiment was devoted to an attempt to estimate the laser bean width. With the ship stationary the laser was slowly scanned horizontally, and shipboard observers reported their

*Size determined from image size and scale defined by camera focal length over distance between the camera and laser.

Figure 34: Laser beam image obtained on 3 October 1976 at 2330 PDT at a range of 3.7 km, f 5.6, 1/125 sec. Image diameter on film ∿100 μm, equivalent to ∿1.8 m beam diameter. Visibility approximately 50 km, RH 85%.

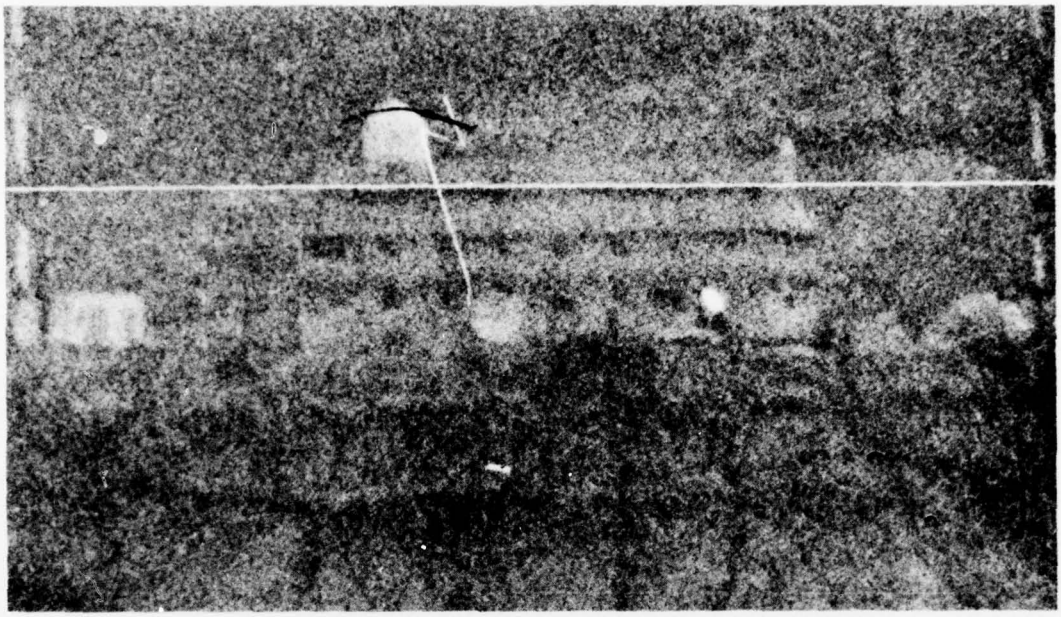

(a)

(b)

Figure 35: Imagery obtained on 22 September 1976 at 0915 PDT at a range of 1.5 km, f 16 (a), 11 (b), 1/125 sec. Image diameter on film ∿160 μm x 80 μm, equivalent to 1.2 m x 0.6 m. Visibility ∿5 km, RH near saturation.

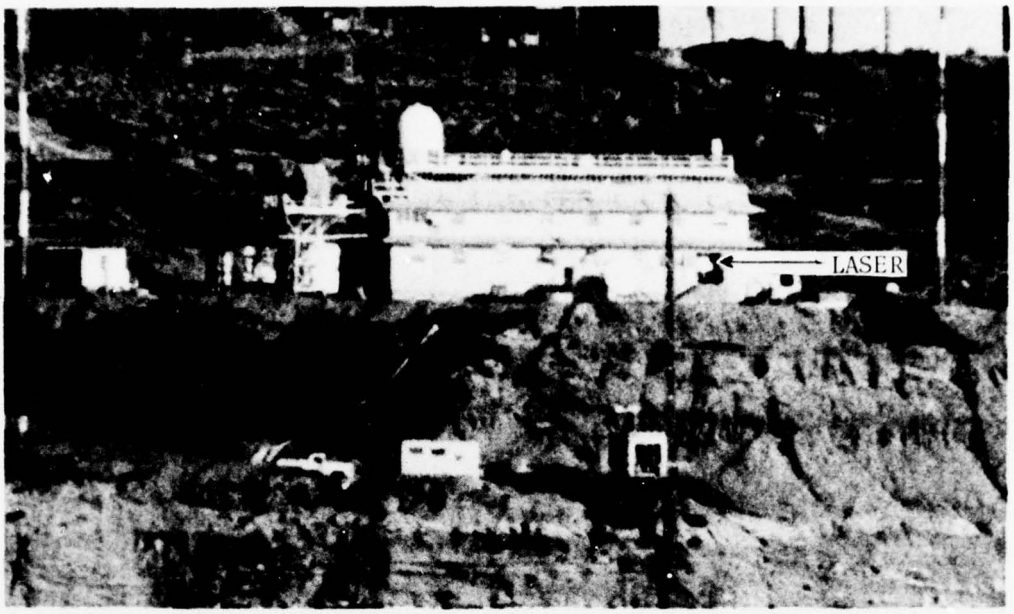

(a)

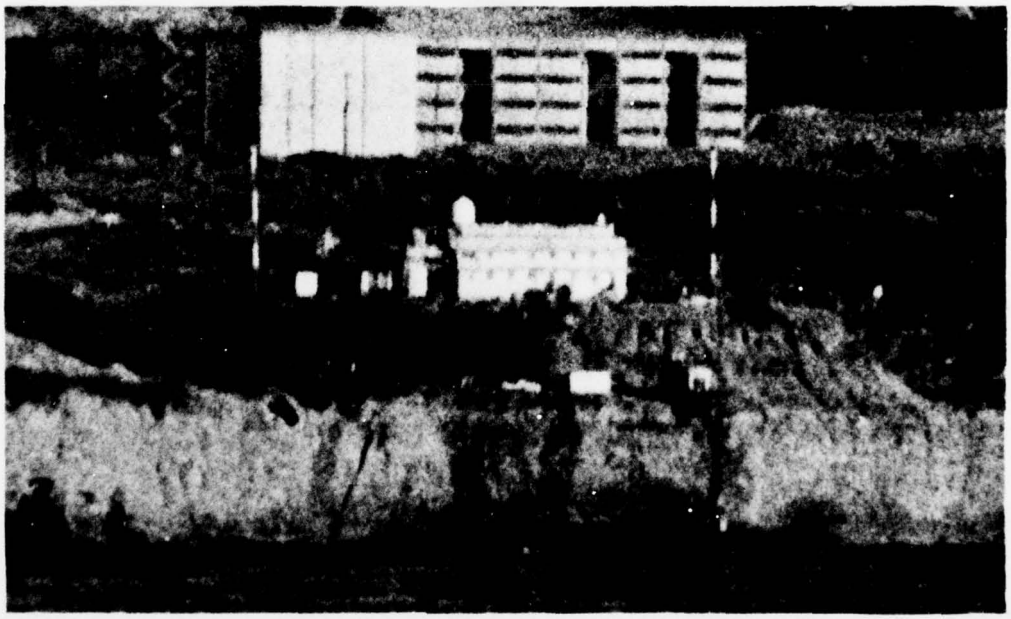

(b)

Figure 36: Laser beam imagery obtained on 3 October 1976 at 1659 (a), 1725 (b) PDT at a range of 1.9 km (a), 3.7 km (b), f 3.5 (a), 8 (b), 1/250 sec. Image diameter on film 100 μm (a), 80 μm (b), equivalent to beam diameter of 0.96 m (a), 1.45 m (b). Visibility ∿50 km, RH 80%.

subjective opinion regarding changes in the brightness of the laser source by radio. These observations were consistent with the 5 milliradian beam width measured in the laboratory.

During these visual observations, it was definitely established that atmospheric scattering was detectable when the beam was slightly misaligned with the observer. No scintillation was observed. The data suggest that the first sidelobe of the beam pattern was visually detectable; i.e., a secondary maximum in beam intensity was occasionally observed on either side of the primary beam. At slightly greater misalignment what appeared to be scattering from the optical components of the source was evident.

4.4 Image Analysis Results - Specific

Initial analysis of the imagery suggested that the shape variations could be due to image motion caused by ship movement or operator instability. Closer examination showed that these effects in most frames were probably caused by optical properties of the atmosphere as the image background was sharp and well defined.

Once the shape variations were accepted as a real phenomenon, probably attributable to atmospheric effects, the analysis proceeded in the direction of establishing a relationship between beam size and intensity versus distance from the laser source. One f stop and shutter speed combination (f 16 @ 1/125) was selected in order to form a complete data set of beam imagery at all ranges using a particular camera setting. Each beam image in this data set was measured using a reticle with 50 μm increments and a 25 μm aperture densitometer. The visual measurements are considered accurate to ± 10 μm, with most errors occurring on beam images for the Florida data because of the light sky background behind the laser. Beam-image areas (m^2) were calculated and plotted against the respective distances from the laser. Figures 37 and 38 are graphs of the regression analyses of these data for 3 October 1976 and 21 February 1977, respectively. The correlation coefficient (r^2) for the 3 October data (0.73) is higher than the value for 21 February (0.66) because of differences in contrast. On 3 October the laser was located in a doorway, providing a dark background for the beam source; thus, more

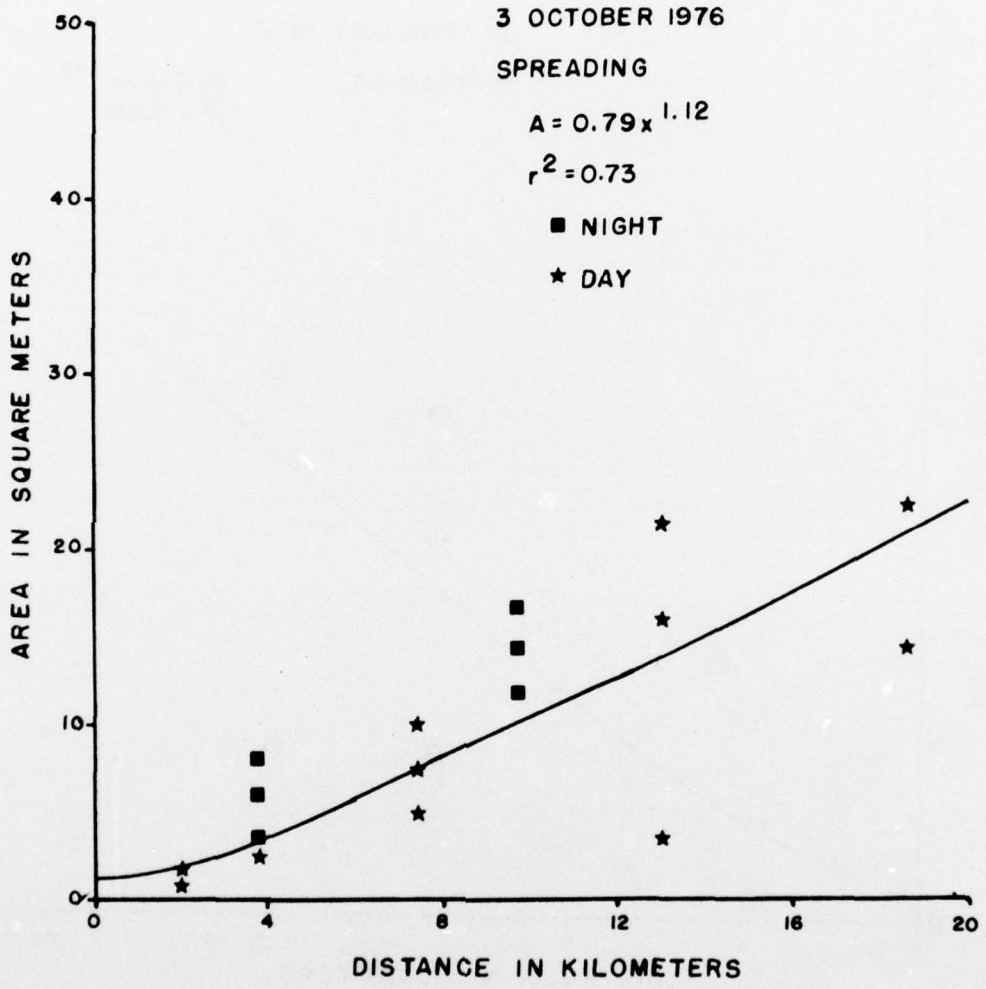

Figure 37: Laser beam spreading (spot area, A) vs. distance (X) from laser, 3 October 1976.

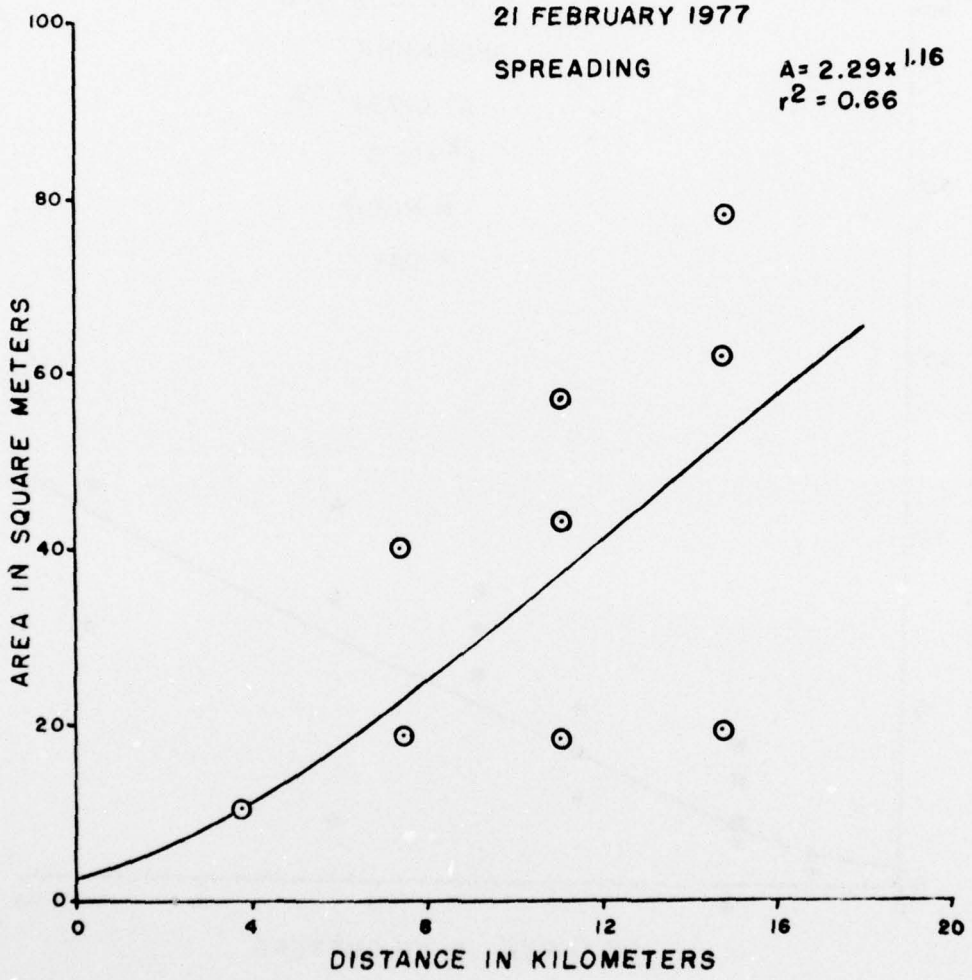

Figure 38: Laser beam spreading (spot area, A) vs. distance (X) from laser, 21 February 1977.

accurate measurement of the beam size could be made because the edges of the spot were more easily distinguishable due to the lack of illumination from behind the source. Additionally, the 3 October data included nighttime imagery which created a highly contrasting background for the beam spot, again providing for more accurate dimensional data. During the experiment in Florida in February, 1977, the laser was located on an off-shore platform with little structural background. The beam background was mostly sky, and the beam image was pale and poorly defined due to low background contrast as well as additional back illumination due to atmospheric scattering. These images were more difficult to measure as the exact edges of the beam spot tended to blend with the sky.

It is evident from Figures 37 and 38 that beam spot diameters on 21 February were about 50% larger than those measured on 3 October. Both days were characterized by dry, clear, sunny conditions; the scattering coefficient (as measured by nephelometry) on 21 February was about half the value recorded on 3 October, whereas total particle concentrations were 8000 cm^{-3} and 1000 cm^{-3} and relative humidities were 42% and 80% respectively, for the two days. More detailed information on the prevailing aerosol size spectra were not obtained in a comparable fashion on the two days, and it is therefore not possible in this case to relate the beam spreading to particular aerosol characteristics. To what extent turbulence was responsible for the observed phenomena cannot be assessed at this time because turbulence data have not been fully evaluated as of this writing.

Images taken on the two hazy days (22 September and 25 February) were even more difficult to measure because beam-spot color was pale and beam edges occasionally exhibited halos. For this reason only a very small number of frames taken on the hazy days could be evaluated, and the resulting data were insufficient for performing a meaningful regression analysis analogous to Figures 37 and 38. Therefore, it was not possible to establish correlations between the amount of beam spreading and atmospheric variables despite the differences in weather conditions between 22 September and 3 October. The difficulty in obtaining meaningful data on the hazy days points to the limitations of low power laser under conditions of restricted visibility.

The second portion of the film analysis attempted to establish a relationship between beam intensity and distance from the source. A microdensitometer was used to measure the density of the film in each of the three layers (red, green, blue) of the color film. Since film density depends upon processing effects, a sensitometric step wedge was exposed onto each roll of film; film density could then be converted to the exposure values causing the density.

The same images used for the size versus distance correlation were used for the intensity analysis. As expected, the laser had much higher exposure in the red band (it was operating at red wavelengths and its color on the film was red). Intensity data for the experiments of 3 October and 21 February are shown in Figures 39 and 40, respectively. These diagrams demonstrate that the beam intensity decreased exponentially with distance and that the atmospheric attenuation increased with distance, as was anticipated. The correlation coefficient for these two data sets is higher than that achieved for the beam size analysis probably because of the more objective nature of the measurements. The only possible errors incurred in the densitometry portion of this analysis would be related to placement of the aperture on the brightest portion of the beam spot.

Intensity measurements of the larger beam spots for the 3 October 1976 data were obtained at various points along the major axis. On circular spots, the center portion had the highest exposure in the blue, green and red bands. At increasing radial distances within the image, exposure density decreased in all bands. On elliptical spots, exposures along the bright centerline on the major axis remained relatively constant until the extreme edges were read, at which point exposure decreased in all bands. The latter behavior would be consistent with beam elongation due to turbulence of a time scale of the order of the exposure time.

On the 21 February 1977 data off Panama City, a different effect was noted, probably due to the placement of the laser against a sky background. Exposures for these beams decreased in the red band with increasing distance from the laser but the green and especially blue exposures increased with

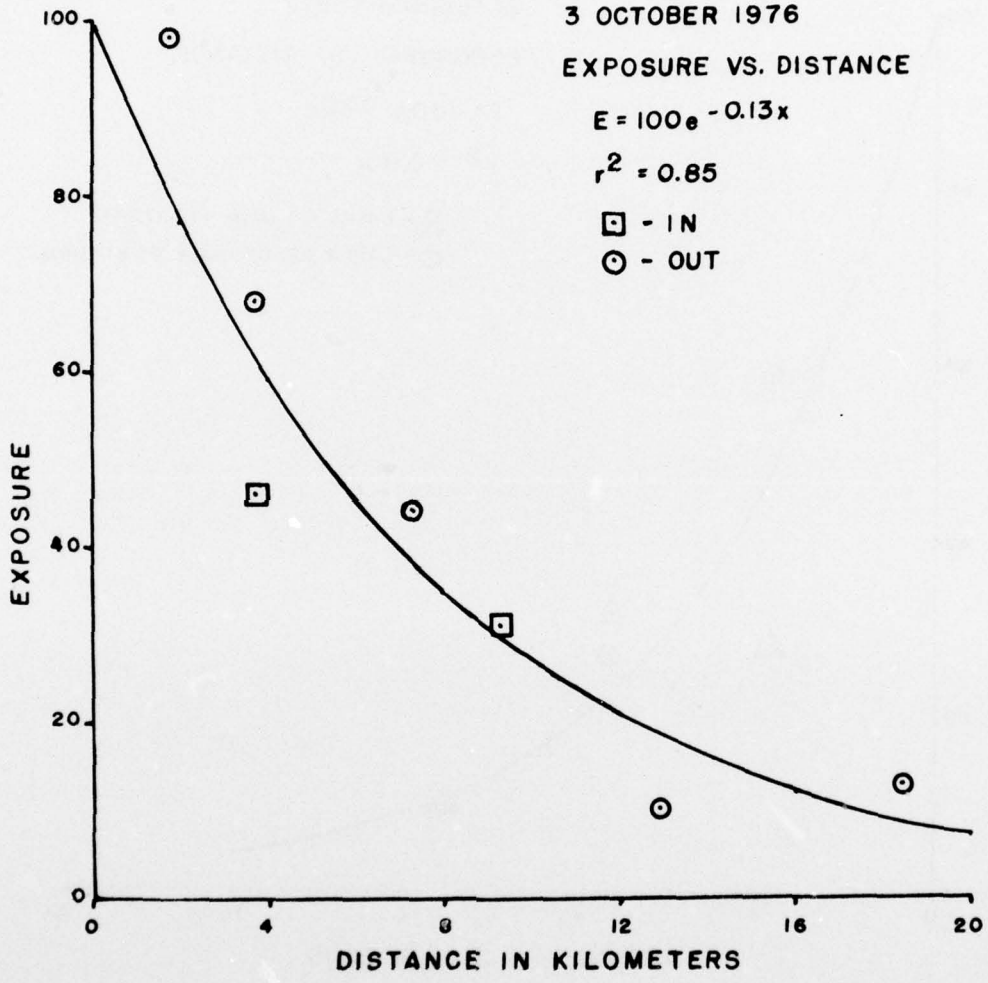

Figure 39: Film exposure (E) vs. distance (X) from laser, 3 October 1976.

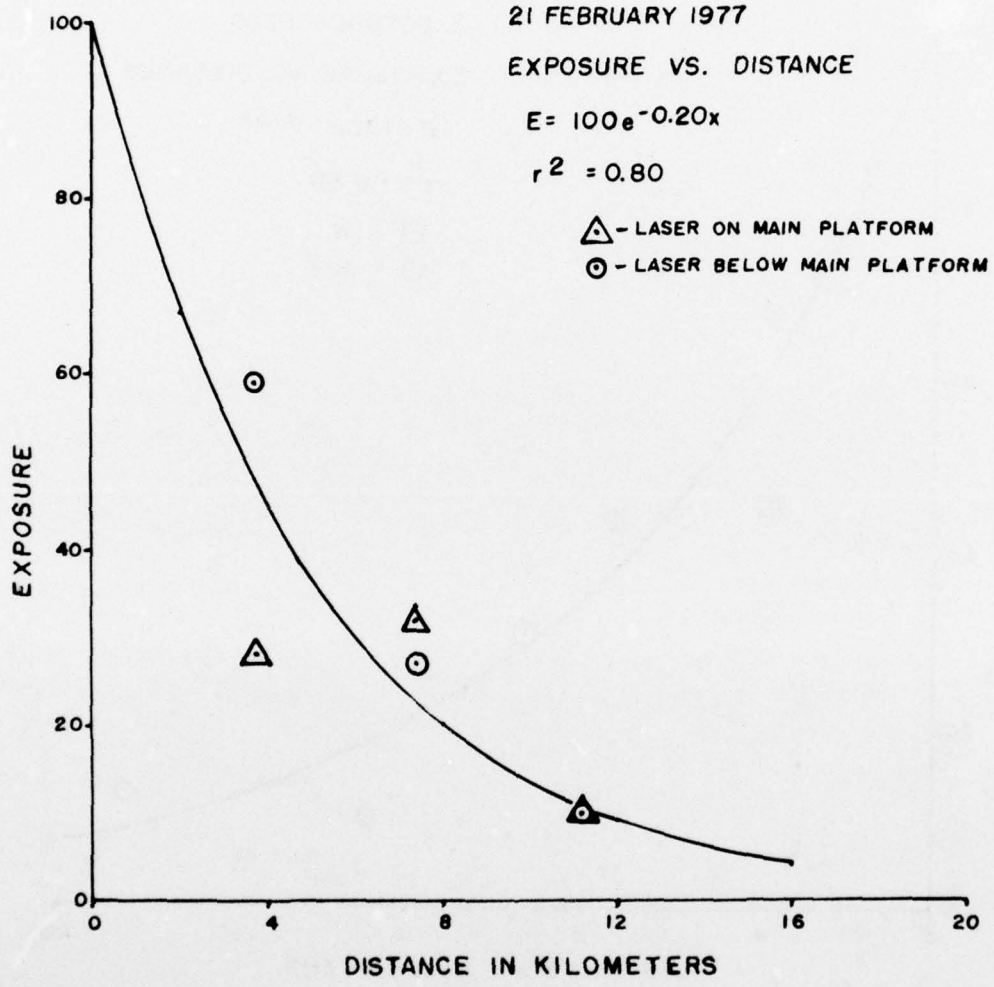

Figure 40: Film exposure (E) vs. distance (X) from laser, 21 February 1977.

increasing distance. This was due primarily to blue light being scattered by the intervening atmosphere as well as by background illumination. These effects were even greater for data recorded on 25 February 1977 when the sky was overcast and a haze persisted.

One frame of imagery taken on 21 February 1977 exhibited a strange anomaly. Two beam spots were recorded on the same scene, one directly above the other. It is felt that the upper spot was the actual laser beam while the lower spot was ascribed to a reflection off the water at some point between the platform and the research vessel. The unexplainable fact about this anomaly is that the upper spot was smaller and less intense in the red band than the lower spot and exhibited higher exposure in the green and blue bands.

4.5 Conclusions and Recommendations

In summary, these simple laser imaging experiments demonstrated that beam enlargement does occur over short propagation paths in the marine boundary layer, that it can be detected from use of a low-power laser under certain circumstances, and that it is attributable to atmospheric scattering effects. The results of analyses of laser imagery data suggest that attenuation of beam size and energy is related to forward scattering of peak energy and therefore is probably a function of particle size in the marine boundary layer. The good correlation of distance versus size and intensity indicates that the derived attenuation coefficients could eventually be applied to a measurement of boundary layer characteristics.

The present analysis concentrated on the imagery collected on clear days because this data set was larger and included samples from all ranges of observation. The data gathered on hazy days did not include any imagery for stations beyond 7.4 km. This data set, though small, did enhance results by demonstrating that the increased haze reduces the red exposure and increases blue exposure as distance increases. A larger data set would provide for the development of a correlation between clear and hazy conditions and could provide the basis for applying laser beam spreading in measurement of particle size

and/or concentrations. A laser of higher power than the 2 mW device used in these experiments will be required for data acquisition during more hazy conditions; i.e., when visibility is < 20 km.

Before laser beam spreading can be used in routine measurements of the marine boundary layer, more experiments are required to refine the attenuation coefficients derived from this study. A larger and better sample could be obtained if the following procedures were incorporated into future experiments.

1. Laser source and collector should be mounted on fixed platforms in order to maintain exact alignment.
2. A laser source of several times higher output should be used in order to provide better imagery under conditions of reduced visibility.
3. Either an electro-optical device or a high speed motion picture camera with f stop and exposure optimized for the laser intensity should be used to image the laser beam. Multiple frames collected at each position would allow an averaging of size and exposure values and allow a more precise measurement of these parameters.
4. The measurement of size and exposure on the processed data should also be performed through a precise electro-optical system where exact edges of the beam spot could be determined and the point of highest beam intensity could be measured.

REFERENCES

1. Mack, E.J., Pilié, R.J., and Kocmond, W.C., 1973: "An Investigation of the Microphysical and Micrometeorological Properties of Sea Fog" Project SEA FOG: First Annual Summary Report, Calspan No. CJ-5237-M-1, Calspan Corp., Buffalo, NY, May 1973.

2. Mack, E.J., Katz, U., Rogers, C.W., and Pilié, R.J., 1974: "The Microstructure of California Coastal Stratus and Fog at Sea" Project SEA FOG: Second Annual Summary Report, Calspan No. CJ-5404-M-1, Calspan Corp., Buffalo, NY, July 1974.

3. Mack, E.J., Pilié, R.J. and Katz, U., 1975: "Marine Fog Studies Off the California Coast" Project SEA FOG: Third Annual Summary Report, Calspan No. CJ-5608-M-1, Calspan Corp., Buffalo, NY, March 1975.

4. Mack, E.J. and Katz, U., 1976: "The Characteristics of Marine Fog Occurring off the Coast of Nova Scotia", Project SEA FOG: Fourth Annual Summary Report, Part 1, Calspan Report No. CJ-5756-M-1, Calspan Corp., Buffalo, NY, June 1976.

5. Alofs, D.J. and Carstens, D.J., 1976: "Numerical Simulation of a Widely Used Cloud Nucleus Counter," J. Appl. Met., Vol 15, pp 350-354.

6. Gerber, H.E., Hoppel, W.A., and Wojciechowski, T.A., 1977: "Experimental Verification of the Relationship Between Size and Critical Supersaturation of Salt Nuclei", Presented at the Fifth Annual Marine Fog Investigation Program Review Meeting, Buffalo, NY, 5-6 April 1977.

7. Blanchard, D.C., 1969: "The Oceanic Production Rate of Cloud Nuclei", J. de Rech. Atmospheriques, Vol. IV, 1, pp 1-6.

AD-A047 613 CALSPAN CORP BUFFALO N Y F/G 8/3
AN INVESTIGATION OF THE METEOROLOGY, PHYSICS, AND CHEMISTRY OF --ETC(U)
OCT 77 E J MACK, U KATZ, C W ROGERS N00019-76-C-0657
UNCLASSIFIED CALSPAN-CJ-6017-M-1 NL

2 OF 2
AD
A047613

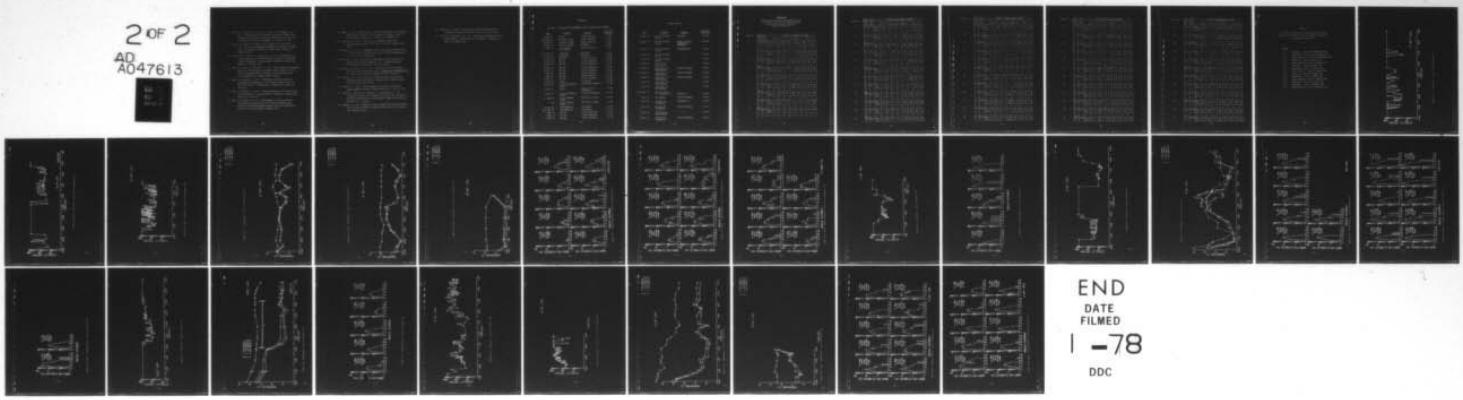

END
DATE
FILMED
1 -78
DDC

8. Mack, E.J., Kocmond, W.C., Pilié, R.J., Katz, U., and Vaughan, C.H. Jr., 1972: "Some Microphysical Features of Coastal and Inland Fogs", presented at the First International Conference on Aerospace and Aeronautical Meteorology, Washington, D.C., May 22-26 1972.

9. Mack, E.J., Eadie, W.J., Rogers, C.W., Kocmond, W.C., and Pilié, R.J., 1972: "A Field Investigation and Numerical Simulation of Coastal Fog", Calspan Report CJ-5055-M-1, Calspan Corp., Buffalo, NY, August 18, 1972.

10. Rogers, C.W.C., Mack, E.J., and Pilié, R.J., 1972: "Experimental Test of Fog Clearing by Ground-Based Heating--Visibility, Temperature and Fog Microphysics", Calspan Report CJ-5076-M-1, Calspan Corp., Buffalo, NY, December 1972.

11. Mack, E.J., Katz, U., and Pilié, R.J., 1976: "The Influence of Continental Aerosols on the Microphysics of Marine Fogs Occurring in Coastal Areas", Proceedings of the Conference on Coastal Meteorology, 21-23 September 1976, Virginia Beach, Virginia.

12. Mack, E.J. and Katz, U., 1977: "Measurements of Aerosol and Micrometeorological Characteristics of the Marine Boundary Layer in the Gulf of Mexico", Calspan Report, Calspan Corp., Buffalo, NY, March 1977.

13. Katz, U. and Mack, E.J., 1977: "Direct Measurement of Sea Spray Droplet Size Distributions", Calspan Report No. CH-6067-M-1, Calspan Corp., Buffalo, NY, April 1977.

14. Katz, U. and Mack, E.J., 1977: "Measurements of Aerosol and Micrometeorological Characteristics of the Marine Boundary Layer During the Transatlantic/Mediterranean Cruise of the USNS HAYES, May-June 1977, Calspan Report, September 1977.

15. Mack, E.J., 1977: "Measurements of Aerosol Characteristics in the Marine Boundary Layer Along the Offshore Margin of Southern California", Calspan Report, Calspan Corp., Buffalo, NY, September 1977.

16. Hodkinson, J.R., 1966: "The Optical Measurement of Aerosols", Aerosol Science, edited by C.N. Davies, New York, Academic Press, 468 pp.

17. Meszaros, A., 1977: "An Attempt to Explain the Relation Between Visual Range and Relative Humidity on the Basis of Aerosol Measurements", J. Aerosol Sci, Vol 8, pp 31-38.

18. Winkler, P., 1973: "The Growth of Atmospheric Aerosol Particles as a Function of the Relative Humidity - II. An Improved Concept of Mixed Nuclei", Aerosol Sci, Vol 4, pp 373-387.

19. Mohnen, V.A., and Yue, G.K., 1974: "Free HCl Acid in the Atmosphere Resulting from Scavenging Processes", Precipitation Scavenging 1974, U.S. Atomic Energy Commission Symposium Series (in press).

20. Anderson, J.B., 1931: "Observations from Airplanes of Cloud and Fog Conditions Along the Southern California Coast," Monthly Weather Review, July 1931, pp 264-270.

21. Leipper, D.F., 1948: "Fog Development at San Diego, California", Sears Foundation; Journal of Marine Research, 7, 3, pp. 337-346.

22. Fairall, C., Davidson, K., Houlihan, T., and Schacher, G., 1977: "Properties of Small Scale Turbulence in Marine Fog", Presented at the Fifth Annual Marine Fog Investigation Program Review Meeting, Buffalo, N.Y., 5-6 April.

23. Schacher, G., 1977: "Unpublish Acoustic Sounder Data from the CEWCOM-76 Cruise of the R/V ACANIA", September-October 1976, Naval Postgrad. Sch., Monterey, Calif.

24. Petterssen, S., 1938: "On the Causes and the Forecasting of the California Fog", Bull Am. Met. Soc., Vol 19, No. 2, pp 49-55.

25. Piech, K.R. and Schott, J.R., 1975: "Evaluation of SKYLAB Earth Laser Beacon Imagery", Calspan Rept. No. KL-5552-M-1, Calspan Corp., Buffalo, NY, March 1975.

Appendix A

FOG LOG: A LISTING OF FOGS OBSERVED AT SEA TO DATE ON THIS PROGRAM

Date	Location	Fog Type	Avg. Min. Visibility
26 Aug '72	MTY Bay	Stratus Lowering	1.5 km
29-30 Aug '72	Farallon Islands	Stratus Lowering	1.0 km
30 Aug '72	Farallon Islands	Stratus Lowering	1.0 km
30 Aug '72	Farallon Islands	Warm Water	0.4 km
31 Aug '72	Coastal near San Francisco	Coastal Radiation	1.0 km
9-10 July '73	Vandenberg	Warm Water	0.3 km
10 July '73	Vandenberg	Warm Water	0.2 km
24 July '73	MTY Bay	Coastal Radiation	0.2 km
25 July '73	MTY Bay	Coastal Radiation	0.2 km
26 July '73	MTY Bay	Coastal Radiation	0.2 km
29 Apr '74	MTY Bay	Coastal Radiation	0.3 km
30 Apr '74	MTY Bay	Coastal Radiation	0.3 km
7 May '74	MTY Bay	Stratus Lowering	1.5 km
8 May '74	MTY Bay	Stratus Lowering	1.0 km
11 May '74	MTY Bay	Coastal Radiation	0.3 km
22 Aug '74	Eureka	Convergence	0.1 km
23 Aug '74	To 40 nmi Offshore Eureka	Fog Patches (numerous)	0.5 km
24 Aug '74	Eureka	Shallow Coastal (numerous)	0.3 km
24 Aug '74	To 50 nmi Offshore Eureka	Fog Patches(numerous)	0.5 km
24 Aug '74	65 nmi Offshore Eureka	Warm Water (single)	0.2 km
[illegible] '74	60 nmi Offshore Eureka	Warm Water (single)	0.1 km
26 Aug '74	Cape Mendocino	Convergence	0.2 km
26-27 Aug '74	Cape Mendocino	Convergence	0.1 km
1 Sept '74	MTY Bay	Coastal Radiation	0.2 km
2 Sept '74	MTY Bay	Coastal Radiation	0.2 km
4 Sept '74	MTY Bay	Coastal Radiation	0.1 km

FOG LOG (Cont.)

Date	Location	Fog Type	Avg. Min. Visibility
2-3 Aug '75	35 n mi off Nova Scotia	Cold Water	0.10 km
3-4 Aug '75	30 n mi off Nova Scotia	Stratus Lowering Augumented by Cold Water	0.20 km
4-5 Aug '75	50 n mi off Nova Scotia	Cold/Warm Water	0.15 km
6-7 Aug '75	40 n mi off Nova Scotia	?	0.15 km
7 Aug '75	50 n mi off Nova Scotia	?	0.15 km
7 Aug '75	60 n mi SE of Nova Scotia	?	0.08 km
7-8 Aug '75	~150 n mi S of Newfoundland	Stratus Lowering	0.08 km
8-9 Aug '75	~150 n mi S of Newfoundland	Stratus Lowering	0.25 km
9 Aug '75	~150 n mi S of Newfoundland	Stratus Lowering	0.10 km
10 Aug '75	~150 n mi S of Newfoundland	?	0.15 km
11 Aug '75	~150 n mi S of Newfoundland	?	0.20 km
27-28 Sep '76	100 n mi SW of Pt. Conception, CA	Frontal (?)	0.20 km
5 Oct '76	Los Angeles	Coastal Radiation	0.15 km
8 Oct '76	10 n mi off Vandenberg	Cold Water (?)	0.10 km
9 Oct '76	45 n mi off Vandenberg	Stratus Lowering	0.8 km
13 Oct '76	75 n mi S of Santa Barbara	?	0.10 km
14 Oct '76	15 n mi off Vandenberg	Coastal Radiation	0.15 km

APPENDIX B

Airborne Concentrations and Sodium Ratios of Constituents of Hi-Vol Bulk Aerosol Samples Obtained Off Southern California, September-October 1976

Sample No.	Date Time			Airborne Concentration ($\mu g/m^3$)							
	day/mo.	Hr PDT		SO_4^{--}	Cl^-	Na	Al	NH_4^+	K	Mg	Ca
1	20 S	13-19	Avg	6.4	7.35	4.05	0	1.05	.09	.50	.20
			X/Na	1.6	1.8	-	-	.26	.02	.12	.05
2	21 S	7-13	Avg	.14	3.8	1.21	0	.05	.025	.12	.10
			X/Na	.12	3.14	-	-	.04	.02	.10	.08
3	21 S	14-20	Avg	5.2	7.0	5.7	.01	.72	.52	.73	.24
			X/Na	.91	1.23	-	.002	.13	.09	.13	.04
4	22/23 S	22-05	Avg	2.4	.18	.17	0	.33	.06	.08	.09
			X/Na	14.1	1.1	-	-	1.94	.35	.47	.53
5	23 S	06-14	Avg	7.9	.16	4.4	0	.17	.15	.12	.04
			X/Na	1.8	.04	0	0	.04	.03	.03	.01
6	23 S	15-22	Avg	7.8	1.7	2.2	.005	.68	.22	.28	.09
			X/Na	3.5	.77	-	.002	.31	.10	.13	.04
7	23/24 S	22-06	Avg	2.7	2.05	1.45	.045	.34	.12	.20	.08
			X/Na	1.9	1.4	-	.03	.23	.08	.14	.05
8	24 S	07-15	Avg	.33	.13	.05	0	0	0	.01	.002
			X/Na	6.6	2.6	-	-	-	-	.2	.04
9	24/25 S	21-01	Avg	1.0	0	0	0	0	0	.01	.005
			X/Na								

Sample No.	Date day/mo.	Time Hr PDT		Airborne Concentration ($\mu g/m^3$) SO_4^{--}	Cl^-	Na	Al	NH_4^+	K	Mg	Ca
10	25 S	01-07	Avg	.38	.13	.78	0	0	0	.04	.03
			X/Na	.49	.17	-	-	-	-	.05	.04
11	25 S	8-17	Avg	.2	.49	.14	0	.02	.02	.02	.01
			X/Na	1.4	3.5	-	-	.14	.14	.14	.07
12	25/26 S	18-04	Avg	1.4	.16	.18	0	.16	.005	.04	.03
			X/Na	7.8	.89	-	-	.89	.03	.22	.17
13	26 S	05-12	Avg	4.3	0	.35	0	.25	.04	.05	.05
			X/Na	12.3	-	-	-	.71	.11	.14	.14
14	26 S	12-20	Avg	1.7	0	.35	0	0	.02	.06	.03
			X/Na	4.9	-	-	-	-	.06	.17	.09
15	26/27 S	20-00	Avg	.2	.6	.67	0	.10	0	.12	.05
			X/Na	.3	.9	-	-	.15	-	.18	.07
16	27 S	12-16	Avg	.5	4.0	1.8	0	0	.01	.26	.07
			X/Na	.28	2.2	-	-	-	.006	.14	.04
17	27 S	16-19	Avg	.2	2.6	1.2	0	0	0	.15	.07
			X/Na	.17	2.2	-	-	-	-	.13	.06
18	28/29 S	19-03	Avg	1.6	8.1	5.4	0	.34	.19	.73	.09
			X/Na	.3	1.5	-	-	.06	.04	.14	.02
19	29 S	05-13	Avg	2.3	5.7	3.5	0	.50	.10	.49	.08
			X/Na	.66	1.6	-	-	.14	.03	.14	.02
20	29 S	13-23	Avg	2.2	5.4	4.0	0	.42	.31	.56	.14
			X/Na	.6	1.4	-	-	.11	.08	.14	.04
21	29/30 S	23-8	Avg	2.4	10.5	4.9	0	.85	.16	.60	.10
			X/Na	.49	2.1	-	-	.17	.03	.12	.02

Sample No.	Date day/mo.	Time Hr PDT		Airborne Concentration ($\mu g/m^3$) SO_4^{--}	Cl^-	Na	Al	NH_4^+	K	Mg	Ca
22	30 S	08-17	Avg	.86	.64	.86	0	0	0	.17	.03
			X/Na	.7	1.1	-	-	-	-	.20	.03
23	30 S	17-24	Avg	1.6	2.4	2.2	0	0	.06	.29	.04
			X/Na	.7	1.1	-	-	-	.03	.13	.02
24	1 O	00-06	Avg	1.6	2.5	2.3	0	.06	.06	.29	.03
			X/Na	.7	1.1	-	-	.03	.03	.13	.01
25	1 O	08-14	Avg	1.2	1.6	1.7	0	0	0	.22	.03
			X/Na	.7	.9	-	-	-	-	.13	.02
26	1 O	15-19	Avg	.3	2.1	.97	0	.14	0	.14	.03
			X/Na								
27	1/2 O	20-01	Avg	0	.05	0	0	0	0	0	0
			X/Na								
28	2 O	01-06	Avg	.59	2.0	.82	0	.09	.06	.18	.07
			X/Na	.72	2.4	-	-	.11	.07	.22	.09
29	2/3 O	24-06	Avg	1.1	2.7	1.5	0	.32	.13	.20	.06
			X/Na	.7	1.8	-	-	.21	.09	.13	.04
30	3 O	16-21	Avg	2.2	1.2	1.2	.01	.36	.09	.17	.09
			X/Na	1.8	1.0	-	.008	.3	.08	.14	.08
31	4 O	01-08	Avg	5.1	2.6	2.3	.005	1.2	.18	.34	.11
			X/Na	2.2	1.13	-	.002	.52	.08	.15	.05
32	4 O	10-14	Avg	6.5	2.6	2.7	0	.79	.22	.39	.10
			X/Na	2.4	.96	-	-	.29	.08	.14	.04
33	4 O	15-19	Avg	3.3	1.7	2.5	.01	.99	.14	.32	.14
			X/Na	1.3	.68	-	.004	.40	.06	.13	.06

Sample No.	Date day/mo.	Time Hr PDT		Airborne Concentration ($\mu g/m^3$) SO_4^{--}	Cl^-	Na	Al	NH_4^+	K	Mg	Ca
34	4 0	19-24	Avg	9.1	4.5	4.5	0	1.15	.30	.54	.12
			X/Na	2.0	1.0	-	-	.26	.07	.12	.03
35	5 0	01-06	Avg	7.5	.35	1.6	.015	2.10	.28	.25	.12
			X/Na	4.7	.22	-	.01	1.3	.18	.16	.08
36	5 0	10-11	Avg	19.1	.22	.42	0	5.6	.15	.18	.32
			X/Na	45.5	.52	-	-	13.3	.36	.43	.76
37	5 0	12-14	Avg	9.2	1.2	1.3	0	.57	.10	.30	.09
			X/Na	7.1	.92	-	-	.44	.08	.23	.07
38	5 0	16-21	Avg	7.7	3.9	3.75	0	1.15	.30	.53	.15
			X/Na	2.1	1.04	-	-	.31	.08	.14	.04
39	6 0	1-12	Avg	6.5	.88	2.12	.025	1.17	.22	.41	.23
			X/Na	3.1	.42	-	.01	.55	.10	.19	.11
40	7 0	19-21	Avg	6.9	3.4	4.0	.10	1.37	.36	.43	.17
			X/Na	1.7	.85	-	.03	.34	.24	.11	.04
41	8 0	00-07	Avg	7.5	2.1	3.5	0	.97	.26	.46	.16
			X/Na	2.1	.6	-	-	.28	.07	.13	.05
42	8 0	12-15	Avg	5.6	4.0	5.1	0	.81	.29	.68	.17
			X/Na	1.1	.8	-	-	.16	.06	.13	.03
43	8/9 0	23-03	Avg	4.0	9.3	8.2	0	.65	.39	1.12	.18
			X/Na	.5	1.1	-	-	.08	.05	.14	.02
44	10 0	9-13	Avg	10.5	1.19	3.49	.06	2.70	.34	.75	.59
			X/Na	3.0	.34	-	.02	.77	.10	.22	.17
45	10/11 0	23-02	Avg	13.6	.23	2.4	.05	2.35	.23	.33	.15
			X/Na	5.7	.10	-	.02	.98	.10	.14	.06

Sample No.	Date day/mo.	Time Hr PDT		Airborne Concentration ($\mu g/m^3$) SO_4^{--}	Cl^-	Na	Al	NH_4^+	K	Mg	Ca
46	11 0	02-07	Avg	15.3	0	1.3	.04	1.34	.28	.18	.19
			X/Na	11.8	-	-	.03	1.03	.22	.14	.15
47	11 0	07-11	Avg	26.4	0	1.6	.04	1.9	.28	.22	.22
			X/Na	16.5	-	-	.025	1.19	.18	.14	.14
48	11 0	1130-1240	Avg	25.8	0	1.1	0	1.9	.22	.13	.23
			X/Na	23.5	-	-	-	1.7	.2	.12	.2
49	11 0	13-18	Avg	13.3	0	3.3	0	1.60	.33	.44	.18
			X/Na								
50	11 0	18-22	Avg	11.1	.12	2.2	0	1.2	.17	.26	.12
			X/Na	5.0	.05	-	-	.55	.08	.12	.05
51	11/12 0	22-1	Avg	5.48	.68	1.9	0	1.2	.2	.32	.23
			X/Na	2.9	.36	-	-	.63	.11	.17	.12
52	12 0	01-05	Avg	4.3	0	3.1	0	.87	.25	.38	.18
			X/Na	1.4	-	-	-	.28	.08	.12	.06
53	12 0	05-10	Avg	5.1	.28	1.9	.02	1.02	.23	.20	.13
			X/Na	2.7	.15	-	.01	.54	.12	.11	.07
54	12 0	17-23	Avg	9.3	.55	2.2	0	1.7	.27	.45	.78
			X/Na	4.2	.25	-	-	.77	.12	.20	.35
55	12/13 0	23-03	Avg	13.7	.42	2.2	.03	1.5	.32	.30	.64
			X/Na	6.2	.19	-	.01	.68	.15	.14	.29
56	13 0	15-18	Avg	3.6	.66	2.8	.05	.63	.25	.35	.22
			X/Na	1.3	.24	-	.02	.23	.09	.13	.08
57	14 0	02-07	Avg	5.6	1.6	3.6	.02	.84	.34	.50	.18
			X/Na	1.6	.44	0	.006	.23	.09	.14	.05

APPENDIX C

Visibility, Temperature and Drop Spectra Records for Marine Fogs Observed Off Coast of Southern California, September-October 1976

Figure

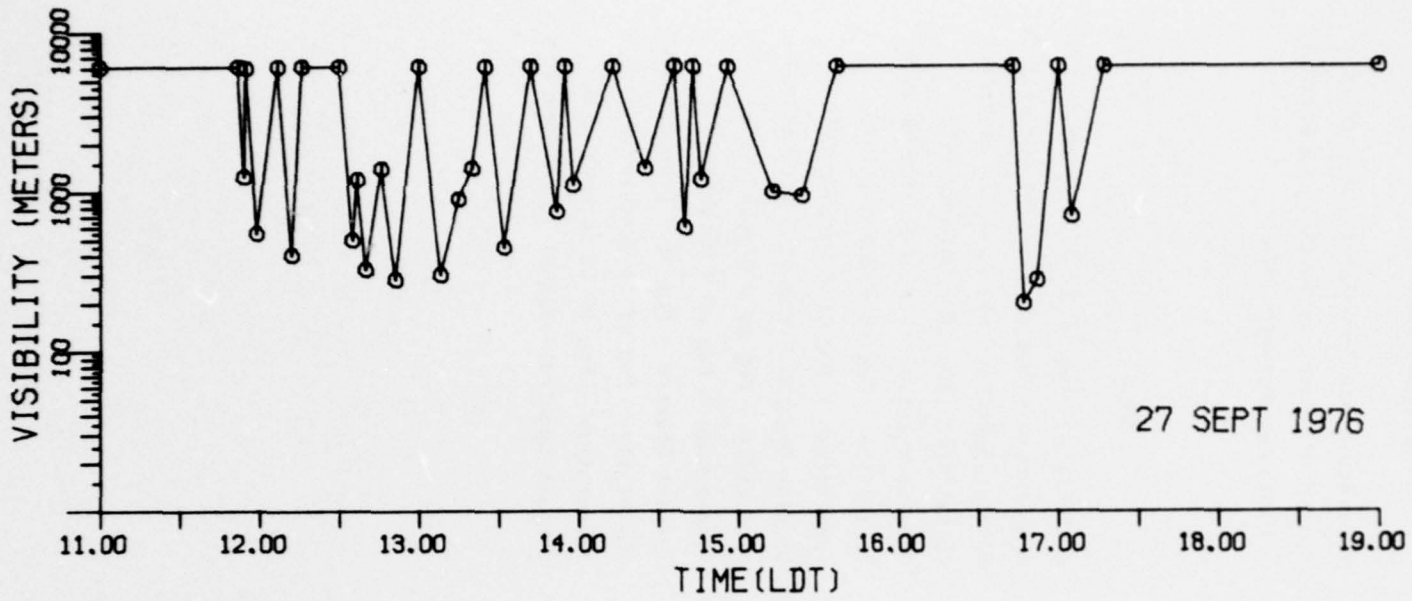

Figure C-1a: Visibility - Fog of 27-28 September 1976

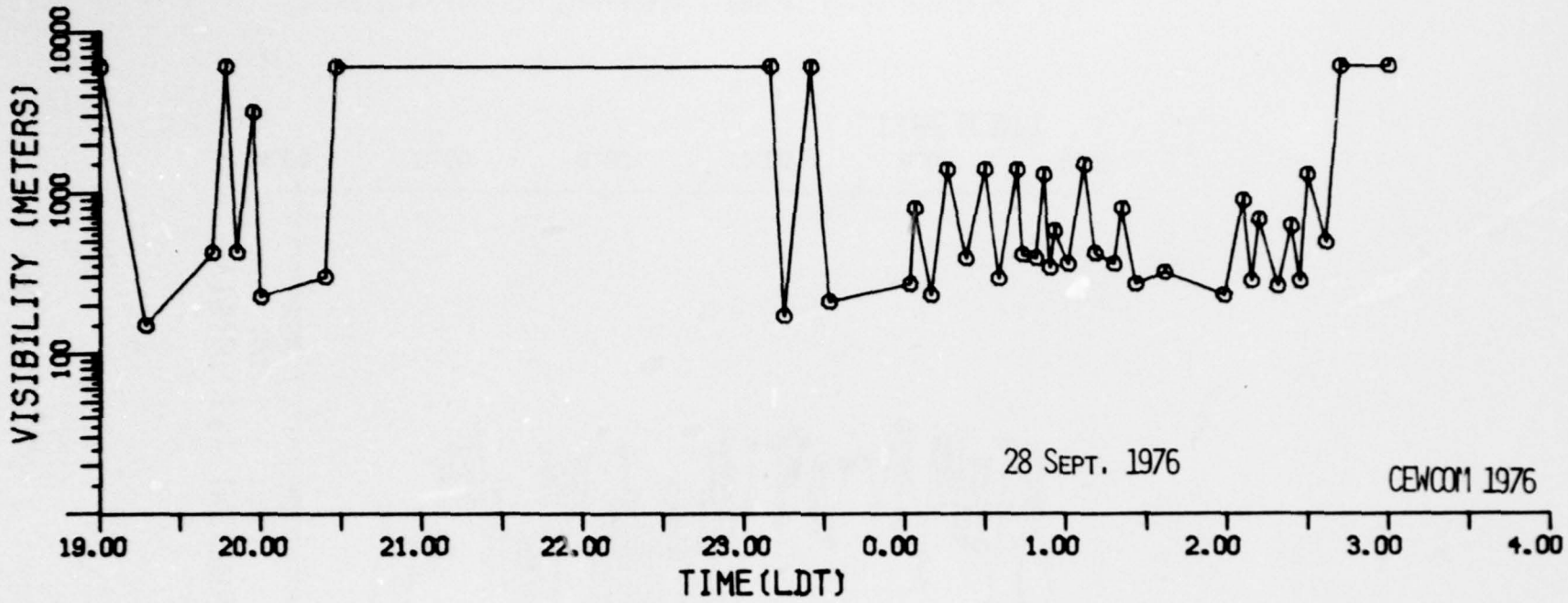

Figure C-1b (Cont): Visibility - Fog of 27-28 September 1976

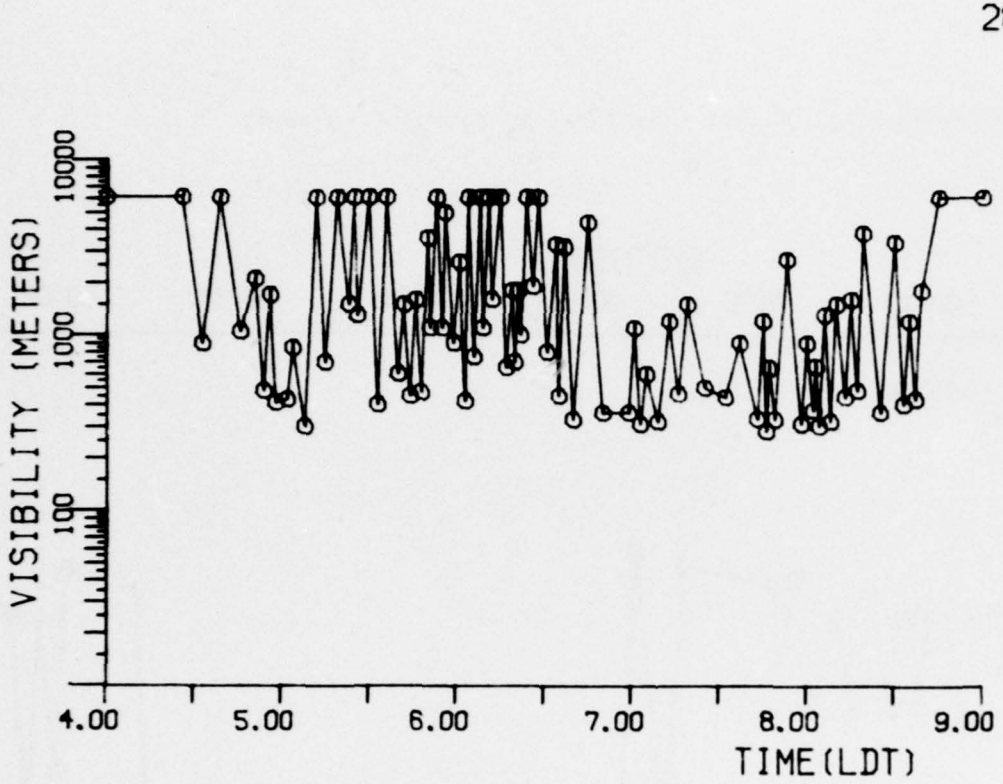

Figure C-1c (Cont): Visibility - Fog of 27-28 September 1976

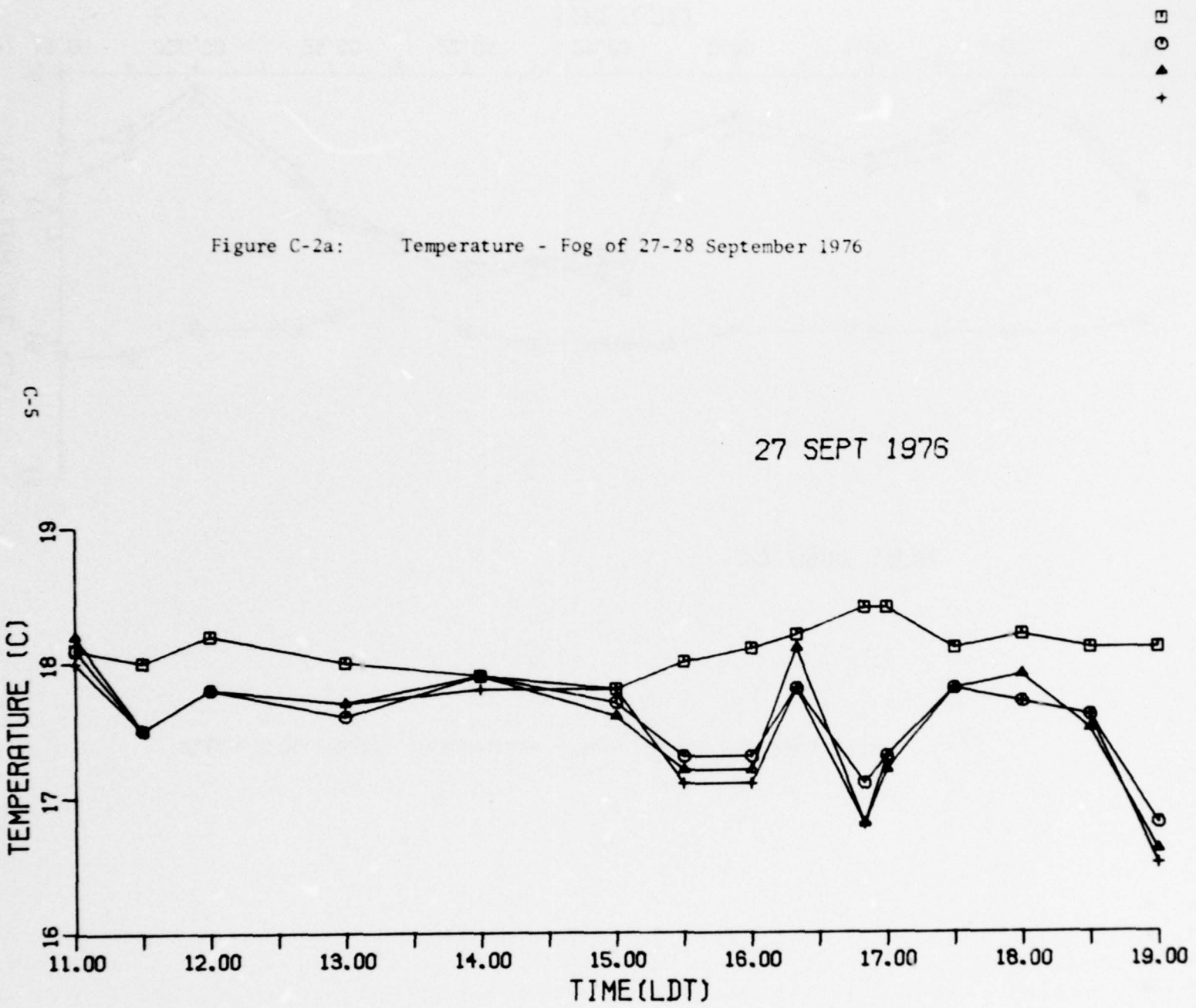

Figure C-2a: Temperature - Fog of 27-28 September 1976

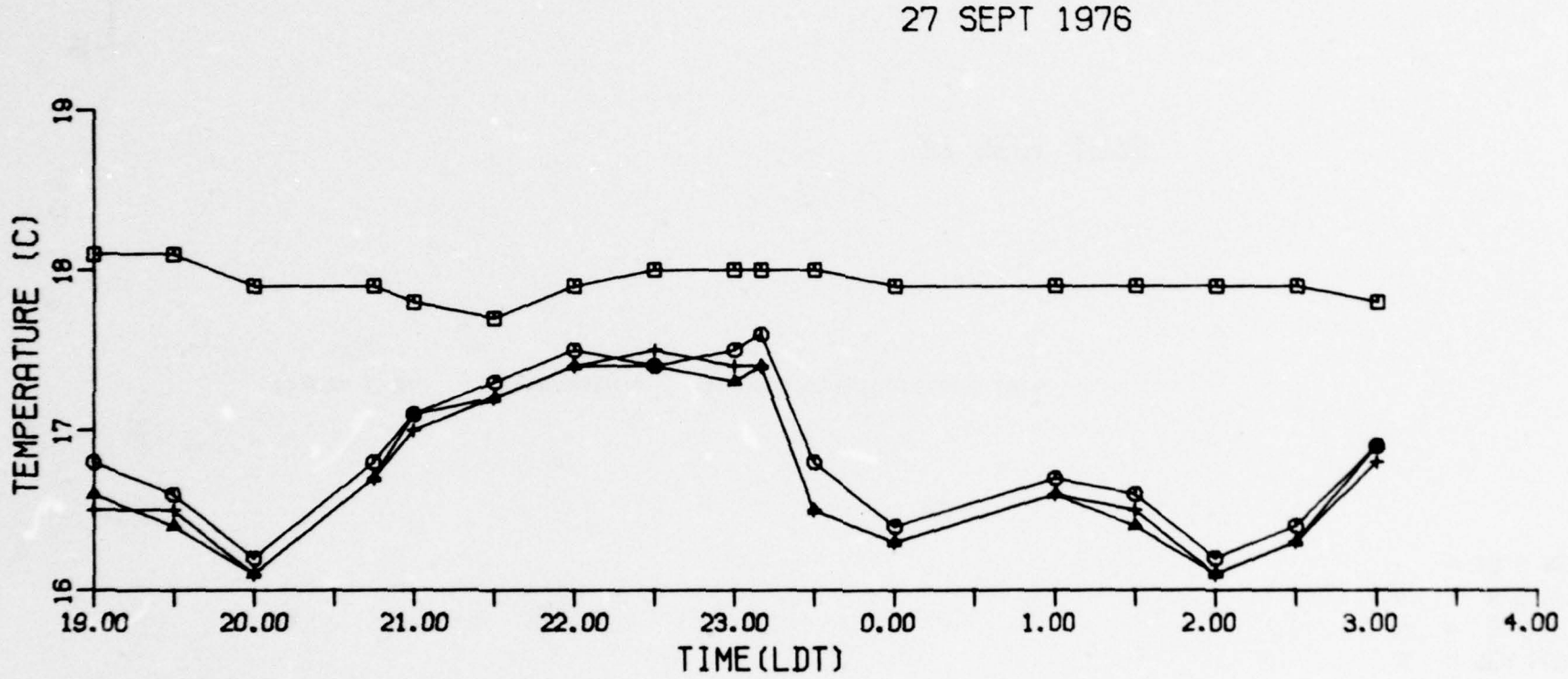

Figure C-2b (Cont): Temperature - Fog of 27-28 September 1976

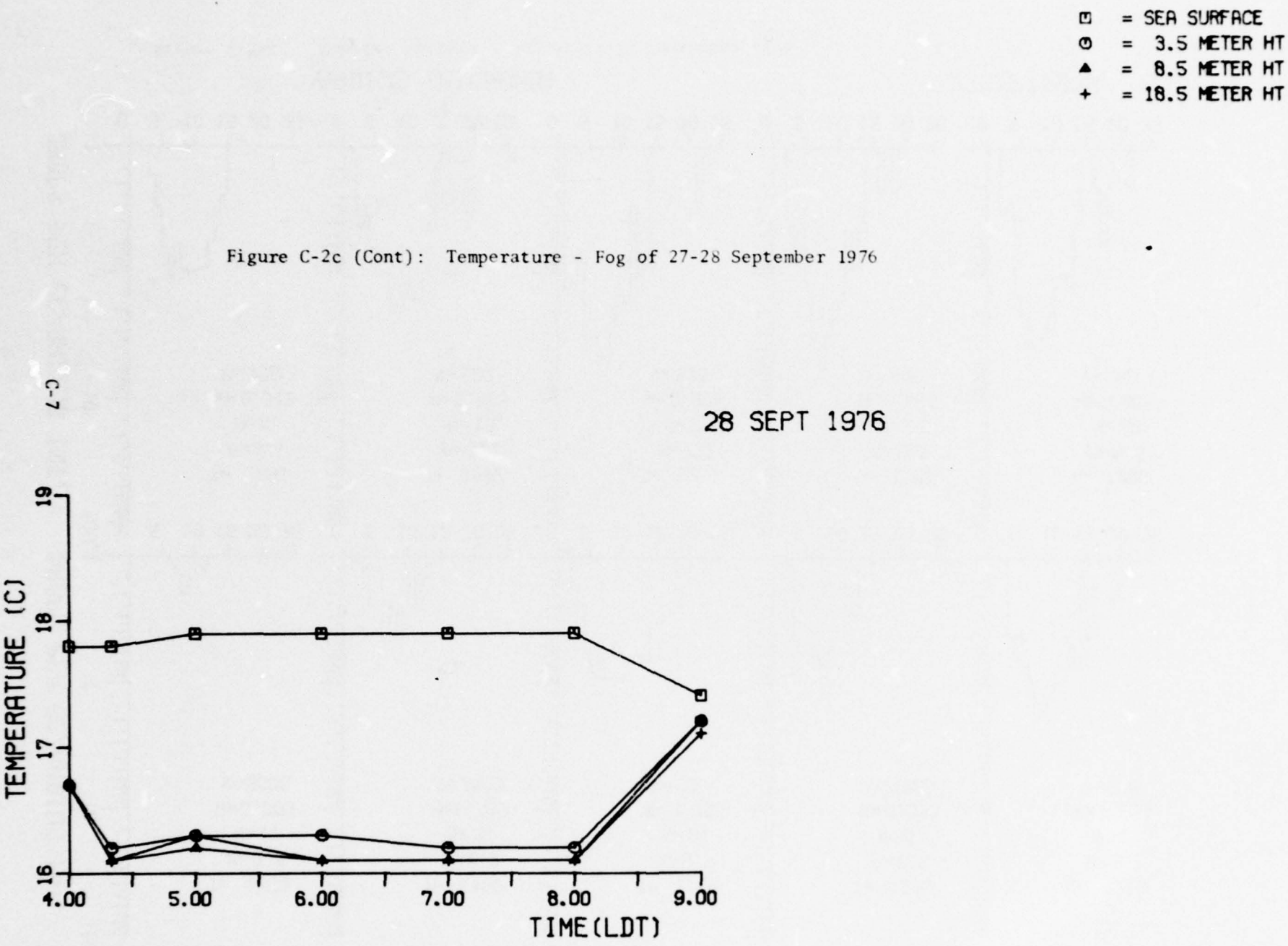

Figure C-2c (Cont): Temperature - Fog of 27-28 September 1976

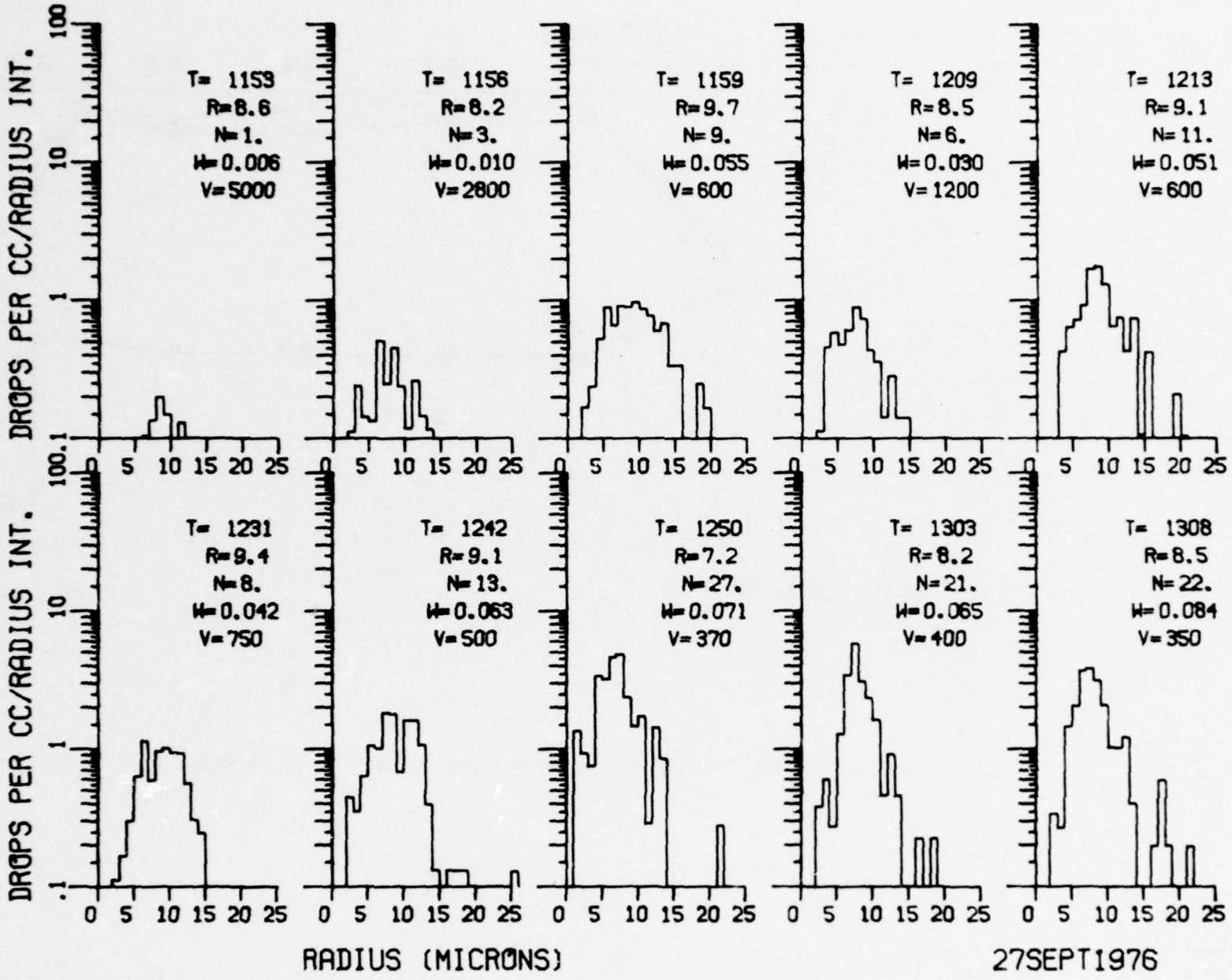

Figure C-3a: Droplet Spectra - Fog of 27-28 September 1976

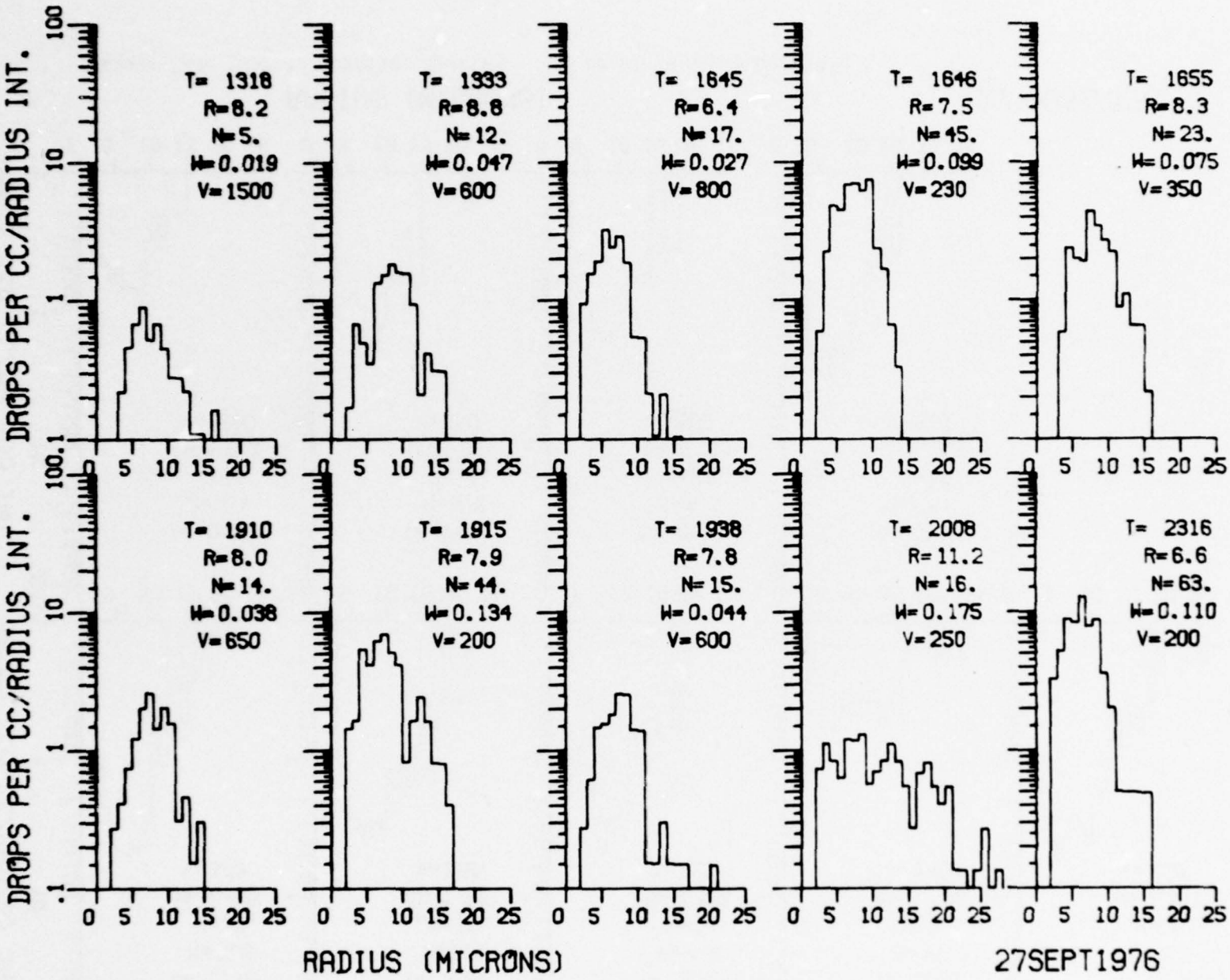

Figure C-3b (Cont): Droplet Spectra - Fog of 27-28 September 1976

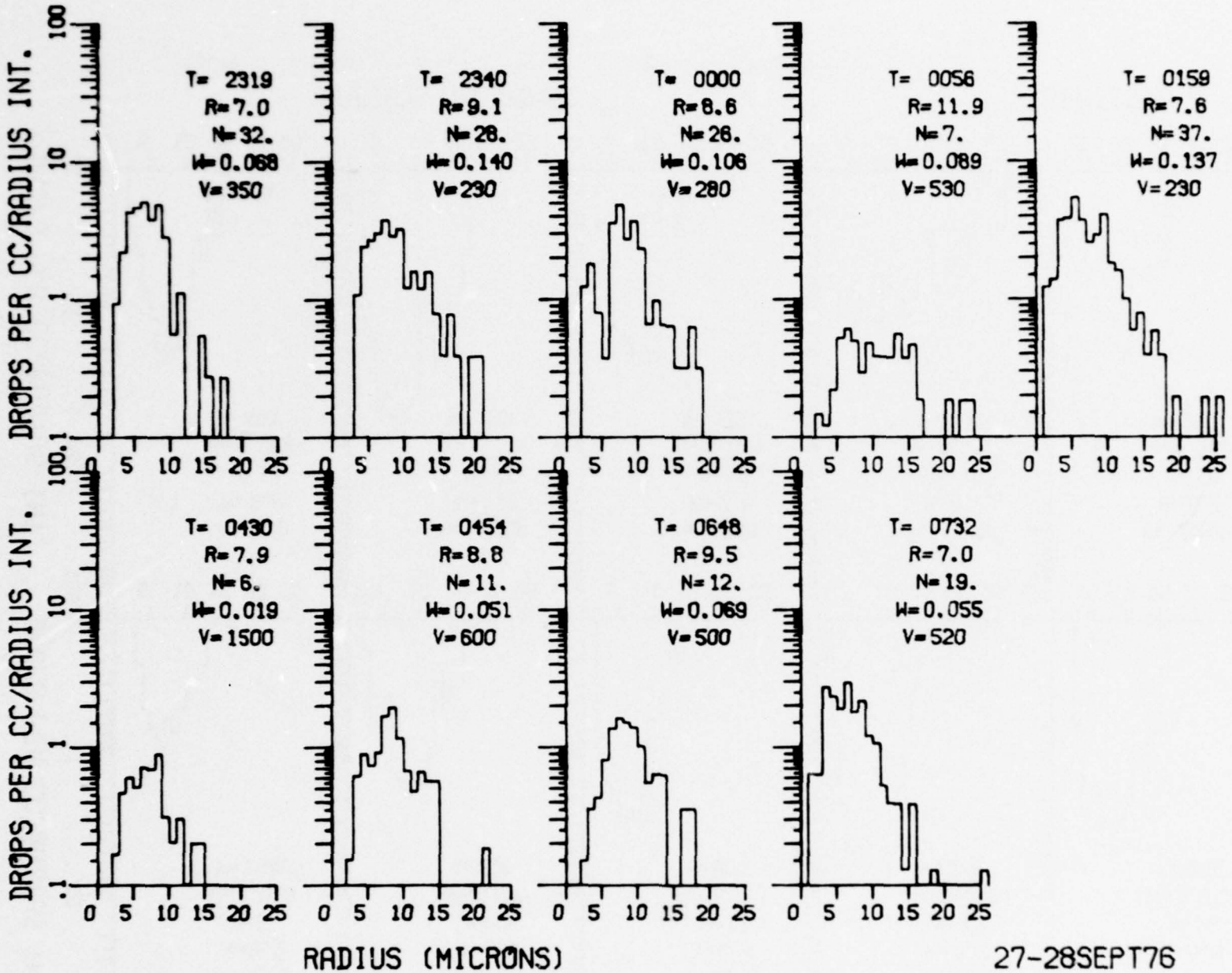

Figure C-3c (Cont): Droplet Spectra - Fog of 27-28 September 1976

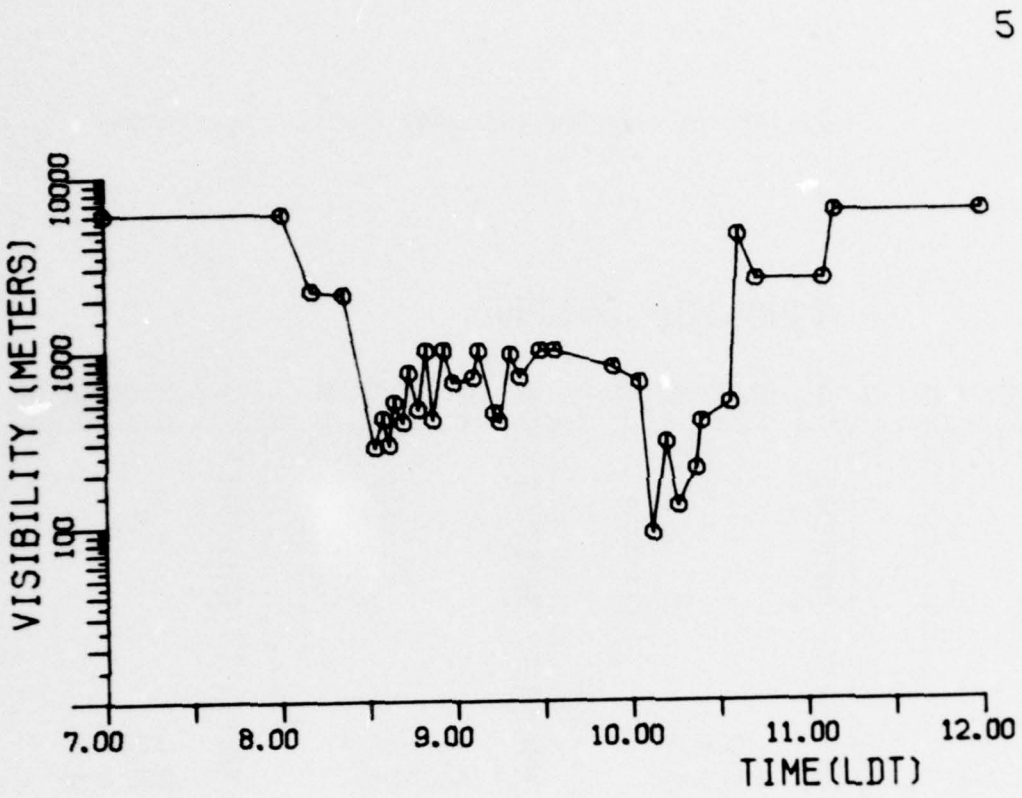

Figure C-4: Visibility - Fog of 5 October 1976

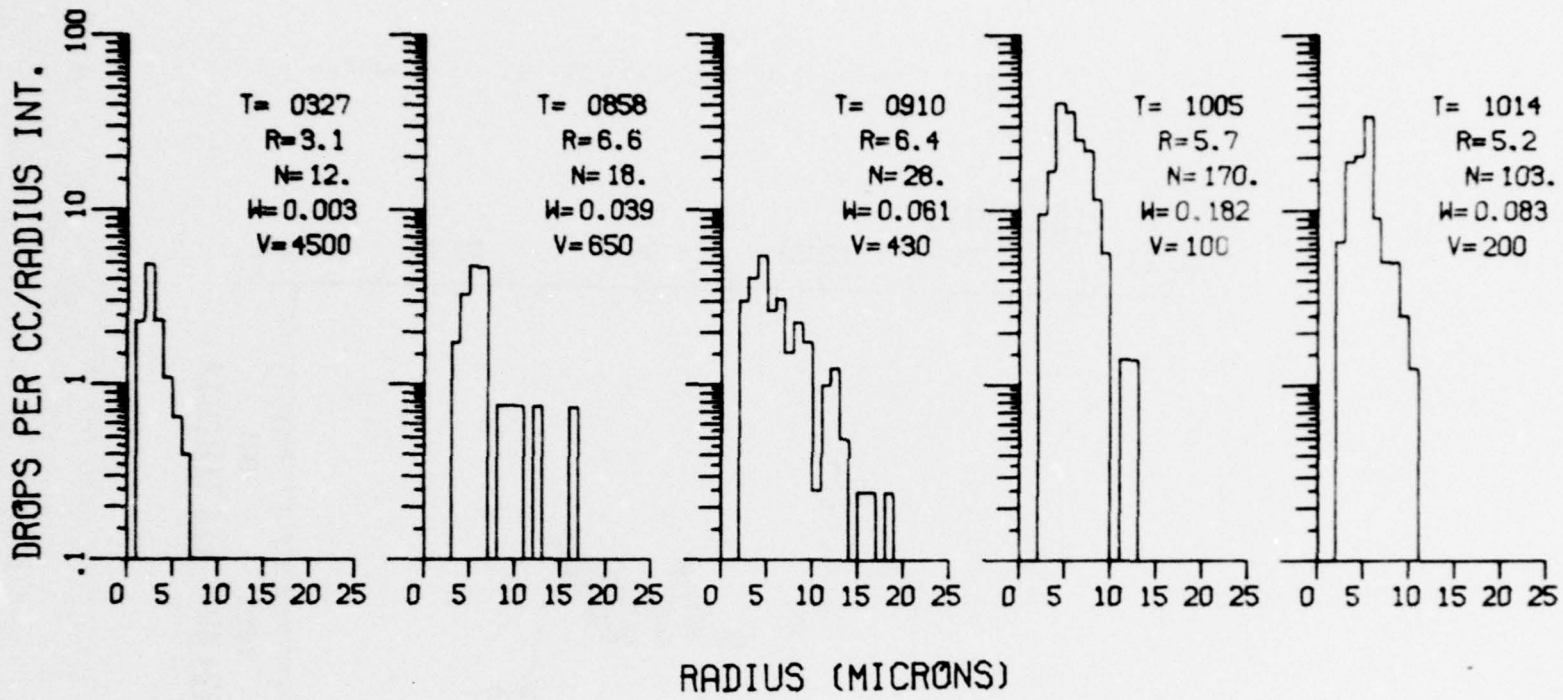

Figure C-5: Droplet Spectra - Fog of 5 October 1976

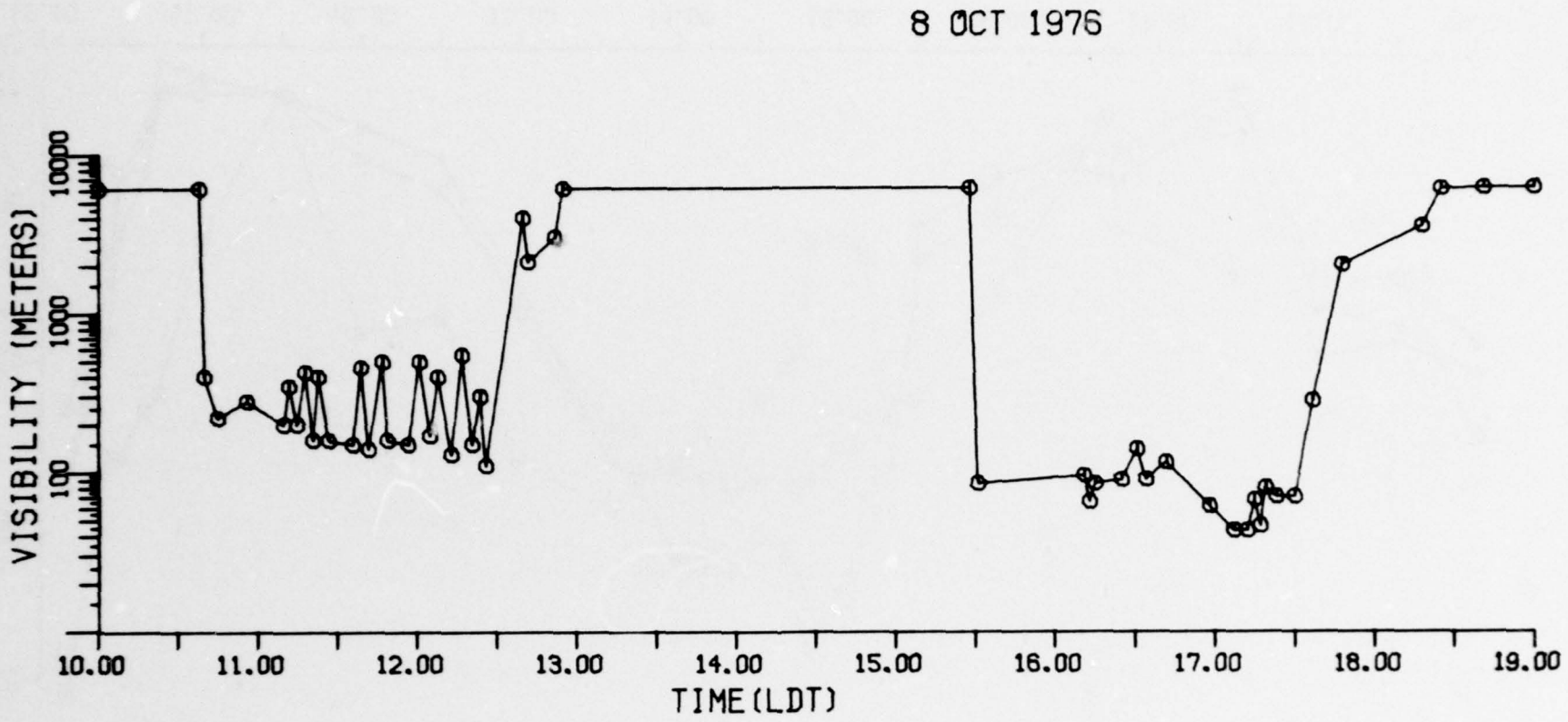

Figure C-6: Visibility - Fog of 8 October 1976

Figure C-7: Temperature - Fog of 8 October 1976

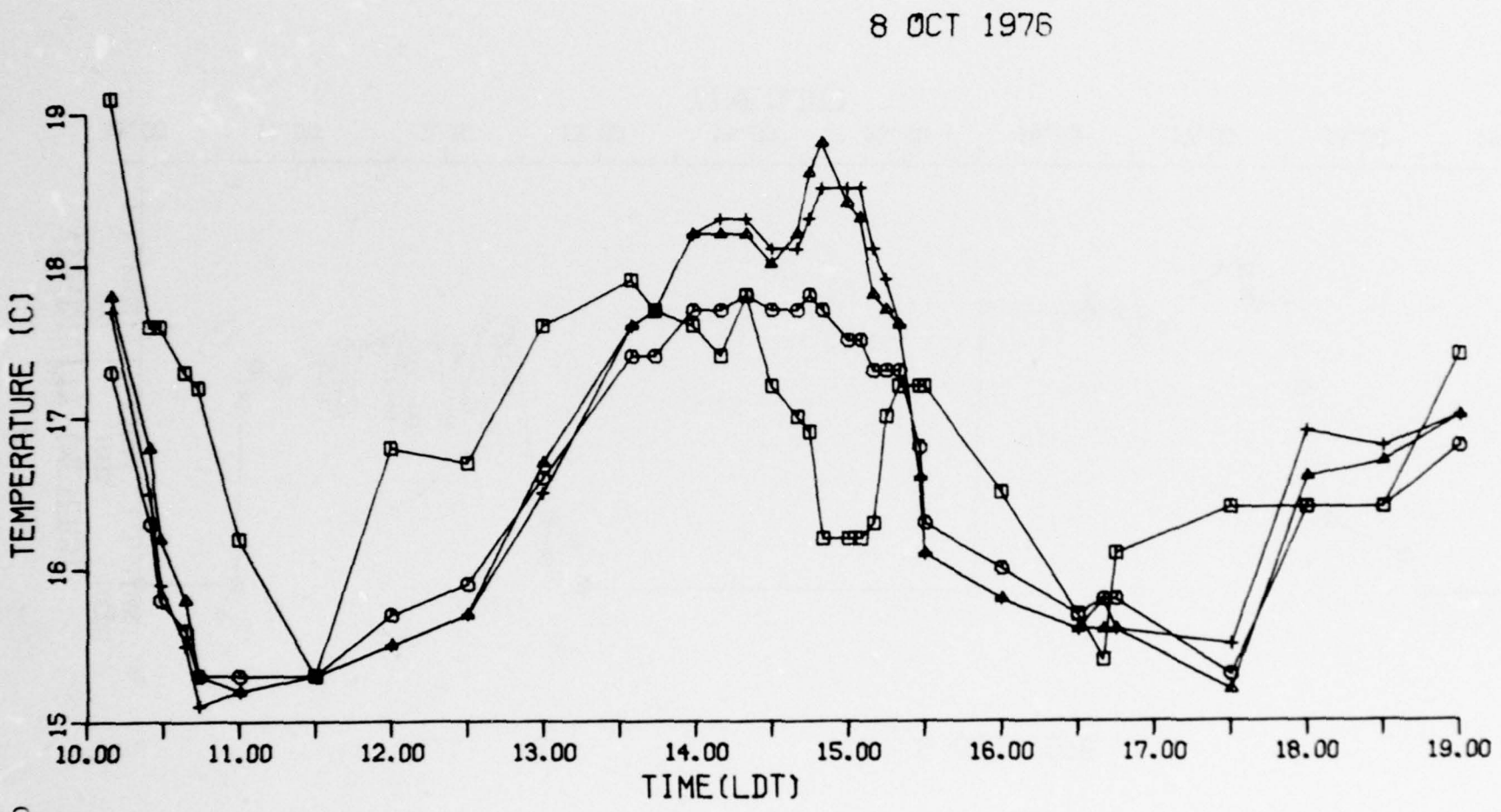

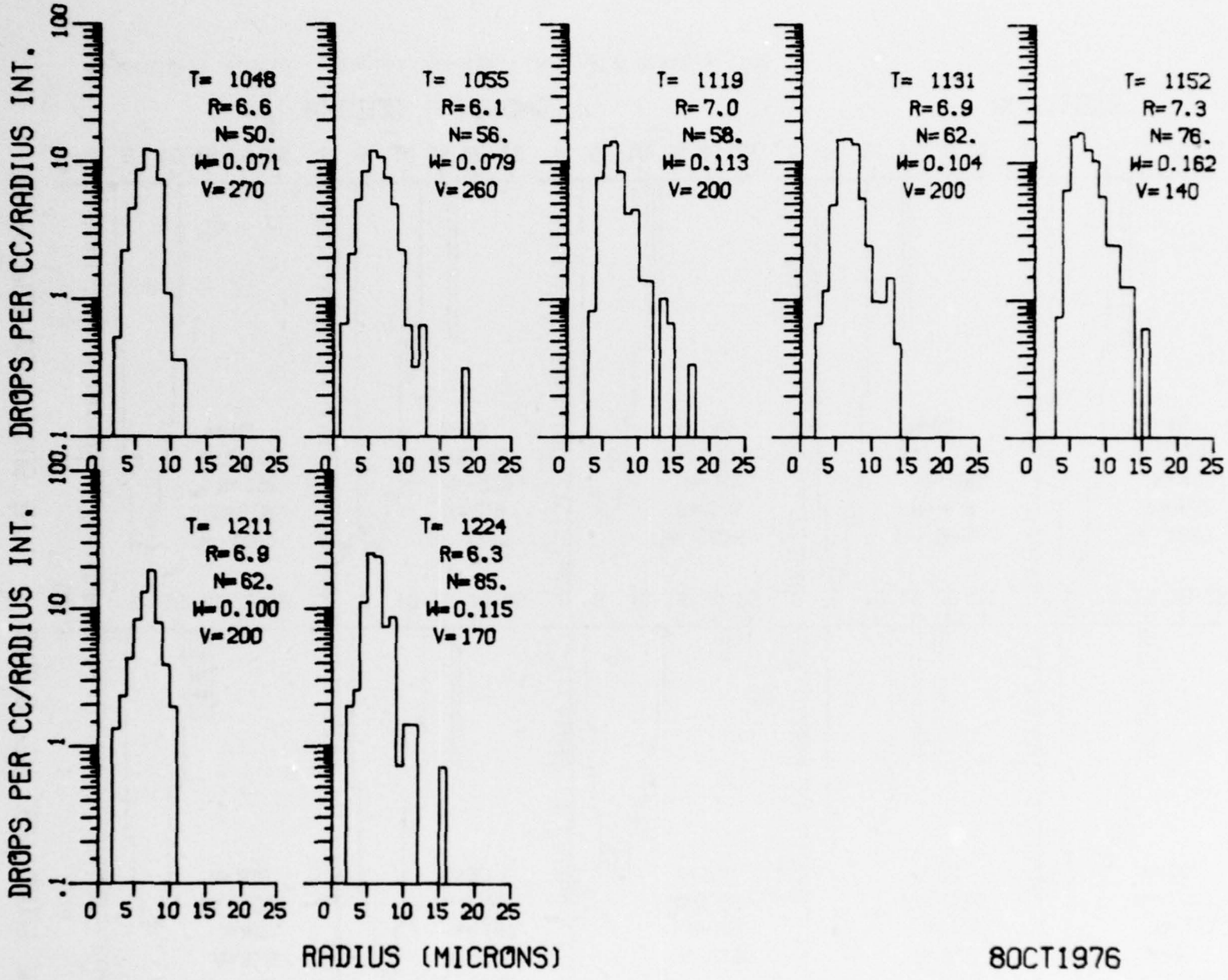

Figure C-8a: Droplet Spectra - Fog of 8 October 1976

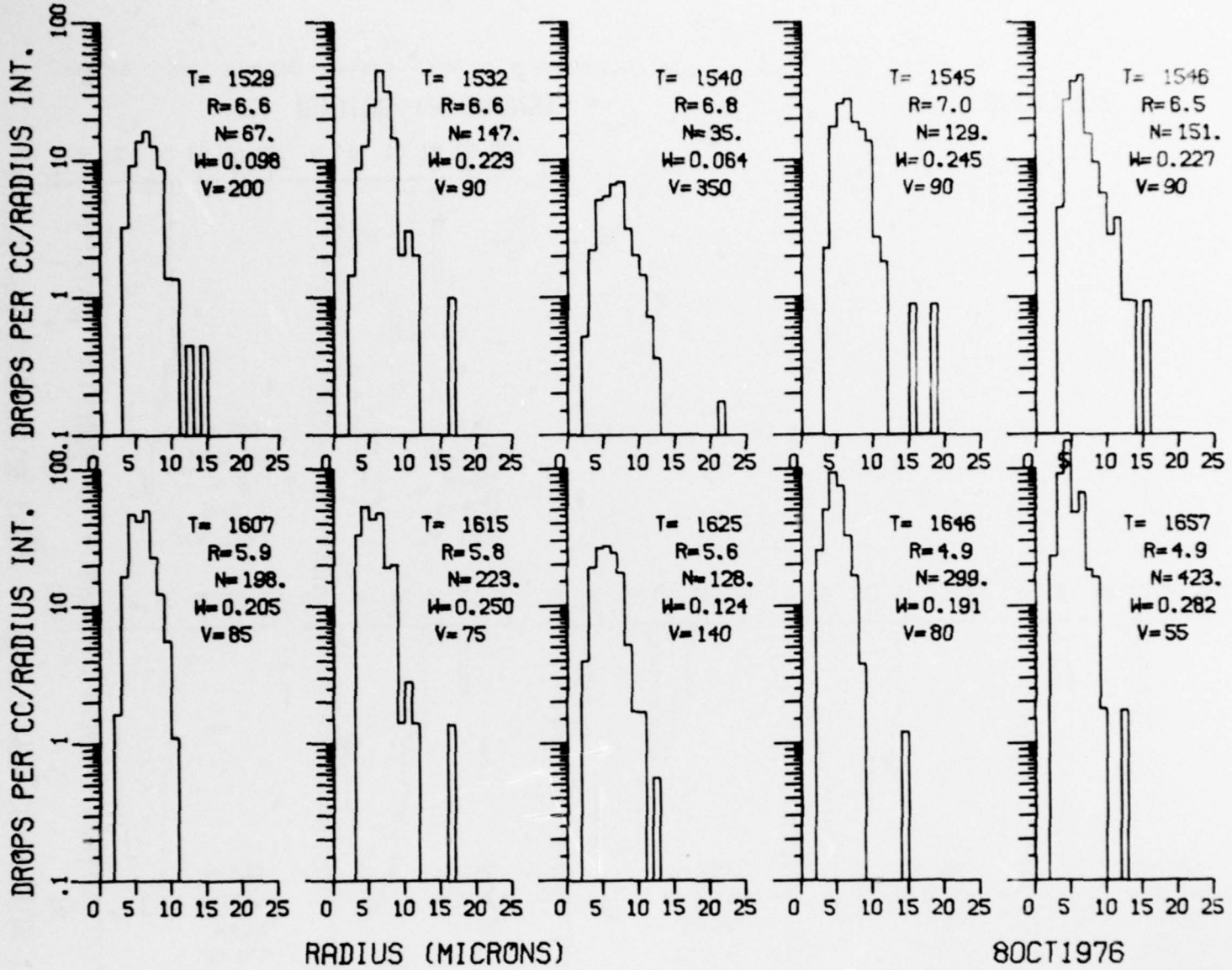

Figure C-8b (Cont): Droplet Spectra - Fog of 8 October 1976

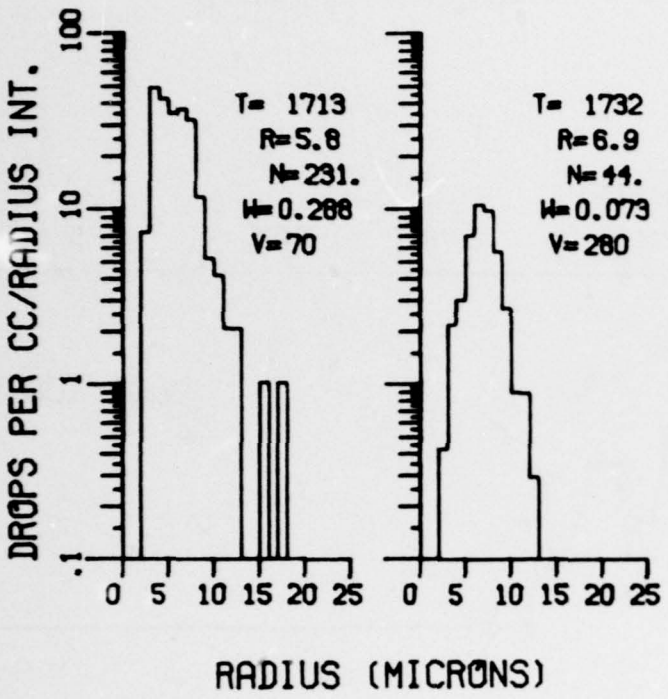

Figure C-8c (Cont): Droplet Spectra - Fog of 8 October 1976

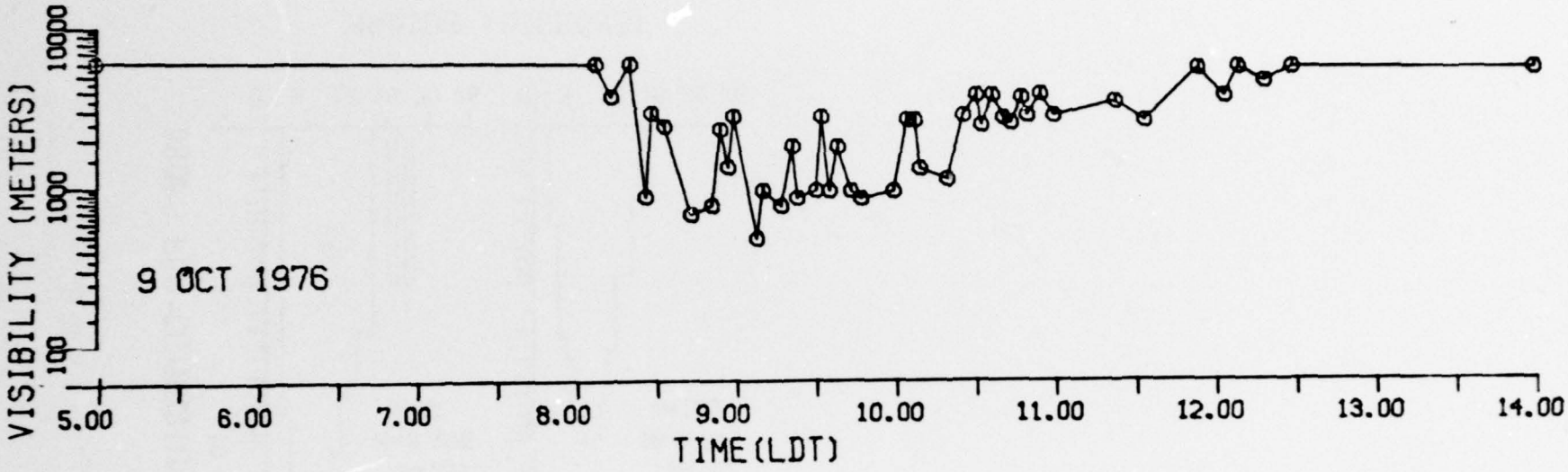

Figure C-9: Visibility - Fog of 9 October 1976

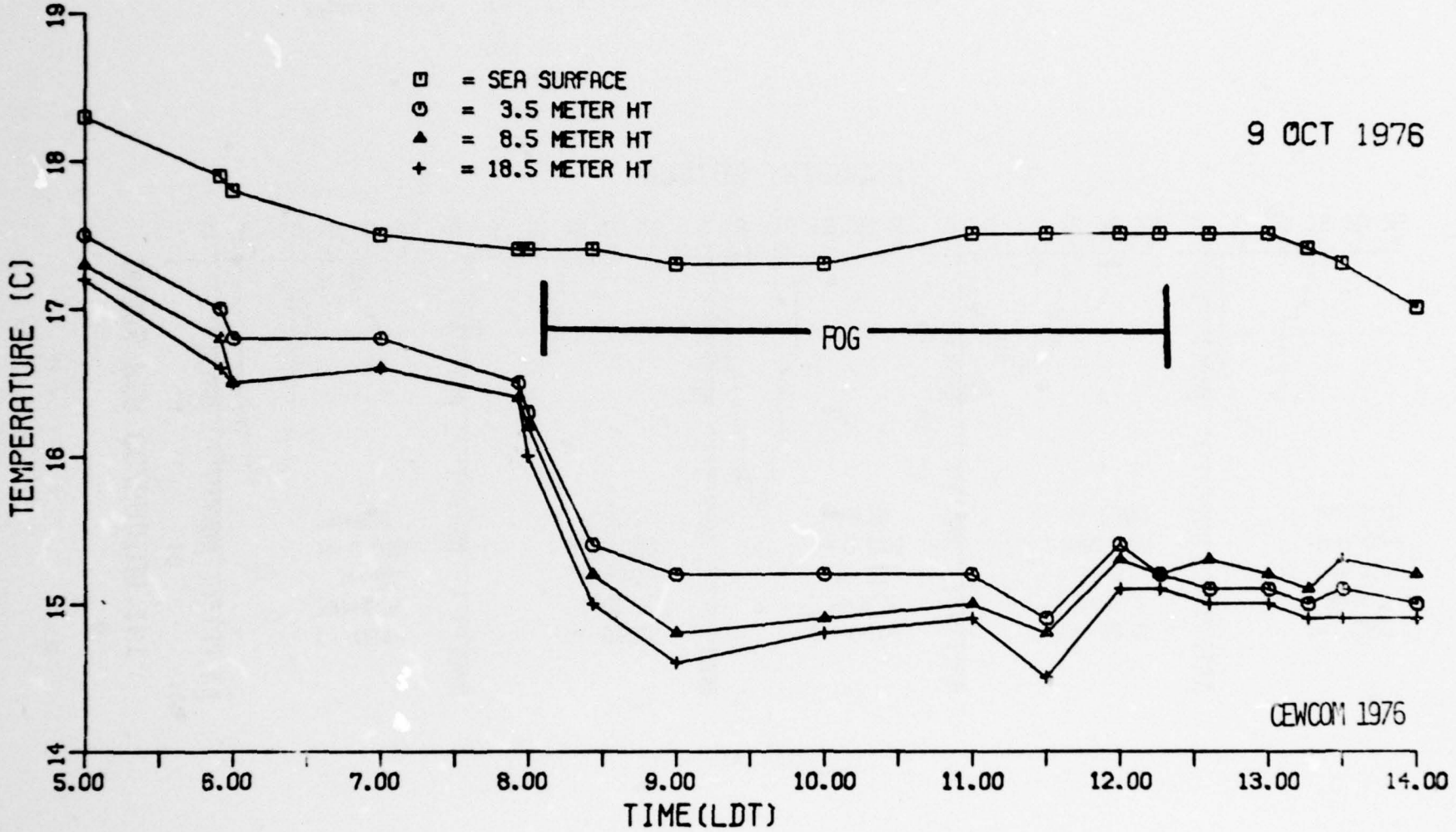

Figure C-10: Temperature - Fog of 9 October 1976

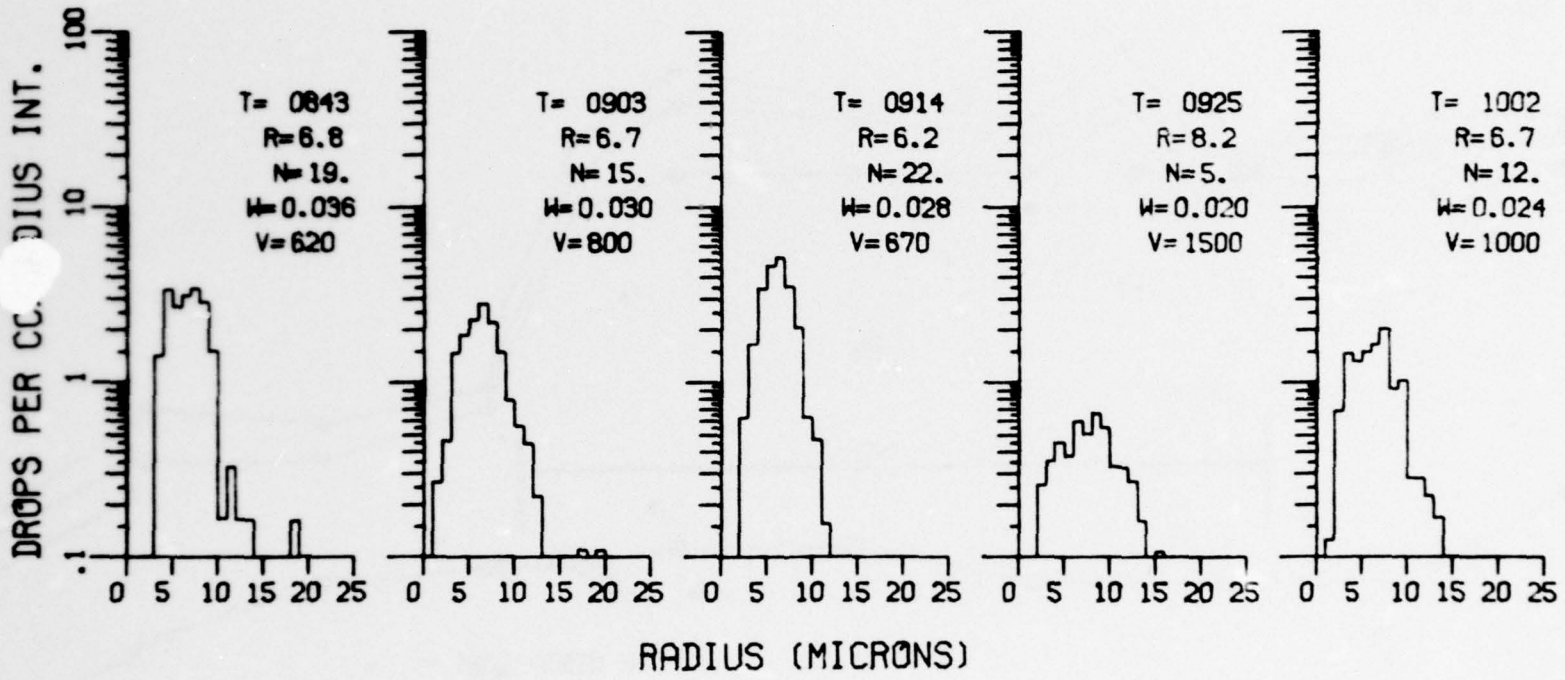

Figure C-11: Droplet Spectra - Fog of 9 October 1976

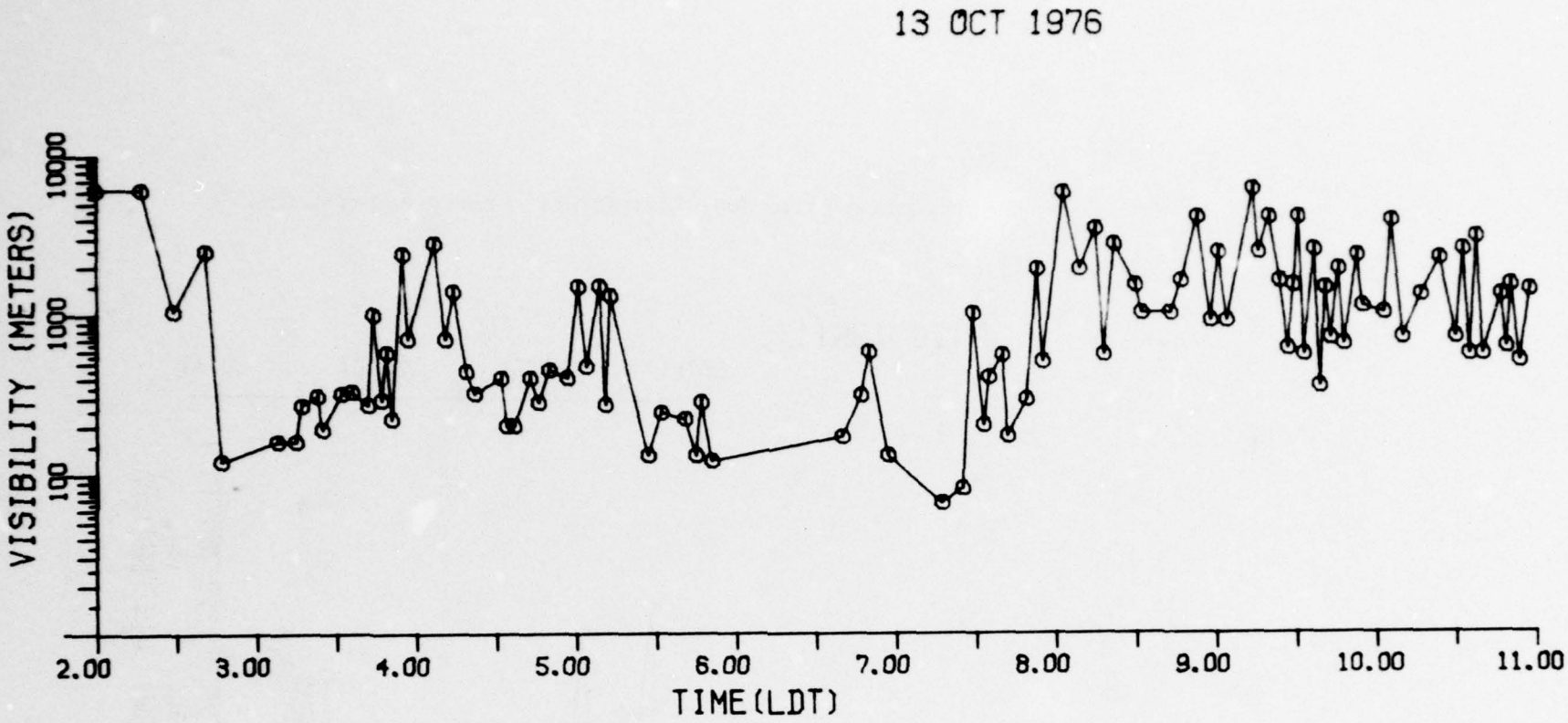

Figure C-12a: Visibility - Fog of 13 October 1976

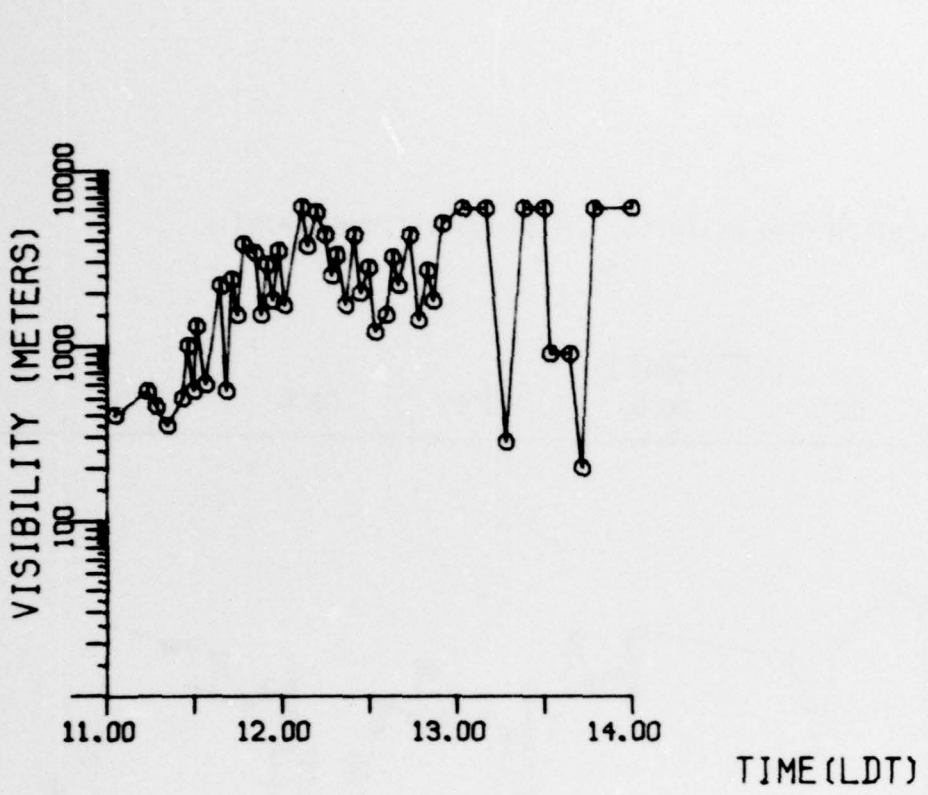

Figure C-12b (Cont): Visibility - Fog of 13 October 1976

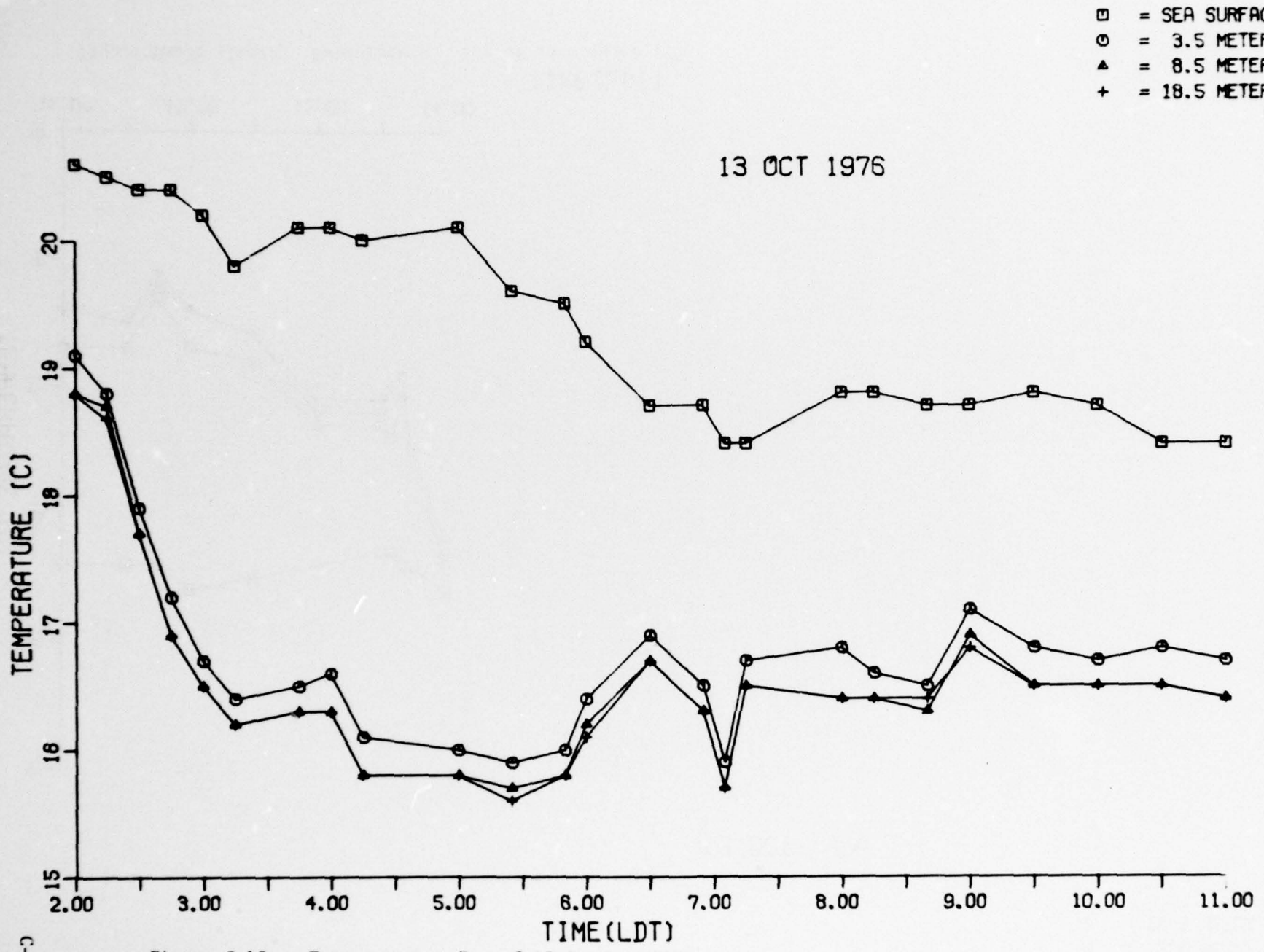

Figure C-13a: Temperature - Fog of 13 October 1976

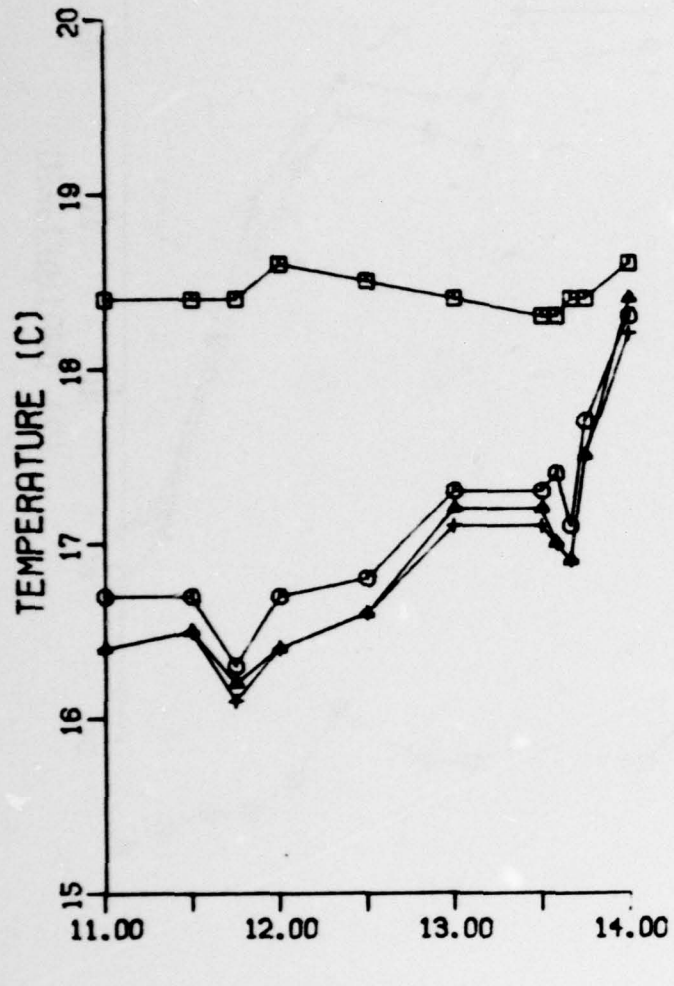

Figure C-13b (Cont): Temperature - Fog of 13 October 1976

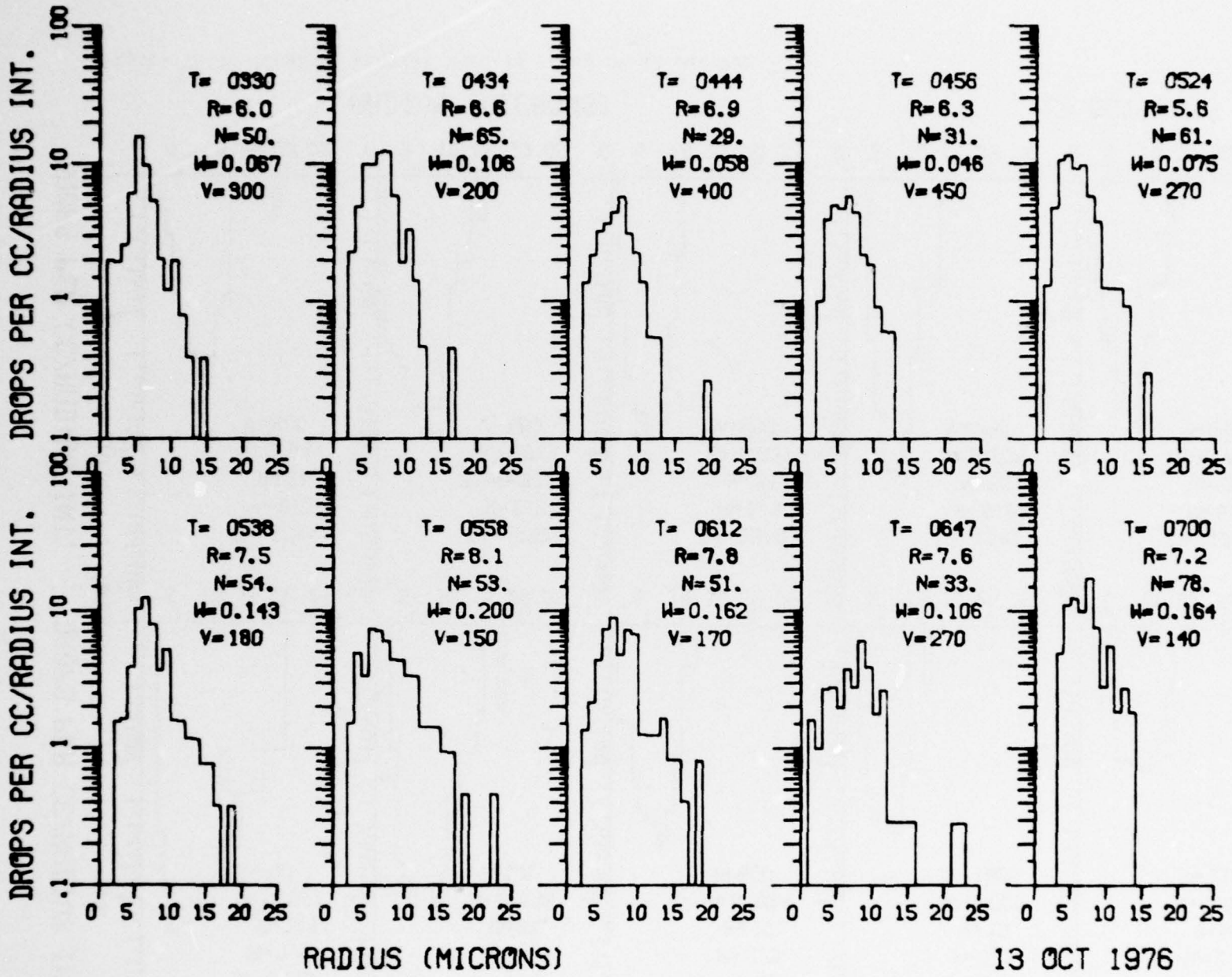

Figure C-14a: Droplet Spectra - Fog of 13 October 1976

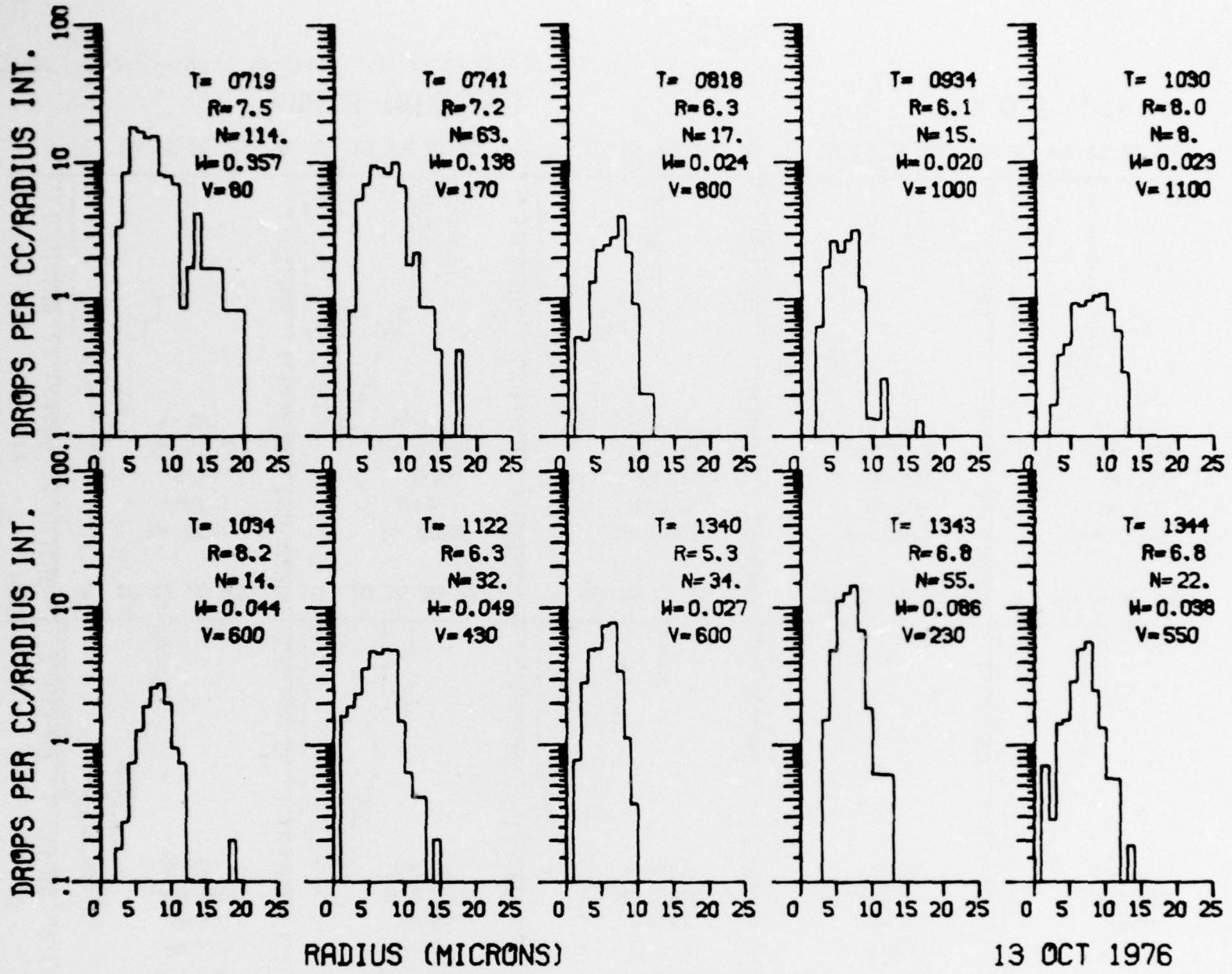

Figure C-14b (Cont): Droplet Spectra - Fog of 13 October 1976